SAARLAND UNIVERSITY

Department of Neuroanatomy,
Institute for Anatomy and Cell Biology,
Faculty of Medicine, Saarland University,
Homburg / Saar, Germany.

ArfGAP3 Is a Component of the Photoreceptor Synaptic Ribbon Complex and Forms an NAD(H)-Regulated, Redox-Sensitive Complex with RIBEYE That Is Important for Endocytosis

A thesis submitted to the Faculty of Medicine in fulfillment of the requirement for the degree of

Doctor of Philosophy (Ph.D.)

Mayur Harish Dembla

Germany 2015

Declaration:

I hereby declare that the Ph.D. thesis entitled "**ArfGAP3 Is a Component of the Photoreceptor Synaptic Ribbon Complex and Forms an NAD(H)-Regulated, Redox-Sensitive Complex with RIBEYE That Is Important for Endocytosis** " is a presentation of my original research work. Where other sources of information have been used, they have been acknowledged. No portion of work contained in this thesis has been submitted in support of any application for any other degree or qualification.

Homburg,

23.09.15

Mayur Harish Dembla.

Supervisor:

Co-supervisor:

Acknowledgement:

It's an immense satisfaction and pleasure feeling to narrate about the people with whose help direct or indirect has contributed in the completion of my thesis work.

First and foremost I would like to express my deepest and highest gratitude to my supervisor Prof. Dr. Frank Schmitz, who gave me the important opportunity for initiating my Doctoral thesis under his guidance. First thing that comes to my mind is his never-ending thrust for science and immense sincereness. His curiosity for research has always excited my work and has taken it to clear path of hard work.

I would like to express my sincere thanks to Prof. Dieter Bruns, Prof. Jens Rettig and other members of their lab for creating an inspiring and debateable environment in the "synapse club" seminar.

I convey my special thanks to Dr. Karin Schwarz for helping me out at various stages of my work with her expert and critical suggestions and also for proof reading the "Zusammenfassung" of my thesis.

I would like to convey my heartly respect to Dr. Chad Grabner for being a nice teacher and a friend during his stay in the lab and also to his family.

I would like to thank Prof. Gerald Thiel for helping me in academic related matters.

I would like to thank Dr. Sivaraman Natarajan and Dr. Jagadish Kumar who were chaperons of my thesis work as nicely stated by Prof. Schmitz. Their help was immense support for me to intiate my work in the starting of Doctoral period.

It is of equal importance to mention Dr. Silke Wahl and Mrs. Rashmi Katiyar who helped me in doing some important experiments of my Doctoral thesis and also providing a pleasant environment in the lab.

I would like to thank Sylvia Brundaler and Gabi Kiefer for being helpful at all the times in the lab regarding scientific and personal work. Many thanks to Gerlinde Kühnreich and all the remaining staff members of my lab.

I feel pleasure to thank my cousin Dr. Sandeep Dembla for initiating my journey and help me out at early stages of my stay in Homburg.

I want to mention Ms. Shweta suiwal, Mr. Hiresh Ayoubian, Ms. Lisa Woc and Dr. Stephan Maxeiner for being a part of my time spent during my doctoral thesis.

The financial support from Sonderforschungsbereichs (SFB 894) and University of Saarland is gratefully acknowledged.

My friends in Homburg, Zweibrucken and other places have been quite good in creating some good memories, which I will cherish for quite a long time.

These in-detailed list of people would be incomplete without mentioning at first, my parents and my brother, who have always stood by my side in all different kinds of situations and Second, my wife Mrs. Ekta Dembla who has helped, supported me and has provided positive and sincere approach toward professional and personal matters.

DEDICATED TO MY PARENTS, MY WIFE AND MY BROTHER

Summary:

Ribbon synapses constitute a distinct type of chemical synapses present in retinal neurons (photoreceptor and bipolar cells), hair cells from the inner ear and pinealocytes from the pineal gland. Ribbon synapses are specialized for continuous synaptic transmission. Ribbon synapses differ morphologically from conventional synapses by the presence of a unique electron-dense presynaptic structure, the synaptic ribbon. In the retina, ribbon synapses enable neurons to transmit light signals over a dynamic range of varying magnitude that is not achievable by conventional synapses.

RIBEYE is a major component of the synaptic ribbon. RIBEYE consists of a unique aminoterminal A-domain and a carboxyterminal B-domain that is identical to the protein CtBP2. RIBEYE(B)-domain consists of a NADH binding subdomain (NBD) and substrate-binding subdomain (SBD). RIBEYE has been proposed to be directly influencing the rate of exocytosis and endocytosis either directly or through its interaction partners. But how RIBEYE and synaptic ribbon functions at the synaptic ribbon is still largely unclear.

In order to obtain a better understanding of the molecular events at the synaptic ribbon, I performed a YTH screen with RIBEYE(B) as bait and obtained the protein ArfGAP3(ADP-ribosylation factor GTPase activating protein 3) as a potential interaction partner of RIBEYE. ArfGAP's in general are typically considered as gatekeepers of vesicle generation. One of the important functions of GTPase-activating proteins (GAP's) is the regulation of small G proteins such as Arf's and Arl's. Furthermore, they are proposed to bind to SNARE proteins. Therefore, this putative interaction appeared to be very interesting to the ribbon synapse and I analyzed it in detail. I verified this interaction in the YTH system with original YTH clone and with multiple ArfGAP3 plasmids cloned from full length (f.l.) ArfGAP3 cDNA. To check for the smallest interactions parts of both proteins, f.l. ArfGAP3 was splitted into two parts, the N-terminal GAP-domain, and the C-terminal SNARE and cargo-binding domain and tested for the interaction with RIBEYE. With help of the YTH, I found that GAP-domain of ArfGAP3 interacts with NBD domain of RIBEYE. Although the GAP-domain was important for the interaction with RIBEYE the enzymatic activity is most likely dispensible. The intial YTH clone had deletion of 8 amino acids in the middle of the zinc finger domain that can be expected to disrupt the enzymatic activity. Despite the loss of its enzymatic activity, the interaction between ArfGAP and RIBEYE was unaffected suggesting a GAP activity-independent interaction. To confirm direct interaction between ArfGAP3 and RIBEYE, I performed fusion protein pull-down assays, in which the proteins were found to bind to each other to a large extend (≥30%). The specificity was confirmed by using various

controls (including irrelevant control proteins and by switching proteins tags to rule out that the interaction depends on the fusion-tags.

I verified the RIBEYE-ArfGAP3 interaction identified by the YTH system by multiple independent approaches. Firstly, I performed co-immunoprecipitation of ArfGAP3 from bovine retina using newly generated rabbit polyclonal antibody generated against the C-terminus region of ArfGAP3 (named Cterm2 and Cterm3). With the use of co-immunoprecpitation (Co-IP) techniques, I demonstrated that ArfGAP3 co-immunoprecipitated RIBEYE from bovine retina and analyses confirmed that these proteins do interact in the retina. Polyclonal antibodies generated against ArfGAP3 were further used to check the localization of the ArfGAP3 in retina at the light microscopic level. With the use of 0.5µm semi-thin sections of the mouse retina and high-resolution microscopy techniques (including SR-SIM) the immunolabeling analyses showed a close localization of ArfGAP3 to the synaptic ribbon. Double Immunolabeling of ArfGAP3 and Bassoon also showed a close localization of the proteins at the active zone, suggesting the ArfGAP3 could be localized at the base of the ribbon. Unfortunately, the ultra-structural localization of ArfGAP3 could not be resolved with Cterm2 and 3 antibodies or with several tested commercial antibodies. Triple labeling of ArfGAP3, RIBEYE and Dynamin also showed close localization of ArfGAP3 in vicinity of synaptic ribbon. Pulldown analyses indicated that the interaction is redox-sensitive. With removal of ß-mercaptoethanol from pull-down buffer, interaction between GAP-domain of ArfGAP3 and RIBEYE(B) was strongly reduced, implying that a more reduced environment is favourable for the interaction between ArfGAP3 and RIBEYE. By testing increasing concentrations of either NAD^+ or NADH (in absence of ß-ME), I showed that the GAP-domain of ArfGAP3 binds more efficiently to RIBEYE(B) in presence of the reduced form, i.e. NADH, compared to the NAD^+, the oxidized form. The half maximum binding for GAP-domain in presence of NADH was ≈450 nM and ≈700 nM for NAD^+. This difference in binding of NADH/NAD^+ suggests that ratio of NADH/NAD^+ could act as a metabolic switch for the interaction of GAP-domain of ArfGAP3 and RIBEYE(B). Heterologous over-expression of GAP domain-mcherry together with RIBEYE(B)-EGFP in COS cells also showed recruitment of RIBEYE(B) to ArfGAP3 further confirming interaction between RIBEYE and ArfGAP3 in COS cells.

As indicated above, GAP domain containing proteins such as, ArfGAP3 regulate the function of ADP ribosylation factor proteins Arf's and Arl's, by promoting GTP hydrolysis. Therefore it was important to identify the effector molecule of ArfGAP3. I found out that Arf1, but not Arf6, interacts with ArfGAP3. Light microscopic analysis revealed Arf1 localization in close vicinity of synaptic ribbon. Both RIBEYE(B) and Arf1 interacted with

GAP domain of ArfGAP3 as judged by YTH analyses and not with each other raising the possibility that they could compete for their binding to the GAP-domain. By performing triple pull-down assay with GAP domain, RIBEYE(B) and Arf1, I found that there is decrease in binding of one of partner [RIBEYE(B) or Arf1] with increasing concentration of the other protein and vice versa, while common binding protein, ArfGAP3 was kept at a constant molar concentration. This indicates a competitive binding of RIBEYE(B)/Arf1 to ArfGAP3.

Overexpression of ArfGAP3 in electroporated photoreceptors of the mouse retina resulted in a strong inhibition of endocytic membrane retrieval as judged by an inhibited uptake of FM1–43. One of the explanations could be that over-expressing ArfGAP3 could cause uncontrolled hydrolysis of Arf1 thereby disturbing its balance between active and inactive state eventually affecting the recycling of the vesicles. Therefore, I propose that the RIBEYE/ArfGAP3 complex is important for endocytic membrane retrieval at the synaptic ribbon.

Zusammenfassung:

Band-Synapsen (Ribbonsynapsen) sind spezialisierte chemische Synapsen in Netzhautneuronen (Photorezeptoren und Bipolarzellen), Haarzellen aus dem Innenohr und Pinealozyten der Zirbeldrüse. Band-Synapsen sind für eine langanhaltende kontinuierliche synaptischen Übertragung spezialisiert. Morphologisch unterscheiden sich die Band-Synapsen durch das Vorhandensein einer einzigartigen, elektronendichten präsynaptischen Struktur, dem sogenannten synaptischen Ribbon (Band), von den herkömmlichen chemischen Synapsen. Die Photorezeptoren der Netzhaut besitzen Band-Synapsen, damit sie in der Lage sind, die empfangenen visuellen informationen über eine große Bandbreite in graduierte chemische Signale umzuwandeln, eine Eigenschaft, die von herkömmlichen chemischen Synapsen nicht geleistet werden kann.

Das Protein RIBEYE ist eine Hauptkomponente des synaptischen Ribbon. RIBEYE besteht aus einer nur in RIBEYE vorkommenden aminoterminalen A-Domäne und einer carboxyterminalen B-Domäne, die weitestgehend identisch ist mit dem Protein CTBP2. Die RIBEYE(B)-Domäne wiederum besteht aus einer NADH-Bindungsdomäne (NBD) und einer Substratbindungsdomäne (SBD). Einer Hypothese zur Folge beeinflusst RIBEYE entweder direkt oder indirekt über seine Interaktionspartner die Vorgänge der Exo- und Endozytose. Wie RIBEYE und der synaptische Ribbon dies jedoch machen, ist bisher noch weitestgehend ungeklärt.

Um ein besseres Verständnis über die molekularen Vorgänge am synaptischen Ribbon zu gewinnen, führte ich zunächst einen Hefe-zwei-Hybrid-Versuch (YTH) durch. In diesem YTH-Ansatz habe ich die RIBEYE(B)-Domöne als Köder eingesetzt und als möglichen Bindungspartner von RIBEYE das Protein ArfGAP3 (ADP-Ribosylierung Faktor GTPase-aktivierendes Protein 3) identifiziert. ArfGAP's gelten als wichtige Regulatoren des Vesikelzyklus. Eine wichtige Funktion der GTPase-aktivierenden Proteine (GAP's) besteht in der Steuerung kleiner G-Proteine, wie z.B. Arf und Arl, Darüber hinaus interagieren die GAP's mit SNARE-Proteinen. Diese mögliche Interaktion zwischen RIBEYE und ArfGAP3 könnte somit eine Verbindung des synaptischen Ribbons mit den Vorgängen bei Exo- und Endozytose darstellen. Um die Interaktion zu verifizieren, habe ich zunächst den YTH-Versuch mit dem ursprünglichen ArfGAP3-Klon und mit weiteren ArfGAP-Konstrukten (alle von der vollständigen ArfGAP-cDNA-Sequenz kloniert) wiederholt. Zur Kartierung der Interaktion, wurde full length (f.l.) ArfGAP3 in zwei Teile, die N-terminalen GAP-Domäne und die C-terminale SNARE und Fracht-Bindungsdomäne gespalten und auf Wechselwirkung mit RIBEYE getestet. In vergleichbarer Weise habe ich auch die

RIBEYE(B)-Domäne in kleinere Einheiten zerlegt. Auf diese Weise konnte ich die GAP-Domäne von ArfGAP3 als Interaktionsstelle mit der NBD von RIBEYE identifizieren. Obwohl die GAP-Domäne von ArfGAP3 wichtig ist für die Bindung an RIBEYE, spielt deren enzymatische Aktivität wohl keine Rolle, denn der ursprünglich gefischte ArfGAP3-Klon besitzt eine Deletion von 8 Aminosäuren in dieser Domäne. Die fehlenden 8 Aminosäuren liegen in der Mitte der Zinkfingerdomäne der GAP und haben damit vermutlich einen störenden Einfluss auf die Enzymaktivität. Aufgrund dieser Tatsache ist davon auszugehen, dass die Bindung an RIBEYE unabhängig von der GTPase-Aktivität erfolgt. Um die direkte Interaktion zwischen ArfGAP3 und RIBEYE zu bestätigen, habe ich Interaktionsstudien mit aufgereinigten Fusionsproteinen durchgeführt (Pull-down-Assays). In diesen Studien konnte ich zeigen, dass die beiden Proteine im großen Umfang an einander binden. Mehr als 30% der eingesetzten Bindungspartner konnten gemeinsam präzipitiert werden. Die Spezifität des Pull-down-Assays wurde mit Hilfe von verschiedenen Kontrollen (z.B. Einsatz von irrelevanten Kontrollproteinen oder tauschen der Protein-Tags, um auszuschließen, dass die Interaktion von den Fusion-Tags beeinflusst wird) verifiziert.

In weiteren Schritten überprüfte ich die im YTH gefundene RIBEYE-ArfGAP3 Interaktion, Als erstes führte ich Co-Immunpräzipitationen mit zwei unabhängigen gegen ArfGAP3 gerichteten polyklonalen Antikörpern durch. Beide Antikörper (Cterm2 und Cterm3) sind gegen unterschiedliche Regionen des C-terminus von ArfGAP gerichtet und wurden von mir neu generiert. Wie erwartet, haben beide Antikörper ArfGAP3 aus der Rinderetina präzipitiert. Darüber hinaus konnte ich RIBEYE in den ArfGAP-Präzipitaten detektieren. Diese Co-Immunpräzipitationen belegen, dass ArfGAP3 und RIBEYE in vivo in der Retina mit einander interagieren. Ich verwendete die von mir generierten Antikörper, um die Verteilung von ArfGAP in der Retina zu lokalisieren. Unter Verwendung von 0,5 µm dünnen Gewebeschnitten und mit Hilfe hochauflösender lichtmikroskopischer Techniken (Konfokalmikroskopie und SR-SIM) konnte ich zeigen, dass sich ArfGAP3 in unmittelbarer. Nähe des synaptischen Ribbons befindet. Doppel-Immunmarkierungen von ArfGAP3 und Bassoon zeigten, dass sich beide Proteine in Nachbarschaft der aktiven Zone der Ribbonsnapse befinden. Die Co-Lokalisation von ArfGAP3 und Bassoon deutet daraufhin, das sich ArfGAP3 an der Basis des Ribbons befindet. Leider konnte die ultra-strukturelle Lokalisierung (Elektronenmikroskopie) von ArfGAP3 mit den zur Verfügung-stehenden Antikörpern (Cterm2, Cterm3 und verschiedene kommerzielle Antikörper) nicht gezeigt werden, da keiner der verwendeten Antikörper mit dieser Technik funktionierte. Dreifach-Immunmarkierungen von ArfGAP3, RIBEYE und Dynamin belegten die enge räumliche Nachbarschaft von ArfGAP3 und dem synaptischen Ribbon.

Mit Hilfe von Pulldown-Analysen konnte ich zeigen, dass die Interaktion zwischen RIBEYE(B) und ArfGAP3 redox-sensitiv ist. Wenn ß-Mercaptoethanol aus dem Pull down Puffer entfernt wurde, war die Bindung zwischen der GAP-Domäne von ArfGAP3 und RIBEYE (B) stark vermindert. Dies bedeutet, dass ein stärker reduziertes Umfeld die Interaktion zwischen ArfGAP3 und RIBEYE begünstigt. Durch Zugabe von aufgehende aufsteigenden Konzentrationen von entweder NAD^+ oder NADH in den Co-Präzipitations-Ansatz (in Abwesenheit von ß-ME), konnte ich nachweisen, dass die GAP-Domäne von ArfGAP3 in Gegenwart der reduzierten Form (NADH), effizienter an RIBEYE (B) bindet, als in der Gegenwart der oxidierten Form (NAD^+). Die halbmaximale Binding der GAP-Domäne an RIBEYE(B) wurde in Gegenwart von NADH bei einer Konzentration von ≈450 nM erreicht, in Gegenwart von NAD^+ erst bei einer Konzentation ≈700 nM für NAD^+. Dieser Unterschied in der Bindung in Gegenwart von NADH/NAD^+ legt nahe, dass Verhältnis von NADH/NAD^+ als Stoffwechselschalter für die Interaktion der GAP-Domäne von ArfGAP3 mit RIBEYE (B) fungieren könnte. Heterologe Überexpression von GAP-mCherry zusammen mit RIBEYE (B)-EGFP in COS-Zellen zeigte die Rekrutierung von RIBEYE (B) zum Expressionsort von GAP-mCherry und bestätigte somit die Interaktion zwischen RIBEYE und ArfGAP3.

GAP-Domänen enthaltende Proteine, wie z.B ArfGAP3, regulieren die Funktion von ADP-Ribosylierungsfaktorproteinen (z.B. Arf und Arl), unter Förderung der GTP-Hydrolyse. Deshalb war es wichtig, das Effektor-Molekül von ArfGAP3 zu identifizieren. Ich konnte zeigen, dass Arf1, aber nicht Arf6, mit ArfGAP3 interagiert. Lichtmikroskopische Analysen lokalisierten Arf1 in unmittelbarer Nähe des synaptischen Ribbons, also dort wo auch ArfGAP3 zu finden ist. Sowohl RIBEYE (B) und Arf1 interagieren mit der GAP Domäne von ArfGAP3 (aber nicht miteinander), was auf die Möglichkeit hinweist, dass sie für ihre Bindung an die GAP-Domäne konkurrieren könnten. Um zu testen, ob tatsächlich eine kompetitive Bindung beider Proteine (RIBEYE(B) und Arf1) an ArfGAP3 vorliegt, führte ich Co-Präzipitations versuche durch. In diesen Versuchen wurde die molare Konzentration der GAP-Domäene von ArfGAP3 konstant gehalten und mit den beiden Kandidatenproteinen (RIBEYE(B) und Arf1) inkubiert. Ich konnte zeigen, dass die Bindung des einen Kandidatenproteins an die GAP-Domäne von ArfGAP3 abnahm, wenn die Konzentration des anderen Bindungskandidaten erhöht wurde und umgekehrt. Dies deutet auf eine kompetitive Bindung von RIBEYE (B) und Arf1 an ArfGAP3 hin.

Die Überexpression von ArfGAP3 in isolierten Maus-Photorezeptoren führte zu einer starken Hemmung der Endozytose in diesen Zellen. Im Vergleich zu nicht transfizierten

Photorezepotoren nahmen die ArfGAP3 überexprimierende Zellen nur sehr wenig FM1-43 auf. Eine Erklärung hier für könnte darin bestehen dass Überexpression von ArfGAP3 zu einer unkontrollierte Hydrolyse von Arf1 führt, wodurch das Gleichgewicht zwischen aktiven und inaktiven Zustand gestört und dadurch die Endozytose inhibiert wird. Basierend auf meinen Daten ist der RIBEYE/ArfGAP3 Komplex wichtig für die endozytotischen Vorgänge am synaptischen Ribbon.

CONTENTS

1 INTRODUCTION:

1.1 Structural Organization of the Eye:

The eye is a three-layered fluid-filled tissue, which is the prime organ for vision. The outer layer is the sclera at the posterior end and this opaque layer is transformed into the cornea, a specialized light transparent tissue that permits light rays to enter into the eye. The middle layer of tissue includes three distinct but continuous structures: the iris, the ciliary body, and the choroid. The innermost layer of the eye, the retina, contains neurons that are sensitive to light and are capable of transmitting visual signals to higher brain centre via optic nerve. Despite its peripheral location, the retina or neural portion of the eye is actually part of the central nervous system (for review, see Purves et al., 2001).

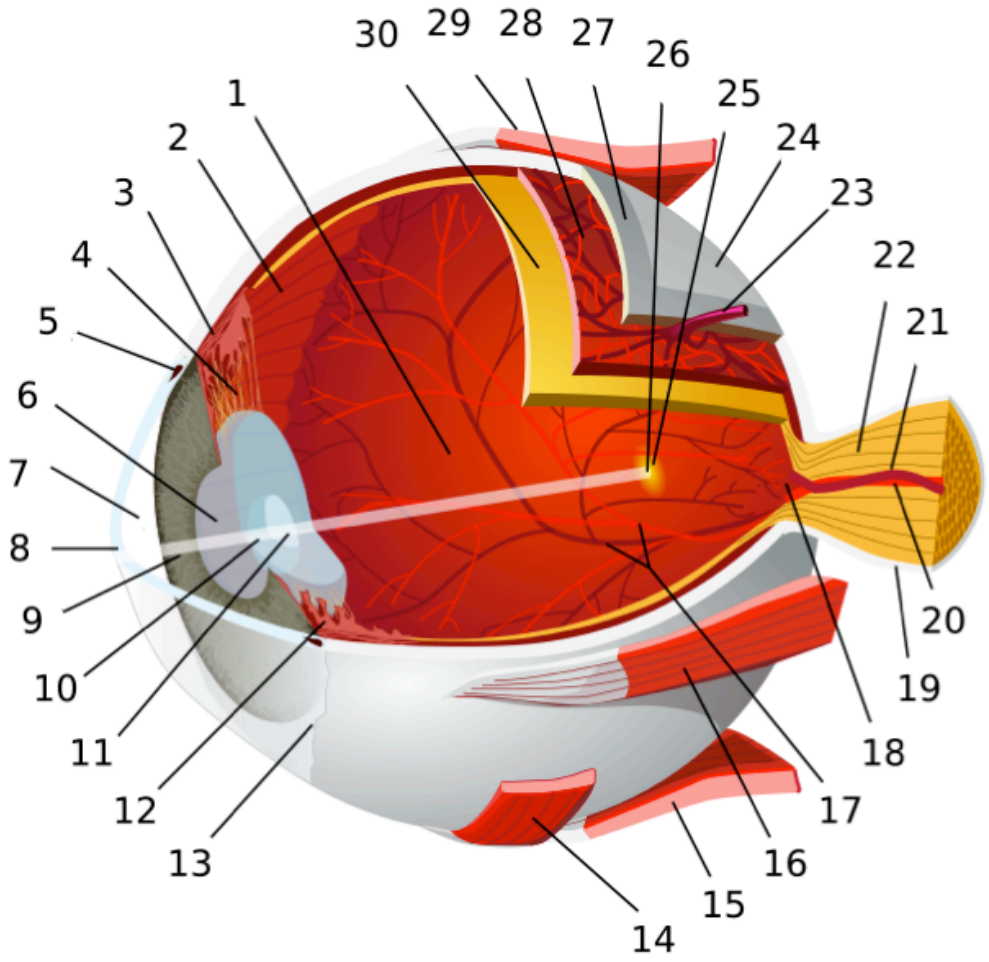

Figure 1: Diagramatic representation of EYE. 1: posterior segment of eyeball 2:Ora serrata 3:Ciliary muscle 4: Ciliary zonules 5: canal of Schlemm 6: pupil 7: Anterior chamber 8: Cornea 9: Iris 10: lens cortex 11: lens nucleus 12: Ciliary process 13: Conjunctiva 14: Inferior oblique muscle 15: Inferior rectus muscle 16: Medial rectus muscle 17: Retinal arteries and veins 18: Optic disc 19: Dura mater 20: Central retinal artery 21: Central retinal vein 22: Optic nerve 23: Vorticose vein 24: Bulbar sheath 25: Macula 26: Fovea 27: Sclera 28: Choroid 29: Superior rectus muscle 30: Retina (http://en.wikipedia.org/wiki/Humaneye)

1.2 Synaptic Complexity of the Retina

The retina itself is a part of central nervous system lining the posterior part of eye. Retinal arc (the maximum length of retina) of human is approximately 51mm in length (Panda-Jonas S et al., 1994; Polyak et al., 1941; Van Buren et al., 1963; Kolb et al., 1991) and that of mouse is 4.9mm (Jeon et al., 1998). The total retina of mouse is a circular disc of approximately 200µm in thickness (Gollisch and Meister et al., 2010). Charles Darwin famously wrote that the eye caused him to doubt that random selection could create the intricacies of nature.

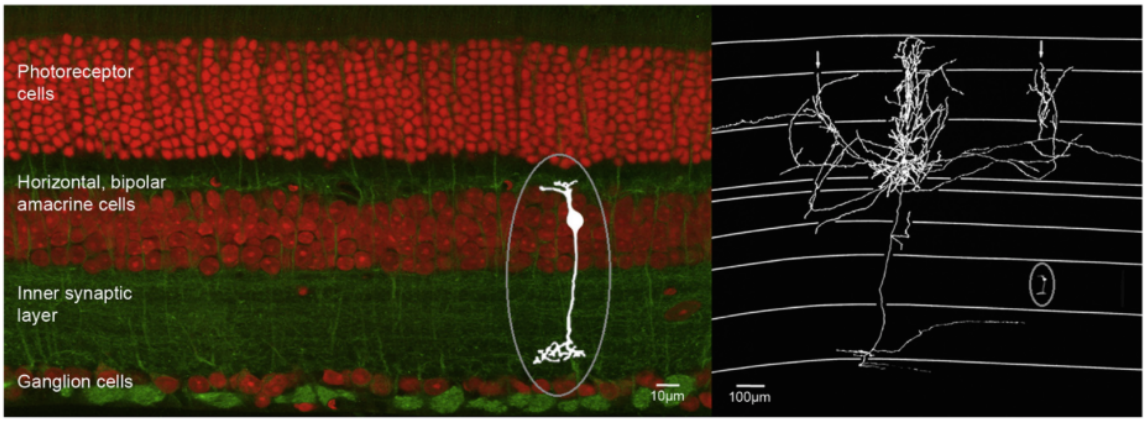

Figure 2: By the standards of other CNS regions, retinal neurons are miniscule (A) The layers of the mouse retina. A single bipolar cell is shown in white (adapted with permission from Wässle et al. (2009)). (B) The bipolar cell shown in A is reproduced at its correct scale on an image showing a cortical pyramidal cell (Masland et al., 2012).

Among several wonders of the retina, first most is its tiny size as shown in Figure 2 in comparison with cortical pyramidal cell (Gilbert et al., 1992). A radial section of a portion of the retina reveals that the ganglion cells (output neurons of the retina) lie innermost in the retina closest to the lens and front of the eye, and the photoreceptor cells (rods and cones) lie outermost in the retina touching the pigment epithelium and choroid (figure 3). In mouse, the average cone density is 12,400 cells/mm^2 and that of rod photoreceptor cells average density is about 437,000cells/ mm^2, giving a total number of rods of 6.4 million per retina. Thus, on average, rods are 97.2%, and cones are 2.8% of all photoreceptors (Jeon et al., 1998). Rod photoreceptors appear to be second most numerous neurons of the human body, after only the cerebellar granule cells. The retina's projection neuron, the retinal ganglion cell also a part of inner plexiform layer (Figure 2,3) has less than 1% the soma-dendritic volume of a cortical or hippocampal pyramidal cell. Although the retina forms a sheet of tissue only 200µm thick, its neural networks carry out feats of image processing that were unimagined even a few years ago (Gollisch and Meister, 2010). There is essential requirement of a rethinking not only of the retina's function, but also of the brain mechanisms that shape these signals into behaviorally useful visual perception.

The optic nerve marking the outermost layer of the retina contains the ganglion cell axons extending into higher visual center and additionally, incoming blood vessels that open into the retina to vascularize the retinal layers and neurons. Light must, therefore, travel through thickness of the retina before striking and activating the rods and cones.

The retina's processing of information begins with the sampling of the mosaic of rod and cone photoreceptors by the bipolar and horizontal cells at outer plexiform layer (OPL). The signal generated by any individual cone is decomposed into 12 different components, each of which is transmitted separately to the inner retina (inner plexiform layer, IPL) by a structurally and molecularly distinct type of bipolar cell. The outputs of these bipolar cells channels are sampled by different sets of retinal ganglion cells in varying diverse encodings of the visual scene that are further sent to brain (Masland et al., 2012).

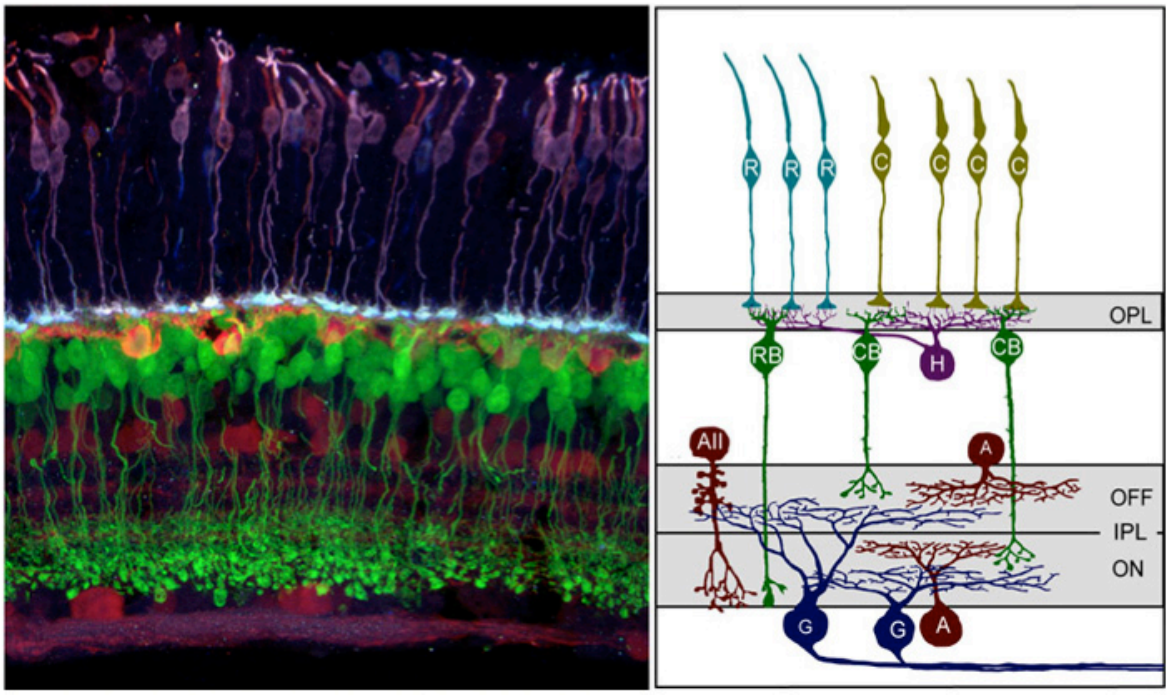

Figure 3: Retina as viewed by under Microscope: Cross-section of an immunostained mature mouse retina showing lamination of cell bodies and synaptic terminals. Cone Photoreceptors (bluish-purple) immunolabeled with anti-cone arrestin; Amacrine and Ganglion cells immunstained for calbindin (red) and bipolar cells immunoreacted for GFP (section from a transgenic animal in which ON bipolar cells express GFP under the mGluR6 promoter;(right) Schematic diagram illustrating the major cell components and their projection patterns in the mature vertebrate retina (Morgans and Wong, Nat. Neuroscience, 2006).

1.3 Ribbon synapses and its unique presynaptic specialization: the synaptic ribbon

In the retina, photoreceptors and bipolar cells form a specialized type of chemical synapse, ribbon synapses, which are characterized by the presence of a presynaptic electron-dense

plate-like structure, the synaptic ribbon, to which synaptic vesicles are tethered via fine filaments (Regus-Leidig et al., 2012; tom Dieck et al., 2006; Schmitz et al., 2009). Ribbon synapses are also seen in the inner ear, where they are formed by hair cells of the auditory and vestibular organ (Sterling and Matthews et al., 2005; Moser et al., 2006; Nouvian et al., 2006). Synaptic ribbons (also called synaptic bodies or electron-dense bodies) are the name given to presynaptic specializations structures of ribbon synapses and have been known since the early days of electron microscopy (Sjöstrand et al., 1953). Conventional neurons encode information by changes in the rate of action potentials, but for complex senses like vision, this is insufficient. Ribbon synapses enable neurons to transmit light signals over a wide dynamic range of several orders of magnitude in intensity. This is achieved by encoding variations in tonic rate of neurotransmitter concentration that requires the release of several hundred to several thousand synaptic vesicles per second. To achieve this level of high performance, the sensory neurons of the retina maintain diverse and large pools of fast releasable vesicles that are equipped with ribbon synapses. This enables the cell to exocytose hundreds of vesicles per second, greatly outreaching the rate of neurons without the specialized ribbon synapse (tom Dieck et al., 2006). Ribbon synapse furnishes a reservoir of readily releasable vesicles and is responsible for the fast and continuous vesicle supply for fusion at the exocytotic site. Therefore, synaptic ribbon comprises of precision machinery required for high-throughput focal exocytosis close to presynaptic membrane in the retina. (for reviews see, von Gersdorff 2001 and Lenzi and von Gersdorff 2001).

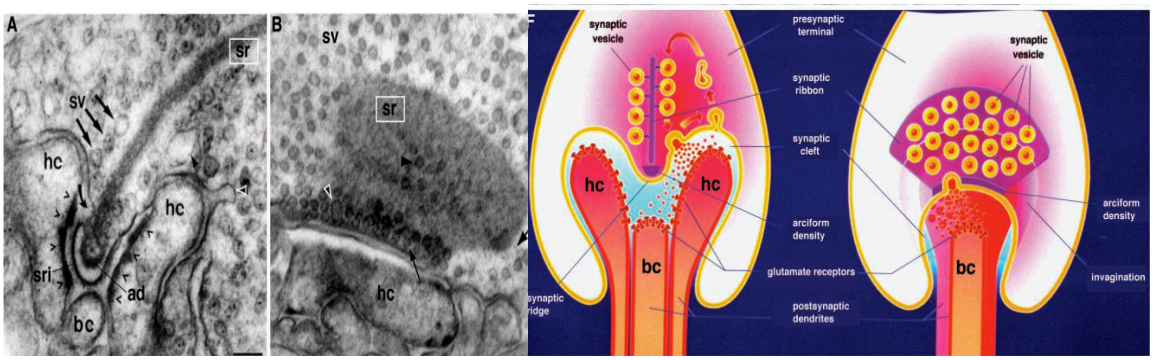

Figure 4: Ultrastructure of synaptic ribbons. (A) Transmission electron micrograph of a rod photoreceptor synapse from the goldfish retina The bar-shaped synaptic ribbon (sr) is anchored at the arciform density (ad), which is located in an evagination of the presynaptic plasma membrane, the synaptic ridge (sri). The active zone, the hot spot of exocytosis, is found at the plasma membrane–anchored end of the synaptic ribbon (curved arrow). Numerous synaptic vesicles (sv, arrows) are associated with the synaptic ribbon (sr). An omega-shaped exocytosis figure is visible at the active zone (curved arrow). The black arrowhead shows a larger membrane compartment in close vicinity to the synaptic ribbon. Membrane retrieval predominantly occurs lateral to the active zones (white arrowhead). Hc, bc denote the postsynaptic dendritic endings of horizontal and bipolar cells. The open black arrowheads denote the postsynaptic densities in these terminals. (B) A synaptic ribbon (sr) is tangentially cut, thus making the plate-like character of synaptic ribbons obvious. The long black arrow points to docked vesicles in physical contact with the presynaptic plasma membrane. The black arrowhead marks a "tethered" vesicle associated with the synaptic ribbon in a more distal position. The white arrowhead denotes a larger membrane structure docked at the base of the synaptic ribbon that could be the result of a compound fusion between vesicles. The short black arrow points to thin, electron-dense stalks that connect vesicles with synaptic ribbons. (F) Photoreceptor synaptic ribbons are schematically depicted. The bar-shaped ribbon (left panel) is actually a cross-section of a plate-like structure that is bended along the invaginated photoreceptor presynaptic plasma membrane in a crescent, horseshoe-shaped manner (right panel). The postsynaptic dendritic profiles of horizontal and bipolar cells are depicted in a simplified manner. sr = synaptic ribbon; sv = synaptic vesicle; pr = presynaptic terminal; en = large, tubular compartment possibly of endosomal origin; ad = arciform density; sri = synaptic ridge; hc, bc = horizontal/bipolar cell dendrites. Scale bars: 100 nm (A, B) (Schmitz et al., 2009).

How this vesicle traffic is organized and precisely regulated in varying types of cells is still largely unknown. Synaptic ribbons, large presynaptic structures associated with numerous synaptic vesicles, appear to play a central role in this process. The basal end of the synaptic ribbon is anchored at the active zone where L-type voltage-gated channels are clustered. This site is a hotspot of exocytosis (Zenisek et al., 2000; Frank et al., 2010; Chen et al., 2013). The synaptic ribbon complex has also been stated to be relevant for vesicle recycling (Spassova et al., 2004; Griesinger et al., 2005; Jackman et al., 2009; Babai et al., 2010; Frank et al., 2010; Schnee et al., 2011; Snellman et al., 2011; Tian et al., 2012; Wahl et al., 2013). In photoreceptor synapses, synaptic vesicle retrieval occurs in the peri-active zone, in close proximity to the synaptic ribbon (Wahl et al., 2013). RIBEYE, an isoform of CTBP2, is a major and unique component of synaptic ribbons (Schmitz et al., 2000; for review, see Schmitz, 2009). RIBEYE consists of an unique N-terminal A-domain and a C-terminal B-domain. The B-domain is largely identical with the protein CtBP2 and binds NAD(H) (for review, see Schmitz, 2009; Schmitz et al., 2012). The RIBEYE(A)-domain is not present in D. melanogaster, C. elegans and other lower vertebrates and invertebrates. This is supporting the notion that RIBEYE and retinal synaptic ribbons are an evolutionary innovation of vertebrates (Schmitz et al., 2000). Except the general knowledge of its architecture, its physiological and functional relevance is still unclear. One of the important discoveries in past few years is close synaptic localization of the Ca^{2+}-binding phosphatase calcineurin, a Ca^{2+} sensor of endocytosis, enriched at in close proximity to synaptic ribbon (Wahl et al., 2013), although molecular and biochemical insights will provide better scope onto its functional relevance.

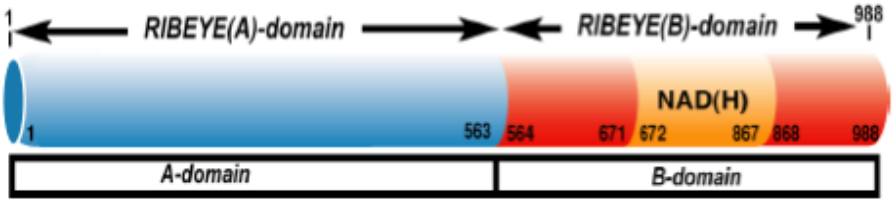

Figure 5: Schematic domain structure of RIBEYE: RIBEYE contains of a large amino-terminal A-domain and a carboxyterminal B-domain. The B-domain of RIBEYE contains the NADH-binding subdomain (NBD, depicted in yellow) and the substrate-binding subdomain (SBD, denoted in red). The A-domain comprises of 563 aa and the B-domain comprises of 425 aa (Magupalli et al., 2008).

Both RIBEYE(B)-domain and CtBP1/CtBP2 bind NAD(H) (Schmitz et al., 2000) CtBP1/CtBP2 are nuclear co-repressors. In case of CtBP1/CtBP2, binding of NADH regulates interaction with nuclear proteins (Fjeld et al., 2003). In the nucleus, this NAD(H)-

regulated interaction can switch on or off distinct target genes relevant, e.g., for cellular migration, adhesion, and apoptosis (Paliwal et al., 2006, 2007, 2012; Chinnadurai, 2009). In the ribbon synapse, NADH(H)/NAD redox state is not only important for interaction of RIBEYE with different proteins but is also required to maintain the architecture of ribbons as demonstrated by the diagrammatic representation of multiple interaction within the domains of RIBEYE (Magupalli et al., 2008) which could be of prime importance as an answer to dynamic rate of exo- and endocytosis occuring due as direct consequence of physiological stimulus in photoreceptor and bipolar cells.

In neurons, both synaptic shuttling and retention of CtBP1 protein levels between cytoplasm and nucleus are co-regulated by neuronal activity that maintains the dynamic pools of CtBP1 at nuclear and presynaptic membrane. Also it has been shown that CtBP1 is targeted and/or anchored to presynapses by direct interaction with the active zone scaffolding proteins Bassoon and Piccolo. This association is regulated by neuronal activity via modulation of cellular NAD^+/NADH levels and restrains the size of the CtBP1 pool available for nuclear import, thus contributing to the control of activity-dependent gene expression (Ivanova et al., 2015). This redox state of NAD^+/NADH levels in photoreceptor cells could also be of significant importance with high abundance of RIBEYE and CTBP1 at ribbon synapse.

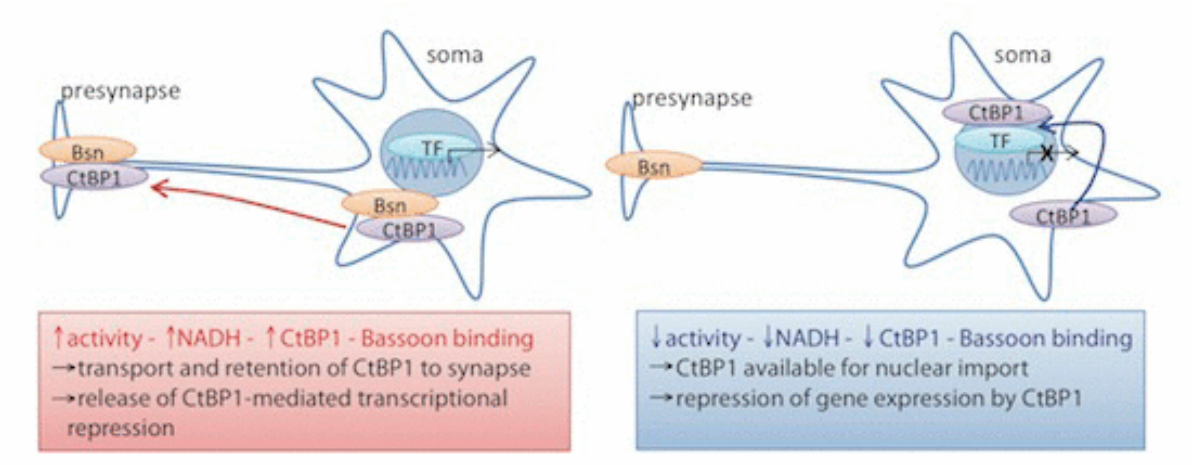

Figure 6: In highly active neurons NADH abundance increases which leads to synaptic enrichment of CtBP1 due to a tighter association with its presynaptic anchor Bassoon/Piccolo. CtBP1-mediated transcriptional repression of activity-dependent genes is released. In conditions of low activity or low NADH levels, CtBP1 dissociates from Bassoon/Piccolo, becomes available for nuclear import and transcriptional repression (Ivanova et al., 2015).

In close vicinity to synaptic ribbon, GCAP2 has been shown to specifically enriched whose interaction with RIBEYE is based on availability of NAD(H). Functional importance, for other proteins like Unc119 or Bassoon, effect of NAD^+/or NADH ratio is either not studied or was found to exert no significant influence (Venkatesan et al., 2010, Alpadi et al., 2008,

tom Dieck et al., 2005). The last few years has lead to the discovery of proteins, which are selectively localized on ribbon or are present in close vicinity of the ribbon. Bassoon in addition to its presence at conventional synapses, it is also found at ribbon synapse of photoreceptor cells, bipolar cells and inner hair cells at cytomatrix active zone (CAZ) similar to conventional synapse (tom Dieck et al., 2005). In the absence of bassoon (in bassoon knock out mice), ribbon are detached from the active zone, displaying a non-plasma membrane-anchored "floating" ribbons in photoreceptor and hair cells (Khimich et al., 2005; tom Dieck et al., 2005) reflecting the role of bassoon and its importance in structural, morphological and functional organization of synaptic ribbon. Recently, Bassoon protein has been linked with presynaptic Ca_v-channels (Nishimune et al., 2004, 2012, Ivanova et al., 2015). Piccolo similar to bassoon, is a very large multidomain-protein, is also present both in conventional and ribbon-type synapses. Recently, a splice variant of piccolo was described, named piccolino, which is preferentially expressed at ribbon synapses (Regus-Leidig et al., 2013). Proteins known to be essential for proper functioning of conventional synapses are the multi-domain rab3-interacting molecule (RIM) protein family (Wang et al., 1997; Kaeser et al., 2011, 2012; for review, see Südhof, 2013). KIF3A, a member of the kinesin motor protein family has been shown to be present along the ribbons at ultrastructural level (Muresan et al., 1999) where KIF3A might transport a synaptic vesicle precursor from the Golgi to the terminal, consistent with the function of KIF3A as a plus-end motor (Kondo et al., 1994). RIM2 appears to be localized at the base of the synaptic ribbon and RIM1 at the body of the synaptic ribbon (tom Dieck et al., 2005). RIM proteins interact with Munc13 proteins in conventional synapses to mediate vesicle priming (Deng et al., 2011). While in conventional synapses, RIMs interact with Munc13-1; Munc13-1 is missing in photoreceptor synapses (Schmitz et al., 2001; Cooper et al., 2012). Instead of Munc13-1, ubMunc13-2 is expressed in photoreceptor synapses (Cooper et al., 2012). Other active zone proteins [e.g., CAST/ELKS; RIM-binding proteins (RIM-BPs)] are also present at photoreceptor ribbon synapses partly differentially distributed in distinct sub-compartments of the synapse (for review, see tom Dieck and Brandstätter et al., 2006; Mercer and Thoreson et al., 2011; Schmitz et al., 2012). At close examination of diversity of proteins found between ribbon synapses and conventional synapses, these synapses do not differ strongly in the composition of the exocytotic machinery, Although ribbon synapse being less studied one among the two synapses, future discoveries of new proteins will provide more insight onto its biological functions. (for review, see Schmitz, 2009; Matthews and Fuchs, 2010; Mercer and Thoreson, 2011; Schmitz et al., 2012). In photoreceptor ribbon synapses, syntaxin-1 is replaced by syntaxin 3b (Curtis et al., 2008, 2010); complexin 1/2 by complexin 3/4 (Reim

et al., 2005, 2009); Munc13-1 by ubMunc13-2 (Schmitz et al., 2001; Cooper et al., 2012); piccolo by piccolino (Regus-Leidig et al., 2013), but key players of exocytosis appears to be remarkably conserved.

CtBP1/BARS, a close relative of RIBEYE(B)-domain/CtBP2 and component of the Golgi complex, is also localized to the synaptic ribbon complex (tom Dieck et al., 2005; for a review, see Corda et al., 2006). At the Golgi apparatus, CtBP1/BARS interacts with ArfGAP1 (Yang et al., 2005). This interaction has been proposed to be essential for vesicle formation and vesicle scission at the Golgi complex (Yang et al., 2002, 2005, 2006; Corda et al., 2006). The function of CtBP1/BARS at the synaptic ribbon is still unclear (Vaithianathan et al., 2013). Figure 7 shows the preferential localization of proteins at synaptic ribbon and CAZ (cytomatrix active zone).

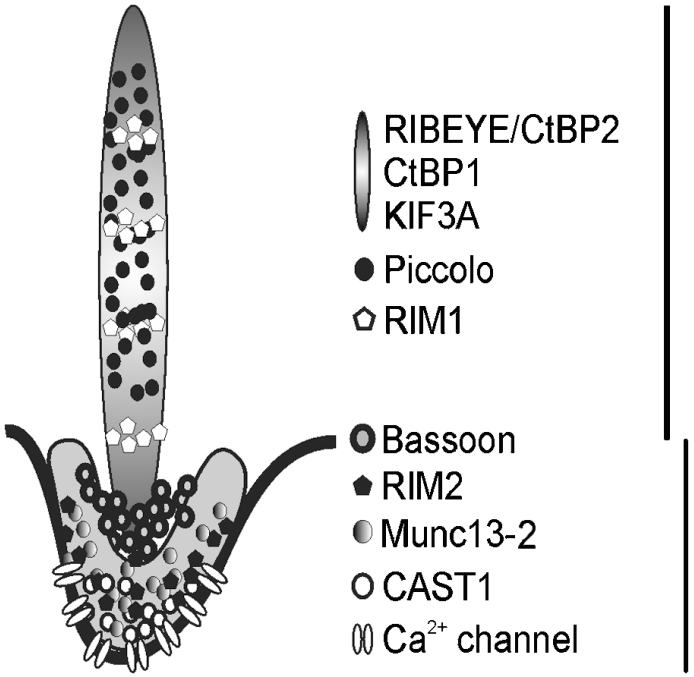

Figure 7: Differential localization of CAZ proteins defines two compartments of the photoreceptor ribbon synaptic complex. The ribbon-associated complex of CAZ proteins includes RIBEYE/CtBP2, CtBP1, KIF3A, Piccolo, and RIM1; the plasma membrane/arciform density-associated complex includes RIM2, Munc13-2, ERC2/CAST1, and a Ca^{2} channel 1 subunit. Bassoon localizes at the border between the two compartments (Modified from tom Dieck et al., 2005)

The diversification of proteins present at ribbon synapse suggest its multifunctional role in maintaining the integrity of synapses and its subtle role in proper functioning of photoreceptor and bipolar cell.

1.4 Understanding mechanisms of synaptic vesicles recycling:

With ongoing high and sustained rates of exocytosis there is a need for a compensatory endocytosis to prevent synaptic depletion. Several of modes of endocytosis including

clathrin-dependent endocytosis, bulk endocytosis retrieval, and kiss and run endocytosis are proposed to contribute to membranc retrieval in ribbon synapses, depending on the phase, stimulus strength, and duration (Lo Giudice and Matthews et al., 2007). Regarding the site of endocytosis, it was recently proposed that the periactive zone is bilaterally located in close vicinity to the synaptic ribbon. Peri-active zone is a hotspot of clathrin-mediated endocytosis in photoreceptor ribbon synapses postulated on the basis of immuno-histochemical findings of prime endocytic components (Figure 8) including clathrin heavy chain, dynamin, amphiphysin, and syndapin and endophilin were found to be synaptically enriched (Wahl et al., 2013).

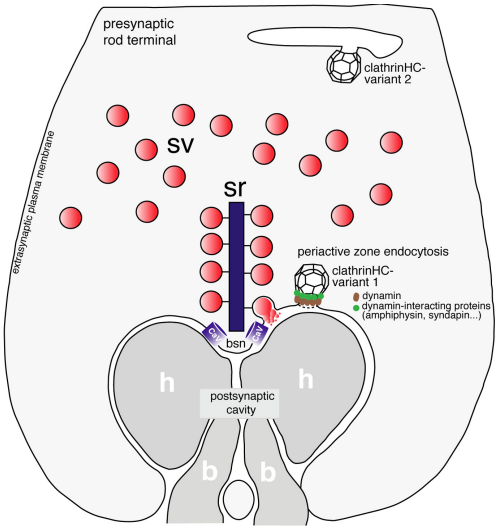

Figure 8: Simplified, schematic summary of key players of endocytic membrane traffic, including dynamin, dynamin-binding proteins, and CHC-V1, are enriched in a periactive zone of photoreceptor synapses. Besides CHC-V1, CHC-V2 is also present in the presynaptic photoreceptor terminal. In contrast to CHC-V1, CHC-V2 is located a large distance from the periactive zone, possibly on an endosomal compartment in the proximal region of the presynaptic terminal. Endosomal-like membrane compartments have been previously observed by transmission electron microscopy in this part of the photoreceptor terminal (Ripps et al., 1976; Schacher et al., 1976; Schaeffer and Raviola, 1978; Cooper and McLaughlin, 1983). The drawing of the photoreceptor terminal is modified based on a drawing of Gray and Pease (1971) . sr, Synaptic ribbon; sv, synaptic vesicles; clathrinHC-V1, clathrin heavy chain variant 1, CHC-V1; clathrinHC-V2, CHC-V2; CaV, voltage-gated calcium channels of the photoreceptor active zone; h, postsynaptic dendritic tip of a horizontal cell; b, postsynaptic dendritic tip of an invaginating bipolar cell; bsn, bassoon (Wahl et al., 2013).

Recently, also PIP5KIγ was shown to be enriched in close vicinity to ribbon synapses (Sakagami et al., 2014), The activity of PIP5KIγ is regulated by variety of diverse factors including ADP ribosylation factor (Arf's) and Rho family GTPases, phosphatidic acid, interacting proteins such as talin and AP-2 complex, and post-translational modifications such as phosphorylation and dephosphorylation. Fascinating evidence suggests that Arf6, a member of the Arf small GTPase family that regulates the actin cytoskeleton and membrane traffic, functions as a physiological upstream regulator of PIP5KIγ in neurons. Also, Arf6 was shown to regulate the recruitment of clathrin/AP-2 to the synaptic membrane (Krauss et al., 2003) and the calcium-dependent exocytosis of large dense core vesicles (LDCV) through the activation of PIP5KIγ in neuroendocrine PC12 cells (Aikawa and Martin, 2003).

At postsynapses, Arf6 was also shown to regulate the clathrin-dependent endocytosis of AMPARs during hippocampal longterm depression (Scholz et al., 2010). Presence of PIP5KIγ in close vicinity to synaptic ribbon leads to probability of finding Arf's specifically enriched in the photoreceptor cells synapses.

PIP5KIγ is responsible for formation of PIP2 at the presynapse, PIP2 thus formed mediates almost every step of synaptic vesicle cycle through its interaction with various PIP2-interacting proteins and also it is an integral component of newly formed vesicle (Koch and Holt, 2012; Martin, 2012). During exocytosis, PtdIns(4,5)P2 participates in priming and docking steps of synaptic vesicles through the interaction with Munc13 (Shin et al., 2010), calcium-activated protein for secretion (CAPS) (James et al., 2008; Loyet et al., 1998) and synaptotagmin (Bai et al., 2004). During clathrin-dependent endocytosis, it also mediates various steps including the formation of clathrin-coated vesicles via the interaction with AP-2 (Gaidarov and Keen, 1999), AP180/ CALM (Ford et al., 2001), andepsin (Itoh et al., 2001); the fission of coated vesicles from the plasma membrane via the interaction with dynamin (Lin and Gilman, 1996) and the uncoating of endocytosed clathrin-coated vesicles by hydrolysis of PIP2 mediate by synaptojanin, a PIP2 phosphatase (Cremona et al., 1999). Pre-embedding immunogold electron microscopy revealed the enrichment of PIP5KIγ at the restricted plasma membrane compartment in near vicinity to the photoreceptor synaptic ribbon (Sakagami et al 2014). The PIP5KIγ immunogold labeling well corresponds to the periactive zone compartment that was recently shown to be an endocytic hotspot for various components of the endocytic machinery (Wahl et al., 2013). Since Arf6 is an upstream activator of both PIP5KI and phospholipaseD, it is postulated that Arf6 initiates a positive feed forward loop to increase PIP2 and phosphatidic acid levels required for endocytosis through the recruitment of major endocytic components and by close regulation of the membrane curvature and actin cytoskeleton (Cockcroft et al., 2009). So far, no information is available concerning the expression and localization of phospholipase D at ribbon synapse, it is worth mentioning that RIBEYE, a major structural component of the synaptic ribbon, itself exhibits lysophosphatidic acid acyl-transferase activity, which synthesizes phosphatidic acid from lysophosphatidic acid that is the early precursor for formation of major components of synaptic vesicle (Schwarz et al., 2011).

1.5 ArfGAPs: gatekeepers of vesicle generation?

ArfGAP proteins are a versatile and diverse group of proteins. They control the activity of

the GTP binding proteins of the ARF family by inducing the hydrolysis of GTP that is bound to Arf proteins (Spang et al., 2010). GTP-binding proteins of the ARF/SAR family are key regulators of intracellular traffic. Mainly 2 classes of regulating proteins primarily control these GTP-binding proteins: Guanine nucleotide exchange factors (GEFs) and GTPase activating proteins (GAPs), (Arf-GTPase-activating proteins; for review, see Inoue and Randazzo, 2007; Kahn et al., 2008; Spang et al., 2010).

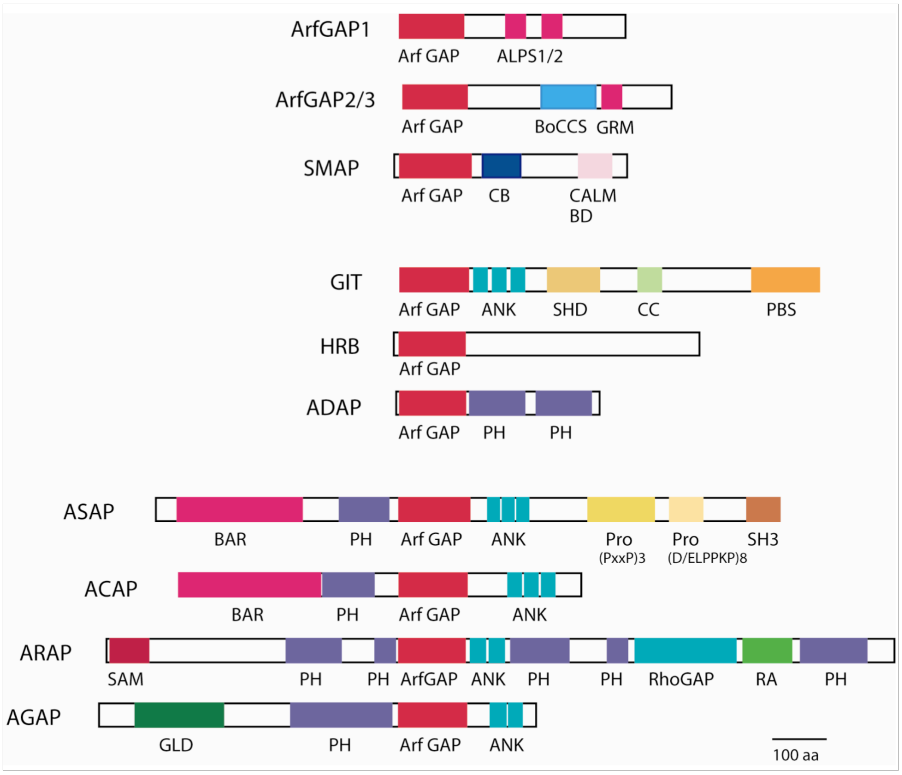

Figure 9: Human ArfGAPs. Domain structures of the human ArfGAP subfamilies are depicted. Abbreviations are: ALPS, ArfGAP1 lipid-packing sensor; ArfGAP, ArfGAP domain; ANK, ankyrin repeat; BAR, Bin/ Amphiphysin/Rvs; BoCCS, *b*inding *o*f *c*oatomer, *c*argo and *S*NARE; CALM, CALM binding domain; CB, clathrin-box; CC, coiled-coil; FG repeats, multiple copies of the XXFG motif; GLD, GTP-binding protein-like domain; GRM, Glo3 regulatory motif; PBS, Paxillin binding site; PH, pleckstrin homology domain; Pro (PxxP)3, cluster of three Proline-rich (PxxP) motifs; Pro(D/ELPPKP)8, eight tandem Proline-rich (D/ELPPKP) motifs; RA, Ras association motif; RhoGAP, RhoGAP domain; SAM, sterile α-motif; SH3, Src homology 3 domain; SHD, Spa- homology domain (Adapted from Kahn et al. 2009).

The GEFs exchange protein bound GDP for GTP to produce the GTP liganded also called activated ARF/SAR proteins. In the activated form, the ARF/SAR proteins are membrane-associated and interact with cargo; SNARE and coat proteins all of these are important for continuously recycled vesicles. The cumulative interactions will then at one point lead to membrane deformation and transport vesicle formation (Spang et al., 2010, Kirchhausen, 2000; McMahon and Mills, 2004).

ArfGAPs were discovered less than 30 years ago, where it was shown that the presence of ArfGAPs in bovine brain extracts vastly decreased the intrinsic activity of Arf1 (Randazzo

and Kahn et al., 1994). Thirty-one genes encoding proteins with ArfGAP's catalytic domains have been identified in humans. Ten subfamilies have been described based on domain structure and phylogenetic analysis. Conserved hallmark of ArfGAPs is ≈136 aa long, catalytically active GAP-domain (AGD) with a central Zn-finger motif that stimulates GTPase activity of the attached Arf (Cukierman et al., 1995; Goldberg, 1999). The regions outside of the AGD are divergent in different ArfGAPs mostly differing from each other on c-terminus region (Figure 9).

As mentioned above in diagrammatic description of ArfGAP's, ArfGAP1 is able to sense membrane curvature through specific motifs called ArfGAP lipid packing sensor (ALPS motif). The central sequence of about 40 amino acids in ArfGAP1 acts as a lipid-packing sensor. This ALPS motif (ArfGAP1 Lipid Packing Sensor) is also found in yeast homologue Gcs1p and is necessary for coupling ArfGAP1 activity with membrane curvature (Bigay et al., 2001). A number of ArfGAP's have been implicated in membrane traffic including SMAPs, ARAP1, AGAP1/2, ArfGAP1 and ArfGAP2/3. ArfGAP1 Gcs1p and the ArfGAP2/3 homologue Glo3p interact with SNARE proteins and induce a conformational change that allows recruitment of Arf1p and coatomer to the SNAREs (Spang et al., 2001). This interaction does not make ArfGAP's as effectors of Arf's per se, but in context of vesicle generation and primer formation, they have the qualities of an effector (Schindler et al., 2009).

1.6 ArfGAP's and effector proteins Arf's:

Small GTP-binding proteins of the Arf family are important regulators of intracellular membrane traffic (for review, see Gillingham and Munro, 2007). ArfGAP's accelerates the low intrinsic GTPase activity of Arfs. A large number of ArfGAPs have been identified in higher organisms. Among the ArfGAPs, the conserved AGD (ArfGAP domain) is located at the N terminus and distinct motifs in their C terminus, one of which mediates membrane binding (Bigay et al., 2005; Kliouchnikov et al., 2009) as well as other functions (for review, see Spang et al., 2010). A common feature of the GAP proteins is presence of conserved $CXXCX_{16}CXXC$ motif (where X is any amino acid) at the NH_2- terminal, which represents the zinc finger structure (Ireland et al., 1995).

Deletion of 20-45 residues of Zinc finger motif and construct less than 120 a.a. starting from NH_2-terminal leads to loss of Zinc finger activity and eventual loss of GAP activity along length of ArfGAPs; indicating both are important for normal functioning of GAP's

(Cukierman et al., 1995).

ADP-ribosylation factor-GTPase-activating proteins (ArfGAP's) are proposed to contribute to site-specific regulation via its control of Arf's. One of important effectors of GAP activity, Arf6 has been to be shown to be potential interacting partner of ArfGAP3 in D. melanogaster (Ruth et al., 2012). Also in adult rat DRG (Dorsal root ganglion) neuron, Arf6 regulates rapid axonal transport of integrins and their tafficking at the cell surface. Arf6 is involved in recycling of plasma membrane components, including certain types of cell surface receptors, as well as in actin-cytoskeleton remodeling at periphery of Hela Cells (Hashimoto et al., 2004).

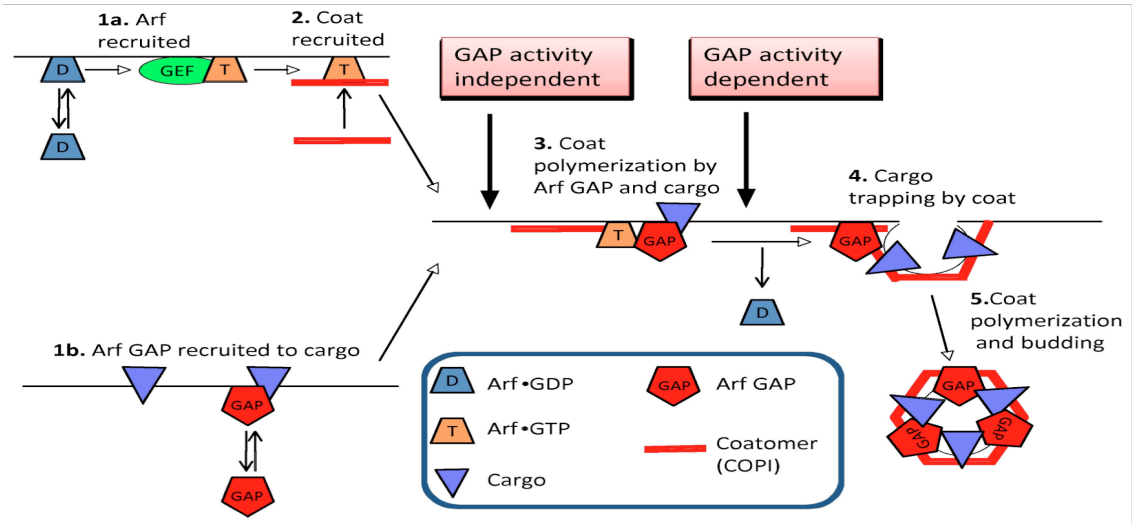

Figure 10: Schematic depiction of dual role of ArfGAP's. ArfGAP has a role as Arf effector in helping to recruit cargo and be a vital part in transport primer formation. This role does not require GAP activity. The second, and more established role is in functioning together with Arf as a heterodimeric GTPase, which promotes coat-cargo association and coat polymerization (Spang et al., 2010).

One of well studied regulatory proteins of Arf's is IQ-ArfGEF / BRAG1, a guanine nucleotide exchange factor for ADP ribosylation factors Arf1 and Arf6, which are implicated in membrane trafficking and actin cytoskeleton dynamics (Murphy et al., 2006; Sakagami et al., 2008). Immuno-Electron microscopic analysis showed that the IQ-ArfGEF⁄BRAG1 was localized at the synaptic ribbons of photoreceptors (Katsumata et al., 2009). Presence of BRAG1 the "GEF" regulator at the synapses implies to the possibility of finding the "GAP" regulators at the ribbon synapses, as both are important for maintaining the active/inactive state of Arf's and Arl's in cells. Figure10 shows the general structure of Arf's and Arl's and their interaction with the membrane.

It has been shown that Golgi localization of ArfGAP's depends on both a central basic

stretch and a carboxy-amphipathic motif. The basic stretch interacts directly with coatomer,

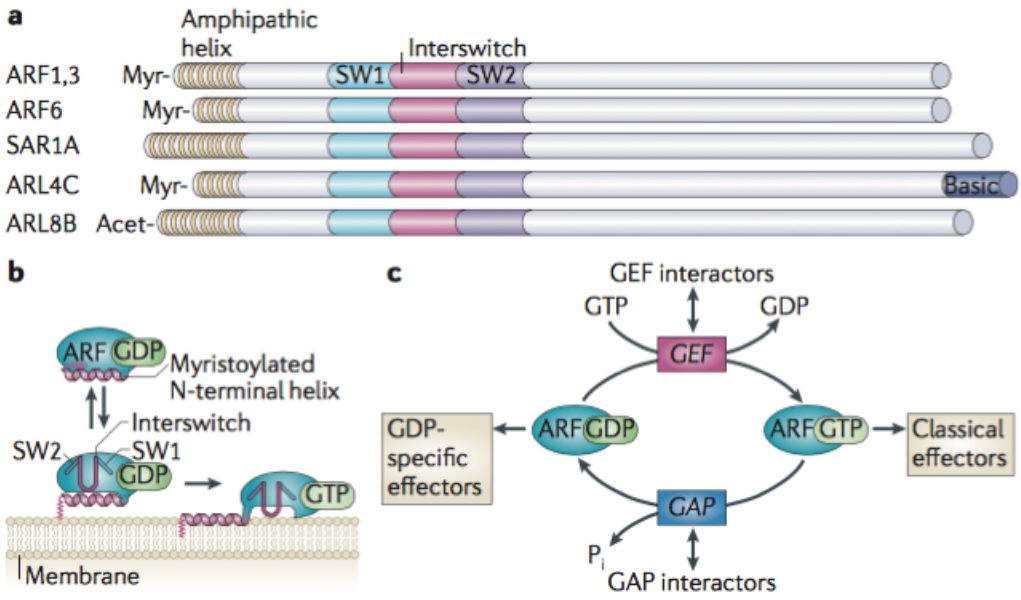

Figure11: The domain structure and regulation of ARF and ARLs. a A schematic of representative ADP-ribosylation factor (ARF), SAR1 and ARF-like (ARL) proteins, indicating the conserved amino-terminal amphipathic helix and the protein-specific lipid modifications at the N terminus. These include myristoylation (Myr) and acetylation (Acet), both of which ensure tight membrane association. The effector regions of the guanine-nucleotide-binding (G) protein, switch 1 (SW1) and SW2, and the interswitch region between them, are depicted. These regions change conformation upon exchange of GDP for GTP and are involved in interactions with effectors. b ARF•GDP reversibly associates with the membrane surface, and the myristoylated N-terminal helix ensures tight membrane association of ARF•GTP. The switch and interswitch regions are also shown, and these undergo a conformational change upon GTP binding to enter the hydrophobic pocket that the N-terminal amphipathic helix occupies in the GDP-bound form. c ARF family G proteins undergo a cycle of GTP binding and hydrolysis, mediated by guanine nucleotide exchange factors (GEFs) and GTPase-activating proteins (GAPs), respectively. The GTP-bound form is thought to carry out G protein functions through interaction with 'classical effectors', including vesicle coat proteins and enzymes that can modify membrane lipid composition; however, increased attention has focused on networks of effectors that are targeted by proteins that interact with GEFs and GAPs themselves and unique effectors that associate specifically with the GDP-bound form of ARF proteins (Donaldson and Jackson, 2011).

which is essential for the catalytic activity of ArfGAP3 on Arf1-GTP, whereas the carboxy-amphipathic motif interacts directly with lipid membranes but has minor role in the regulation of ArfGAP's activity. These findings indicate that the two types of ArfGAP proteins that reside at the Golgi use a different combination of protein–protein and protein–lipid interactions to promote GTP hydrolysis in Arf1-GTP (Kliouchnikov et al., 2009). Treatment with Brefeldin A (BFA), an inhibitor of GTPase activity for 5mins causes redistribution of ArfGAP1 and ß-COP from Golgi like distribution to cytoplasmic and washing out of drug followed by 30mins recovery period leads to reappearances of proteins in Golgi-like pattern. This suggests the important role of ArfGAP in recovery period that could also be an involvement in recycling of vesicles. BFA inhibits the exchange of GDP to GTP on Arf's thereby preventing Arf1 dependent recruitment of coat proteins at Golgi. Cytosolic redistribution of GAP's after BFA washout suggests that GAP is recruited back to Golgi by Arf1-Dependent manner (Cukierman et al., 1995).

Arf1 is an important regulator of vesicle traffic at various intracellular compartments, including the Golgi apparatus and endosomal compartments (Gillingham and Munro, 2007;

Kahn et al., 2008; Donaldson and Jackson, 2011) and might perform a similar role at the photoreceptor synaptic ribbon complex. Although Arf's has been shown to be involved in various biological process of signaling in different complex organ they are not widely studied in retina.

With the summarization of GAP's related proteins function pertaining to recycling of vesicles there is also an important discovery of RP2 protein which is GAP protein found in inner segment of Photoreceptor cell; a known regulator of Arl3 which is important of retrograde transport and ciliogenesis as depicted below in figure11.

One of the other important aspects of ArfGAP/Arf cycles is their interaction with NSF and SNARES proteins. Arf1p is activated through its interaction with an ARF guanine nucleotide exchange factor (ArfGEF) at the membrane (Donaldson and Jackson, 2000). Subsequently, coatomer is recruited and forms a complex with Arf1p, cargo, or soluble *N*-ethylmaleimide-sensitive factor attachment protein receptor (SNARE) and an ARF-GTPase activating protein (ArfGAP), a so-called primer (Springer *et al*., 1999; Spang, 2002). This interaction does not require the deactivation of Arf1p by a GAP.

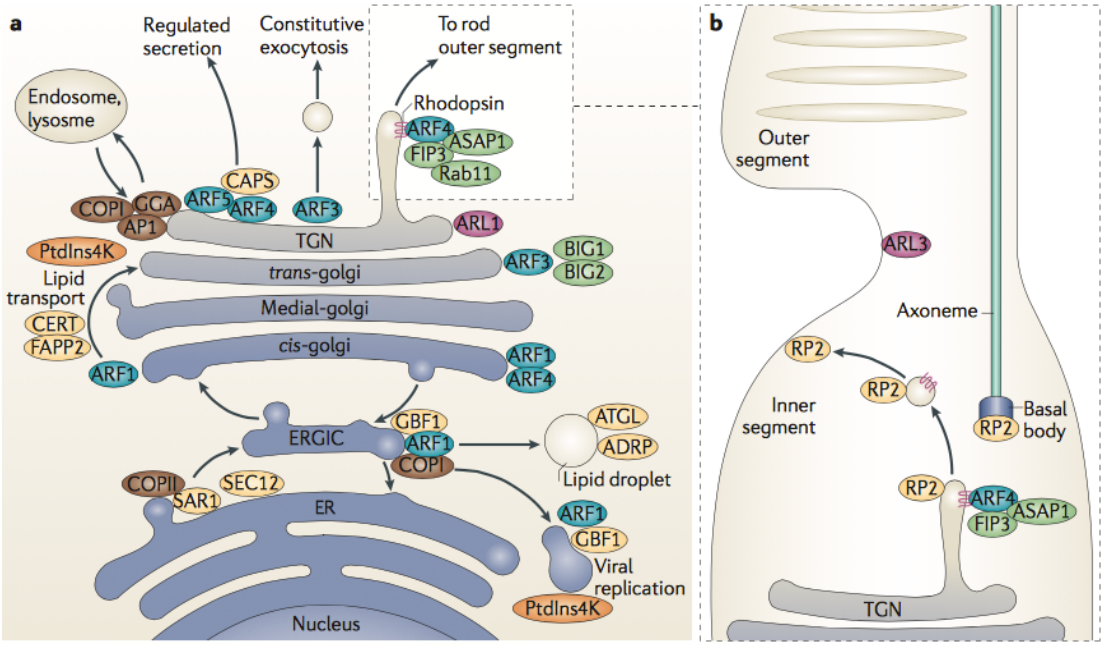

Figure12: ARF and ARL functions in the secretory pathway and in specialized transport. a ADP-ribosylation factor (ARF) proteins have distinct localizations and functions in the endoplasmic reticulum (ER)–Golgi system. ARF1 Lipid droplets Lipid storage organelles that are surrounded by a phospholipid monolayer. PtdIns4K, phosphatidylinositol 4-kinase with findings of ARF4 localization to, and ARF4 and ARF5 functioning at, the early Golgi in other cells[8,15,16] is not known. Recent discoveries show that ARF1 regulates lipid transfer proteins within the Golgi and promotes the formation of lipid droplets at the ERGIC (FIG. 2a). At the Golgi, ARF1 recruits the lipid transfer proteins ceramide transfer (CERT) and FAPP2 (REF. 14) through interaction with their PH domains, which can also bind PtdIns4P. CERT mediates the non-vesicular transport of ceramide from the ER to the Golgi and FAPP2 mediates the transfer of glucosylceramide from the cytosolic side of the early Golgi to the *trans*-Golgi[22]. Exactly how the directionality of this transfer occurs, and the role that ARF1 has, is not yet clear. The finding that ARF1 associates with GBF1 and COPI during lipid droplet formation was unexpected (Donaldson and Jackson, 2011).

If more such priming complexes are formed, the coat polymerizes laterally and deforms the membrane until the donor membrane is severed from the nascent vesicle. Thus, ArfGAPs are not only important to stimulate GTP hydrolysis on Arf1p but also are important at a much earlier step in vesicle biogenesis. Also ArfGAP Gcs1p accelerates vesicle (v)-target membrane (t)-SNARE complex formation in vitro, indicating that ArfGAP's may act as folding chaperones (Spang et al., 2007).

This mechanism can be postulated to be functional in retina specifically in synaptic layers also during the dark and light cycle. Arrestin-1 (visual arrestin/S-antigen) has been found to interact with NSF with enhanced Dark environment, where exocytosis rate is elevated. NSF, SNARES, Arr1 and ArfGAP's in photoreceptor could be functioning in a complex Dark/light dependent manner, as former is critical for normal vision. In in-vivo experiments in mouse retinas with the Arr1 gene knocked out, the expression levels of NSF and other synapse-enriched components, including vGLUT1 (vesicular glutamate transporter 1), EAAT5 (excitatory amino acid transporter 5), and VAMP2 (vesicle-associated membrane protein 2) were markedly reduced, which leads to a substantial decrease in exo/endocytics rate as shown with FM1-43 uptake. That suggests NSF and Arr1 interaction is an important modulator of normal synaptic function in mouse photoreceptors. This study demonstrates a vital alternative function for Arr1 in photoreceptor synapse and provides key insights into the potential molecular mechanisms of inherited retinal diseases, such as Oguchi disease and Arr1-associated retinitis pigmentosa (Huang et al., 2010).
The importance of ArfGAP's has also been shown in yeast, where deletion of either the GLO3 or GCS1 gene results in a relatively mild phenotype. However, deletion of both genes is lethal in yeast. Cell survival of an RNAi-oligo-mediated knockdown of ARFGAP1, ARFGAP2 and ARFGAP3 either in single or pairwise knockdowns showed no significant cell death in, compared with cells transfected with a control oligo. In contrast, a triple knockdown of ARFGAP1, ARFGAP2 and ARFGAP3 resulted in significant cell death in Hela cells. More than 75% cell death was routinely observed after three sets of siRNA transfections at the 72-h time-point after the last transfection. That concludes that at least one of the three ARFGAPs is required to maintain cell viability, elucidating the importance of ArfGAP's in proper functioning of the cells (Frigerio et al., 2007).

1.7 Aim of the present study:

In order to obtain a better understanding of Ribeye function, I performed a YTH screen with RIBEYE(B) as bait and obtained protein ArfGAP3 as a potential interacting partner of Ribeye. The objective of the present study was to characterize the RIBEYE-ArfGAP3 interaction using various molecular and biochemical techniques. Also I wanted to check the cellular localization of ArfGAP3 in retina and whether it supported the intial YTH data of strong interaction. One of the important AIMS of the study was to check the functional and physiological significance of ArfGAP3 in the retina by overexpressing ArfGAP3 f.l. construct and to study its consequent effect.

2 MATERIALS AND METHODS:

2.1 Materials

2.1.1 Host Strains

2.1.1.1 Bacterial strains

Bacterial Strains	Genotype	Sources and Reference
E.coli DH10B	F- mcrA Δ(mrr-hsdRMS-mcrBC) φ80lacZΔM15 ΔlacX74 recA1 endA1 araD139 Δ(ara, leu)7697 galUgalK λ- rpsL nupG	Invitrogen, Grant et al., 1990.
E.coli BL21 (DE 3)	F- ompT hsdSB(rB -mB) gal dcm (DE3)	Invitrogen, Grodberg und Dunn, 1988.
E.coli BL21 (DE 3) EXPRESS T7	BL21 (DE 3) EXPRESS T7	NEB; #C2566

2.1.1.2 Saccharomyces cerevisiae strains

Yeast strain	Genotype	Sources and Reference
Y2H GOLD	MATa, trp1-901, leu2-3, 112, ura3-52, his3-200, gal4Δ, gal80Δ, LYS2 : : GAL1$_{UAS}$–Gal1$_{TATA}$–His3, GAL2$_{UAS}$–Gal2$_{TATA}$–Ade2 URA3 : : MEL1$_{UAS}$–Mel1$_{TATA}$ AUR1-C MEL1.This strain contains distinct ADE2, HIS3, MEL1, and AUR1-C reporter constructs that are only expressed in the presence of GAL4-based protein interactions	Clontech, Nguyen, Unpublished.
Y187	MATα, ura3-52, his3-200, ade2-101, trp1-901, leu2-3, 112, gal4Δ, gal80Δ, met–, URA3 : : GAL1UAS–Gal1TATA–LacZ, MEL1.	Clontech Laboratories Inc. Harper et al., 1993

2.1.1.3 COS 7 cell line

COS7	African green monkey kidney fibroblast-like cell line suitable for transfection by vectors requiring expression of SV40 T-antigen. The presence of T-antigen, retains complete permissiveness for lytic growth of SV40, supports the replication of ts A209 virus at 40°C, and supports the replication of pure population of SV40 mutants with deletions in the early region. The line was derived from the CV-1 cell line (ATCC CCL-70) by transformation with an origin defective mutant of SV40,	Gifted by T. C. Südhof (Gluzman et al.,1981)

2.1.2 Plasmid vectors

2.1.2.1 Escherichia coli cloning vectors

Vectors	Features	Antibiotic	Source and Reference
pGEX-KG	Genes cloned is expressed as fusions to the C-terminus of GST; containing tac promotor and lacq repressor	Ampicillin	Gifted by T. C. Südhof (Schmitz et al., 2000)
pMAL-C2	Genes cloned will be expressed as fusions to the Cterminus of MBP; containing tac promotor and lacq repressor	Ampicillin	New England Bio-Labs (Guan et al., 1988)
pMAL-C2 NEW	It has stop codons inserted on ending of MCS in all the three reading frames with new unique site of SPE-I. Benefit of using pMAL-C2 new is that while expressing MBP-TAG alone protein immediately terminates at the ending of MCS because of insertion of stop codons.	Ampicillin	New England Bio-Labs (Guan et al., 1988)
pSNAPtag -T7-T2	pSNAP-tag(T7)-2 Vector is an *Escherichia coli* expression plasmid encoding the SNAP-tag fusion. Target gene can be cloned as fusion to N- or C-terminus of SNAP-tag.	Ampicillin	Dubendorff, J.W. and Studier, F.W. (1991).

2.1.2.2 Yeast two-hybrid vectors

Vectors	Features	Antibiotic	Source and Reference
pACT2	Production of C-terminal GAL 4 (AD) fusion protein. Fusion protein targeted to yeast nucleus by SV40 NLS. PADH1 constitutive promoter, T7 promotor, HA epitope tag, leucine nutritional marker for selection in yeast. Replicates in E.coli (pUC) and S. cerevisiae (2μ)	Ampicillin	Clontech Laboratories Inc. (Louret et al., 1997).
pGBKT7	Production of C-terminal GAL 4 (BD) fusion protein. PADH1 constitutive promoter, c-Myc tag, tryptophan nutritional marker for selection in yeast. Replicates in E.coli (pUC) and S. cerevisiae (2μ) plasmid.	Kanamycin	Clontech Laboratories Inc. (Louret et al., 1997).
pGADT7	Production of C- terminal GAL 4 (AD) fusion protein. Fusion protein targeted to yeast nucleus by SV40 NLS that have been added to the activation domain sequence. PADH1 constitutive promoter, T7 promotor, HA epitope tag, Leucine nutritional marker for selection in yeast. Replicates in E.coli (pUC) and S. cerevisae (2μ).	Ampicillin	Clontech Laboratories Inc. (Chien et al., 1991).
pSE1111	Negative control vector (Bait) Gal4AD	Ampicillin	Tai et al., 1999.
pSE1112	Negative control vector (Prey) Gal4BD	Kanamycin	Tai et al., 1999.

2.1.2.3 Eukaryotic expression vectors

Vectors	Features	Antibiotic	Source and reference
pEGFP-N1	Genes cloned will be expressed as fusions to the N-terminus of EGFP (Excitation maximum 488nm; emission maximum 507 nm). Immediate early promoter of CMV. SV40 polyadenylation signals downstream of the EGFP gene direct proper processing of the 3´end of the EGFP mRNA. pUC origin of replication and an f1 origin.	Neomycin/ Kanamycin	Clontech
pmCherry-N1	EGFP gene from pEGFP-N1 was replaced with mCherry with PCR cloning using BamH1 and Not1 restriction sites.	Neomycin/ Kanamycin	Lab made

2.1.3 Antibodies

Primary Antibodies used for Immunohistochemistry and Western Blot				
Antibody	Monoclonal or Polyclonal	Raised source	Source reference	Working dilutions
RIBEYE U2656	Polyclonal	Rabbit	Lab made Schmitz et al., 2000	1:10,000
GST	Monoclonal	Mouse	Sigma	1:10,000
MBP	Monoclonal	Mouse	NEB	1:10,000
ArfGAP3 Cterm2 4th IS	Polyclonal	Rabbit	Lab made	1:3,000
ArfGAP3 Cterm3 4th IS	Polyclonal	Rabbit	Lab made	1:3,000
GCAP2 8th IS	Polyclonal	Rabbit	Venkatesan et al. 2010	1:1,000
CTBP2	Monoclonal	Mouse	BD Bioscience	1:1,000
Bassoon	Monoclonal	Mouse	Stressgen, VAM-PS003	1:100
Dynamin Hudy 1	Monoclonal	Mouse	Hudy-1, Millipore	1:50
ARFS 1A9/5	Monoclonal	Mouse	Santa Cruz Biotechnology SC-53168	1:500
Dy-650 Direct labeled CTBP2	Monoclonal	Mouse	CTBP2(BD) Coupled with DY650(Invitrogen)	1:2

Secondary Antibodies used for Immunohistochemistry and Western Blot				
Antibody	Monoclonal or Polyclonal	Raised source	Source reference	Working dilution
Alexa CAM 488	Polyclonal	Chicken	Invitrogen, Molecular probes	1:1,000
Alexa DAR 568	Polyclonal	Donkey	Invitrogen, Molecular probes	1:1,000
Alexa GAM 488	Polyclonal	Goat	Invitrogen,Molecular probes	1:1,000
GAM POX	Polyclonal	Goat	GAM POX(SIGMA) Cat.No: A3673	1:10,000
GAR POX	Polyclonal	Goat	GAR POX(SIGMA) Cat.No: A6154	1:10,000

2.1.4 Fluorescent Dyes

Name	Source	Purpose	Working concentration
SNAP-Vista Green	NEB	Labeling of SNAP-TAG fusion protein	1:50 dilution
Fixable FM1–43: FM1–43FX	Invitrogen, #F35355	Endocytic uptake experiment	20µM

2.1.5 Oligonucleotide

Name	Primer No	Sequence	Vector	Restriction site
GAPdomArfGAP3 For (1-136)	1478	AAAGAATTCTGATCATGGGGAC	pACT2	EcoRI
GAPdomArfGAP3 Rev (1-136)	1479	AAACTCGAGTTAGCTATCAAGCC		XhoI
ArfGAP3 f.l. (1-517) Rev	1481	AAACTCGAGTTAGGAACCGTAGCG		XhoI
CtermArfGAP3 For	1480	AAAGAATTCAGCACGGGCACTGAC		EcoRI
ArfGAP3 f.l. For (1-517)	1499	AAACTCGAGGCCACCATGGGGGACCCCAGCAAG	pmcherry	XhoI

ArfGAP3 F.L. Rev (1-517)	1496	AAAGAATTCCGGAACCG TAGCGATC		EcoRI
pMal-C2 For	1537	AGCTTAGTTAGTTAGTTA GAC TAGT	pMal-C2	SpeI
pMal-C2 Rev	1539	AGCTACTAGTCTAACTA ACTA		
AG Cterm3 for (332-460)	1515	AAAGAATTCAAACACCA ATCACGGCG	pGEX-KG	EcoRI
AG Cterm3 Rev (332-460)	1519	AAACTCGAGAGCTGAGC TGATGGA		XhoI
AG Cterm2 For (226-335)	1514	AAAGAATTCGGGCCAAA AAAGGAAGT		EcoRI
AG Cterm2 Rev (226-335)	1518	AAACTCGAGCGTGATTG GTGTTTC	pGEX-KG	XhoI
GAP Domain F (1-136)	1549	AAAAGAATTCATGGGGG ACCCCAG	pMal-C2	EcoRI
GAP Domain F (1-136)	1550	AAAAGTCGACGCTATCA AGCCAGAG		SalI

2.1.6 Cloned plasmid

GAP-domain (ArfGAP3)-pGEX-KG, encoding aa1-aa136 of bovine ArfGAP3.

The insert was excised from GAP-dom(ArfGAP3)pACT2 (see below) with EcoRI and XhoI and cloned into the EcoRI/XhoI sites of pGEX-KG.

GAP-domain(ArfGAP3)-pMal-C2, encoding aa1-aa136 of bovine ArfGAP3.

The insert was amplified from bovine ArfGAP3 cDNA (BC118087) using the following forward primer (1549) AAAAGAATTCATGGGGGACCCCAG and reverse primer (1550) AAAAGTCGACGCTATCAAGCCAGAG and cloned into the EcoRI/SalI sites of pMal-C2.

ArfGAP3Cterm2-pGEX-KG, encoding aa226-aa335 of bovine ArfGAP3.

The insert was amplified from bovine ArfGAP3 cDNA using the following forward primer (1514) AAAGAATTCGGGCCAAAAAAGGAAGT and reverse primer (1518) AAACTCGAGCGTGATTGGTGTTTC and cloned into the EcoRI/XhoI sites of pGEX-KG.

ArfGAP3Cterm3-pGEX-KG, encoding aa332-aa460 of bovine ArfGAP3.

The insert was amplified from bovine ArfGAP3 cDNA using the following forward primer (1515) AAAGAATTCAAACACCAATCACGGCG and reverse primer (1519) AAACTCGAGAGCTGAGCTGATGGA and cloned into the EcoRI/XhoI sites of pGEX-KG.

RIBEYE(B)-MBP (Magupalli et al., 2008).

pMal-C2 new.

This plasmid corresponds to the commercial pMal-C2 vector (NEB) to whom multiple STOP codons have been added in all reading frames. For this purpose, 7.5µl forward primer (1537; 20mM) AGCTTAGTTAGTTAGTTAGACTAGT and 7.5µl reverse primer (1539; 20mM) AGCTACTAGTCTAACTAACTA were annealed by a temperature touchdown procedure (95°C 5mins, 85°C 1min, 70°C 1min, 55°C 1min, 50°C, 1min, 45°C 1min, 43°C 1min, 40°C 1min, 35°C 1min). pMal-C2 (NEB) was digested with HindIII and treated with calf intestinal alkaline phosphatase (CIAP) to prevent re-ligation of the parental plasmid. The annealed primer dimer was ligated into the HindIII/CIAP-treated pMal-C2 backbone. Successful insertion was verified by double restriction digestion with NcoI and SpeI (which was newly introduced by the newly inserted primer construct). This newly generated pMal-C2 vector contains STOP codons in all reading frames at the end of the multiple cloning site.

RE(B)pGEX-KG (Schmitz et al., 2000)

RE(B)G730ApGEX-KG (Alpadi et al., 2008; Venkatesan et al., 2010).

Eucaryotic expression constructs

ArfGAP3-mCherry, encoding aa1-aa517 of bovine ArfGAP3.

Full-length ArfGAP3 was amplified by PCR using forward primer (1499) AAACTCGAGGCCACCATGGGGGACCCCAGCAAG, reverse primer (1496) AAAGAATTCCGGAACCGTAGCGATC and ArfGAP3 cDNA as template. The ≈1.5kB PCR product was cloned into the XhoI/EcoRI sites of pCherry-N1 (Alpadi et al., 2008)

RE(B)-EGFP (Schmitz et al., 2000).

Yeast vectors

ArfGAP3-pACT2.

ArfGAP3-pACT2 encoding full-length bovine ArfGAP3 was obtained by YTH screening with RIBEYE as bait construct

ArfGAP3cDNA-pACT2, encoding aa1–aa517 of bovine ArfGAP3.

Full-length ArfGAP3 was amplified from the full-length ArfGAP3 IMAGE clone #8081904 (BC118087) using forward primer (1478) AAAGAATTCTGATCATGGGGAC and reverse primer (1481) AAACTCGAGTTAGGAACCGTAGCG and cloned into the EcoRI/XhoI sites of pACT2.

GAP-Dom(ArfGAP3)pACT2, encoding the ArfGAP-domain (aa1-aa136) of ArfGAP3

The insert was amplified by PCR using forward primer (1478) AAAGAATTCTGATCATGGGGAC, reverse primer (1479) AAACTCGAGTTAGCTATCAAGCCA and bovine ArfGAP3 cDNA (BC118087) as template. The PCR product was cloned into the EcoRI/XhoI sites of pACT2.

CtermArfGAP3pACT2

The insert (≈1.0kb) encoding aa127 to aa517 of bovine ArfGAP3 was amplified from bovine cDNA (BC118087) using forward primer AAAGAATTCAGCACGGGCACTGAC (1480) and reverse primer AAACTCGAGTTAGGAACCGTAGCG (1481) and cloned into EcoRI/XhoI sites of pACT2.

f.l. ArfGAP3pACT2

The insert (≈1.5kb) was amplified from bovine ArfGAP3 cDNA (BC118087) using the following forward primer AAAGAATTCTGATCATGGGGAC (1478) and reverse primer (AAACTCGAGTTAGGAACCGTAGCG (1481) and cloned into the EcoRI/XhoI sites of pACT2. This constructs encodes for full-length (f.l.) ArfGAP3.

RE(AB)pGBK-T7 (Magupalli et al., 2008) , RE(B)pGBK-T7 (Magupalli et al., 2008) RE(B)NBD-pGBK-T7 (Alpadi et al., 2008), RE(B)SBD-pGBK-T7 (Alpadi et al., 2008), RE(B)G730A-pGBK-T7 (Alpadi et al., 2008), RE(A)pACT2 (Magupalli et al., 2008).

pGBKT7 (empty bait plasmid) (Tai et al., 1999; Magupalli et al., 2008).

pSE1112 (control bait plasmid) (Tai et al., 1999; Magupalli et al., 2008).

pACT2 (empty prey plasmid) (Magupalli et al., 2008).

pSE1111 (control prey plasmid) (Tai et al., 1999; Magupalli et al., 2008)

Munc119pACT2 (Alpadi et al., 2008). Munc119 is known to interact with RIBEYE(B)-domain and was used as a positive control for yeast matings.

Bassoon pGAD-T7 was cloned by RT-PCR using cDNA isolated from rat R28 cells (Alpadi et al., 2008), forward primer (573) TTTTCATATGTGCCGGATCTCCTCTGTCCCT and reverse primer (574) TTTTGAATTCCTGGGCCAGGCTGGCCTCCTG. The PCR product was cloned into the NdeI/EcoRI sites of pGADT7. This PCR product encodes for aa1638-2081 of rat bassoon (NP062019.2). This stretch is known to interact with RIBEYE(B)-domain (tom Dieck et al., 2005) and was used as a positive control for the indicated yeast matings.

2.1.7 Reagents and chemicals

Name	Company
Acetic acid	Roth
Agar-Agar	
Agarose	PEQLab
3-amino-1,2,4-trazole (ATZ)	Sigma
Ammonium peroxodisulfate	Roth
Ampicillin	
AMES medium	A1420
Benzoyl peroxide	Sigma
Biotin	Calbiochem
Bovine Serum albumin (BSA)	Roth
Bradford protein assay reagent, 5X dye	
Chloroquine	Sigma
Concavlin A	Sigma, #C7275-250 mg
Coomassie Brilliant Blue R 250	Roth
CSM-HIS	QBiogene
DEAE Dextran Dihydrochloride	Fluka
Dimethylsulfoxide (DMSO)	Roth
Disodiumhydrogen phosphate	
Dithiothreitol (DTT)	Sigma
DNase	Sigma, #DN25-110MG
DNTP's PCR Grade	Roth
EDTA	
Ethanol	
Ethidiumbromide	
Glucose	
Glutamine (200mM)	PAA
Glutathione-Sepharose beads	Fluka

Glycerin	Roth
Glycid ether	Serva
Glycine	Roth
IPTG	MP biomedicals
Isopropanol	Roth
Kanamycin	
L-Glutathione reduced	Fluka
Lithium acetate	Sigma
Magnesium chloride	Roth
Magnesium chloride hexahydrate	
Maltose	Sigma
MEM 100X vitamins	
B-mercapotethanol	Roth
Methanol	Roth
NAD+ (Oxidised)	Sigma
NADH (Reduced)	
N,N-Dimethylformamide (DMF)	Roth
Non-essential amino acids (100X)	Roth
GIBCO Non-fat dry milk powder	Supermarket
Nonidet P-40 Sigma (n-Propyl gallate) NPG	Sigma
Papain	Sigma, #76220-25G
Paraformaldehyde	Roth
PCR buffer 10X	Sigma
Peptone	Roth
Phenylmethylsulfonylfluoride (PMSF)	Sigma
Ponceau-S	Roth
Potassium Chloride	
Potassium Hydrogen phosphate	
Potassium phosphate	
Rotiphorese Gel 30	
Saccharose	MP Biomedicals
SNAP-TAG pulldown resins	S9144S
Sodium acetate	Roth
Sodium azide	Merck
Sodium bicarbonate (7.5% solution)	PAA
Sodium Carbonate	Merck
Sodium Chloride	VWR
Sodium dihydrogen phosphate	Fluka
Sorbitol	Roth
Streptomycin	Fluka
TEMED	Roth
TRIZMA BASE	
Triton X-100	
Tryptone	
Whatman filter paper	
Yeast extract	MP Biomedicals
Yeast Nitrogen Base with ammonium sulfate without amino acid	Clontech
X-Gal (5-Bromo-4-Chloro-3-indoyl-β-galactoside)	MP Biomedicals

2.1.8 Buffer and media

Name	Composition
Agarose gel electrophoresis buffer (TAE) 50X stock Note: Working concentration 1X	242.0 g Tris base 57.1 ml glacial acetic acid 100.0 ml of 0.5M EDTA pH 8.0 Made up to 1 liter with distilled water
Acetate buffer (Plasmid preparation)	3M Potassium acetate, pH 5.5
Alkaline lysis solution 2(Plasmid preparation)	0.2N Sodium Hydroxide 1% (w/v) SDS
3-amino-1,2,4-trazole (ATZ)	10mM in double distilled water (filter sterilized)
Aureobasidin	1mg/ml in absolute alcohol
Ampicillin	100mg/ml in dd water, filter sterilized
Binding buffer	100 mM Tris-HCl, pH8.0 150 mM NaCl, 1 mM EDTA 1% Triton X-100
Blocking buffer for Immunohistochemistry	0.5% BSA in 1XPBS
Bradford-reagent Roti®- Quant	1:5 dilution in dd water
Breaking buffer (Saccharomyces cerevisiae)	100mM Tris-HCl, pH8.0 1 mM β-Mercaptoethanol 20% glycerol
BSA for restriction digestion	10 mg/ml (100X) 1:10 dilution dd water
Chloroquine	10mM stock in sterile dH_2O water
Coomassie stain	600.0 ml Isopropanol 1560.0 ml dd water 240.0 ml acetic acid 0.6 grams Coomassie Brilliant Blue R-250
COS cells lysis buffer	100mM Tris-HCl, pH 7.9 150mM NaCl 1mM EDTA 1% Triton X-100
Coomassie destaining solution (Polyacrylamide gel electrophoresis)	100.0ml Acetic acid 300.0ml Ethanol Made up to 1 liter with dd H_2Owater
Dulbecco's modified Eagle's medium/ 10% FCS (DMEM) (For COS cells)	900 ml DMEM 100.0 ml FCS (per liter)
ECL (Chemiluminescence detection system)	1:1 v/v with ECL 1 & ECL 2 (ECL1) 5.0ml 1M Tris-HCl, pH 8.5

	500µl luminol, 220µl PCA Made up to 50ml with dd water (ECL2) 5.0ml 1 M Tris-HCl, pH 8.5 32µl Hydrogen peroxide (30%) Made up to 50.0 ml with dd H_2O water
IPTG	0.1M in dd H_2O
Kanamycin	50mg/ml in dd water, filter sterilized
LB Nutrient medium for Bacteria	Invitrogen GmbH, Karlsruhe
Lithium acetate/ Tris-EDTA/ β-Mercaptoethanol (For making of electrocompetent Saccharomyces cerevisiae)	100mM Lithium acetate 10mM β-Mercaptoethanol 1X Tris-EDTA Make up to 20.0 ml with dd water
Na_2CO_3	1 M in dd H_2O
PBS (for cell culture)	Commercial preparation (PAA)
5x PBS (Western Blots, Immunohistochemistry)	40 g NaCl 1 g KCl 7.2 g Na_2HPO_4 1.2 g KH_2PO_4 Make up to 1 litre with dd H_2O
PMSF-Stock solution	40mM in 100% Isopropanol
Polyacrylamidgel 10%	1.5 ml ddH_2O 1.5 ml 50% Glycerol 1.95 ml 1 M Tris pH 8.8 2.40 ml 30% Acrylamide 50 µl 10% SDS 50 µl 10% APS 5.0 µl TEMED
Ponceau S-stain	30 g Trichloroacetic acid 5 g Ponceau S Make up to 1 litre with dd H_2O
10x restriction enzyme buffer	New England Bio Labs
Resuspension buffer (P1) (Plasmid preparation)	50 mM Tris-HCL, pH 8.0 10 mM EDTA 100 µg/ml RNase A
Dropout Nitrogen base Medium (Minimal medium)	Clontech biosciences 27.0 g/l
Yeast selective medium -L medium -W medium -LW medium -ALWH medium	+0.69 g -Leu-DO +0.74 g -TRP-DO +0.64 g-Leu-TRP-DO +0.6 g-Ala-Leu-Trp-HIS All medium was made up to 1litre with dd H_2O Adjusted to pH 5.8

SDS-PAGE Electrophoresis buffer	3.03 g Tris 14.4 g Glycine 1.0 g SDS Make up to 1 litre with dd H_2O
SDS-loading buffer	4 x 1.6 g SDS 4 ml β-Mercaptoethanol 2 ml Glycerol 2 ml 1M Tris pH 7.0 4 mg Bromophenol blue, 2 ml of dd H_2O.
2X TBS	28 ml 5 M NaCl 3 ml 1 M KCl 1 ml 1 M $CaCl_2$ 0.5 ml $MgCl_2$ 4.5 ml 200 mM Na_2PO_4, pH 7.4 20 ml 1 M Tris-HCl, pH 7.9 Make up to 500 ml of filter dd H_2O
1xTAE-Puffer	40 mM Tris pH 7.8 10 mM Sodium acetate, 1 mM EDTA
Transfer Buffer (Western Blot)	TRIS 15.125 g Glycine 72.05 g Methanol 1 litre Make up to 5 litres with dd H_2O
X-Gal solution	20 mg/ml in N,N Dimethylformamid (DMF)
X-Gal detection solution	350µl X-Gal solution 150 µl β-Mercaptoethanol Make up to 10 ml with Z-Puffer
YPD-Medium Clontech	50g YPD dissolved in 1 litre of ddH_2O. Autoclave
Z-Buffer:	60mM Na_2HPO_4 40mM NaH_2PO_4 10mM KCl 1mM $MgSO_4$ 50mM β-mercaptoethanol pH 7.0 Do not autoclave
LCS (Low calcium saline solution)	132 mM NaCl, 3 mM KCl, 1 mM $MgCl_2X6H_2O$, 0.5 mM $CaCl_2$, 10 mM sodium pyruvate, 10 mM glucose, 10 mM HEPES, pH 7.4 (≈300 mOsm/L)
Artificial Cerebrospinal spinal Fluid (ACSF)	(in mM): 119 NaCl, 2.5 KCL, 2.5 $CaCl_2$, 1.3 $MgCl_2$, 1 NaH_2PO_4, 20 glucose, and 11 HEPES, pH 7.4, osmolarity ≈300 mOsm/L
AMES medium	Prepared as mentioned in datasheet of product number A1420 (Sigma)

2.1.9 Miscellaneous consumables/materials

Product	Supplier
Blotting paper	GE healthcare
Electroporation cuvettes, 0.1, 0.2 &0.4 cm gapped	PeqLab
Glass beads (0.5mm)	Roth
Disposable petri dishes (85mm)	VWR
Polypropylene falcon tubes 15 ml and 50 ml Greiner bio-one Culture flasks	SCHOTT & GEN, Mainz
PVDF membranes	GE healthcare
QIAprep spin colums	Qiagen

2.1.10 Laboratory hardware equipments

Name	Company
Adjustable pipettes	Eppendorf
Agarose gel electrophoresis system	Peq-lab
Axiovert 200, AxioCam MRm (Camera)	Zeiss
Autoclave	Tuttnauer Systec 5050ELCV
Biofuge fresco	Heraeus
Biofuge primo R	
Biofuge stratos	
Chemidoc XRS system	Bio-Rad
Electroporator ECM399	BTX
Fluorescence microscope	Axiovert 200 M Zeiss
Freezer -80°C	Heraeus
100-mesh gold grid	Plano, Wetzlar, Germany
Hot air oven	Heraeus
Incubator for Bacteria /Yeast	Memmert
Incubator for cell culture	Thermo
Laminar Flow Model 1,2	Holten
Magnetic stirrer (Complete Set)	Neolab
Multifuge S-R	Heraeus
Orbital Shaker	Edmund Bühler Labortechnik
PCR master cycler gradient	Eppendorf
pH meter	Inolab
Polyacrylamide Gel system	GE healthcare
Power pack for Gel system	
Rotary wheel	Neolab
Refrigerated Incubator Shaker Innova 4320	New Brunswick Scientific
Steri cycle CO_2 incubator	Thermo ELECTRON CORPORATION
Sterile filtration device	Millipore
Thermomixer compact	Eppendorff
Transmission Electron Microscopy	FEI, Tecnai G 2
Ultracut Microtome (UltraCut S)	Leica

Ultrasound bandelin sonoplus	Bandelin Electronic, Berlin
Vortex	VWR International
Western blot transfer apparatus	HOEFER SCIENTIFIC INSTRUMENTS
Weighing balance CP64	Sartorius
Square wave pulse Electroporator	ECM 830; BTX
Tweezertrode electroporation device	BTX; #45-0118, #45-0204
Feedback temperature controller	TC324B; Warner Instruments
Incubation chamber	Lab made
Transparent ITO heaters	HI- 25Dp; MicroControls

2.2 Methods:

2.2.1 DNA related techniques and cloning

2.2.1.1 PCR amplification of DNA fragments

The Polymerase Chain Reaction (PCR) is a technique to specifically amplify a segment of DNA using two sequence-specific, complimentary primers to the sequence of target DNA. PCR process comprises of three steps: 1) Denaturation of the double-stranded DNA template to separate strands by heating, 2) cooled to a temperature that allows the oligonucleotide primers to anneal to their target DNA sequence and 3) extension of the DNA strand with thermostable DNA polymerase (Chein et. al., 1976). The cycle of denaturation, annealing, and DNA synthesis were repeated (usually for 40 cycles). Because the products of one round of amplification serve as templates for the next, each successive cycle essentially doubles the amount of the desired DNA product. A 50µl final reaction mixture consisted of:

Tube 1

2µl (sterile double distilled H_20)

1µl (Forward Primer OD 5 or 10 pmoles/µl)

1µl (Reverse Primer OD 5 or 10 pmoles/µl))

1µl (template DNA, 1-10ng)

Tube 2

38 µl (sterile double distilled H_20)

5µl (10X PCR buffer containing 25mM $MgCl_2$)

1µl (10mM dNTPs)

1µl (Taq DNA polymerase 1U/µl)

The PCR reaction mixture was incubated in a thermocycler at the following cycle conditions: 95°C (2- 5 min) - {[95 °C (30 sec) - 55 °C (30 sec) - 72 °C (1 min)] 8 cycles} - {[94 °C (30 sec) - 65 °C (30 sec) - 72 °C (1 min)] 40 cycles} - 72 °C (7 min) - 4°C (∞). The preferred annealing temperatures for oligonucleotides were between 54°C-56°C and extension time of ~1min/1kb fragment was used. The PCR was routinely performed with a ´hot start´ (Erlich et al., 1991) to minimize unspecific priming. Hot start was achieved by mixing the contents of tube1 to tube2 after heating to 95°C. Correct amplification and the

purity of PCR products were analyzed by agarose gel electrophoresis and sequencing.

2.2.1.2 DNA Electrophoresis

Agarose gel electrophoresis was used for separation, identification and purification of DNA fragments. DNA samples were mixed with 4X DNA loading buffer. TAE buffer was used as an electrolyte and the separation was done at 5 volts/cm. Depending upon the size of DNA molecule to be resolved, the agarose concentration varied between 0.8%-2.5% (w/v). By virtue of negative charge, DNA moves towards anode. Under constant voltage the migration speed of linear, double-stranded DNA in agarose gel is proportional to the logarithm of its molecular weight. Fluorescent dye, ethidium bromide (Sharp et al., 1973) which intercalates into the resolved DNA fragments was visualized by UV light. DNA fragment size (5,000bp 100bp), quality and quantity of DNA were determined upon comparison with known molecular weight standards (100 bp DNA-Leiter Roti® Mark, Roth).

2.2.1.3 Purification of DNA

After gel electrophoresis and identification of the respective bands under UV light, the respective bands were excised with a sharp scalpel. DNA/PCR products were purified by using a QIA®quick Gel Extraction Kit (QIAGEN) in accordance with the manufacturer's instructions. Excised gel was solubilized in 1 ml of QX1 buffer containing 10µl of vortexed QIAX silica gel beads. Additionally, 8µl of 3M Sodium acetate (pH 5.2) was added. The solubilization process was carried out at 55°C for 40 minutes on 350 rpm thermoshaker. DNA bound to silica gel was sedimented at 13,000 rpm, RT for 1 minute. Pellet was resuspended completely in 1ml of QX1 buffer and pelleted down. The pellet was washed twice with 1 ml of PE wash buffer. The pellet was air dried completely to remove traces of ethanol. The DNA from dried pellet was eluted with 30µl of pre-heated double-distilled water (heated at 55°C). Elution was carried out at 55°C, 400 rpm for 15 minutes on a thermoshaker. The eluted DNA was collected as supernatant after centifugation at 13,000 rpm, RT for 1 minute.

2.2.1.4 Restriction digestion of DNA

Restriction endonuclease catalyzes a sequence-specific cleavage of double-stranded DNA, resulting in cohesive ends or blunt ends. Restriction digests were performed according to the manufacturer's instruction concerning buffer selection, addition of BSA etc. The amount of restriction enzyme, DNA, buffer, ionic concentrations, temperature and the duration of incubation varies and depends upon the specific application. For a typical 30µl reaction, consisting of 1µg DNA, 3µl of 10X recommended buffer, 3µl of 10X BSA and 0.25 or 1 units of restriction enzyme were used. Digested fragments were separated on agarose gel

electrophoresis followed by purification using QIA®quick Gel Extraction Kit (QIAGEN).

2.2.1.5 Ligation of DNA fragment

The T4 DNA ligase reaction catalyzes the repair of single-stranded nicks in duplex DNA restriction fragments having either blunt or cohesive ends. Ligations were carried out overnight at room temperature or 14°C (unless, otherwise mentioned) using a 1:3 molar ratio of vector to insert. The 20µl reaction mixture consisted of 10-200ng total DNA mass, proportionate quantity of digested vector, 1µl of T4 DNA ligase (1U/µl) and 2µl of T4 DNA ligase buffer (10X).

2.2.1.6 Precipitation of DNA

DNA was precipitated and desalted with ethanol. For this purpose, about 1/10 volume of 0.3M sodium acetate (pH 5.2) and two volumes of isopropanol were added to the DNA solution for precipitation (only in case of yeast plasmid rescue otherwise proceeded with isopropanol alone). The DNA solution was centrifuged for 1 hour at 13,000 rpm, +4°C for 15 minutes. The DNA pellet was carefully resuspended with 1 ml of 70% ethanol and centrifuged at 13,000 rpm, +4°C for 15 minutes. Pellet was air dried and resuspended in 10µl of 1mM Tris HCl, pH 8.5.

2.1.1.7 Preparation of electrocompetent cells

All procedures were carried out in sterile and aseptic environment to prepare electrocompetent *Escherichia coli* cells (DH10B, BL21 and BL21T7 Express). The following paragraphs also cover the methodology used for the preparation of electrocompetent *Saccharomyces cerevisiae*. Glycerol stock of bacteria (*E.coli*) cells were freshly streaked on LB plate and incubated overnight at 37°C. Overnight 100 ml LB preculture was grown at 37°C, 160 rpm after single colony innoculation. 600 ml of main culture (in 2 liters flask) was prepared with inoculation of 20 ml overnight grown preculture. Cells were grown at 37°C, 160 rpm shaking till an optical density (OD) between 0.9-1.0 was achieved at 600nm (OD_{600}) Further steps were carried out at +4°C. The culture was transferred to a sterile falcon tubes and centrifuged at 3,500rpm, +4°C for 15 minutes. The cell pellet was washed thrice in the sterile, ice-cold, double-distilled water and centrifuged at 3,500rpm, +4°C for 15 minutes. The final washed pellet was resuspended in 5 ml sterile, ice-cold 10% glycerol (made in sterile water). Aliquot's of (50µl) cell suspension was made in prechilled 1.5 ml reaction tube, and frozen in liquid nitrogen. Electrocompetent cells were stored at -80°C for long-term storage. Using this method, I achieved $1\text{-}2X10^8$ transformants/µg DNA. Saccharomyces cerevisiae strains (Y2H GOLD and Y187) were streaked on YPD plates, and incubated at 30°C till the colonies appear.

The electrocompetent yeasts were prepared as described by (Helmuth et al., 2001). As a laboratory practice, gene of interest cloned in pGBKT7 and pACT2 were electroporated in Y2H and Y187 respectively. Preculture was set up by inoculating a single yeast colony in 10 ml YPD broth and was incubated at 30°C overnight at 160 rpm in an orbital shaker. Around 100ml main culture (in 200 ml baffled flask) was set up, using 0.5 ml of overnight preculture and was incubated at 30°C overnight at 160 rpm in an orbital shaker. Cells were harvested by centrifuging at 2,000 rpm, +4°C for 5 minutes in a sterile 50 ml falcon tube. Cell pellet was washed twice with 20 ml of sterile, cold, double-distilled water and concentrated every time by centrifugation at 2,000 rpm, +4°C for 5 minutes. Cell pellets were resuspended in 20 ml of 1M Sorbitol and collected by centrifugation. Afterwards, the pellet was resuspended in 20 ml volume of incubation mixture (100 mM LiAc, 10 mM β-mercaptoethanol and 1X TE buffer) and was incubated at 30°C for 30 minutes with 250 rpm shaking. Cells were again pelleted at 2,000 rpm, +4°C for 3 minutes and washed once with 20ml of 1M Sorbitol. Electrocompetent cells pellet were resuspended in a minimal volume (200µl) of 1M Sorbitol. They were used directly for the electroporation.

2.2.1.8 Transformation of electrocompetent cells

Electroporation is a very efficient method of E.coli transformation (Chassy and Flickinger, 1987). In presence of high electric field, the transient membrane opening leads to uptake of DNA by electrocompetent bacteria. For electroporation, 1µl of DNA solution containing (10-100ng) DNA was added to approximately 50µl thawed (on ice) electrocompetent bacteria (DH10ß, BL21 and BL21T7 Express). Resuspended contents were transferred to a prechilled, 1mm electroporation cuvette and subjected to a pulse of strong electric field in the electroporator at 1,200V. Immediately after electroporation, the entire contents of the cuvette was recovered by the addition of sterile LB medium and incubated at 37°C, 160 rpm for 1 hour. The recovered cells were sedimented at 3,500 rpm, RT for 1 minute. The cell pellet was resuspended in (50µl) of residual LB, and spreaded on LB agar petri dishes containing appropriate antibiotics for selection of transformants. The petri dishes were sealed, incubated overnight at 37°C and observed for growth.

Electrocompetent Saccharomyces cerevisiae were also electroporated with the recombinant DNA as described (Helmuth et al., 2001). For this purpose, electrocompetent yeast (120µl) was mixed with 1 µl of DNA and transferred to 0.4mm electroporation cuvette. Cells were pulsed at 1,800V and collected immediately with 1ml YPD medium. Cells were incubated at 30°C for 1 hour with 600 rpm shaking. Transformants were selected on selection plates.

Transformants were identified by plating bait and prey plasmid constructs on -W (lacking amino acid tryptophan) and -L (lacking amino acid leucine) selective plates, respectively. Transformants with bait plasmids convert the Y2H GOLD yeasts to tryptophan protrophy and enables them to grow on -W plates. Similarly Y187 transformed with prey plasmids grow on -L plates. Water treated cells and competent cells alone served as controls. The Petri dishes were sealed, incubated at 30°C for 48 hrs and observed for growth.

2.2.1.9 Plasmid DNA preparation

Plasmid DNA was prepared with alkaline lysis (Birnboim and Doly 1979). For plasmid minipreparation, single bacteria colony was inoculated in 5ml LB medium (in 15ml falcon tubes) containing appropriate antibiotics and incubated overnight at 37°C with 160 rpm shaking. Turbid cultures were centrifuged at 3,500 rpm, +4°C for 15 minutes and the pellet was resuspended in 250µl of alkaline lysis solution 1 (see material section). The contents were transferred to a fresh reaction tube and 250µl of alkaline lysis solution 2 (see material section) was added and gently mixed by inverting the tube. The contents incubated at room temperature for 5 minutes. The lysed cells were neutralized with 350µl of acetate buffer (see material section), and the preparation was centrifuged at 13,000 rpm, +4°C for 30 minutes. Clear supernatant was added with 750µl of isopropanol and centrifuged at 13,000 rpm (radius max/min. 10.7/5.6[cm]), +4°C for 45 minutes to precipitate the DNA. The pellet (containing plasmid DNA) was carefully washed with 1ml of 70% ethanol and centrifuged at 13,000 rpm, +4°C for 20 minutes. The washed pellet was air dried and resuspended in 50µl of 1mM Tris-HCl (pH 8.5). DNA was digested with restriction enzymes to screen positive clones. Confirmed positive clones were inoculated for large-scale plasmid DNA preparation (maxi preparation).

Positive clones were inoculated in 100 ml LB medium (in 200 ml conical flask) containing appropriate antibiotics for plasmid DNA maxi-preparation. Overnight incubation was carried out at 37°C, 160 rpm. The cells were centrifuged at 3,500 rpm, +4°C for 20 minutes. The pellet was resuspended in 5 ml of buffer1 (see material section). The contents were transferred to a fresh falcon tube and 5 ml of lysis buffer 2 (see material section) was added and incubated at room temperature for 15 minutes after gently inverting the tubes. The lysed cells were neutralized with the addition of 8 ml of buffer 3 (see material section). The resuspension was centrifuged at 8,500 rpm, +4°C for 30 minutes. Clear supernatant was collected, and added with 20 ml of isopropanol. DNA was precipitated by centrifugation at

13,000 rpm, +4°C for 1 hour. The pellet obtained was carefully washed with 20ml of 70% ethanol and centrifuged at 13,000 rpm, +4°C for 30 minutes. The washed pellet was air dried and resuspended in 1ml of 1mM Tris-HCl (pH 8.5). The DNA was digested with restriction enzymes to consolidate the proper identity of the large-scale DNA preparation.

2.1.1.10 DNA Sequencing

DNA was sequenced with dideoxynucleotide method (Sanger et al., 1977a). DNA sequences were commercially obtained form MWG Biotech (Martinstried, Germany).

2.2.1.11 Glycerol stocks

For long-term storage, 0.85ml of a logarithmic-phase E. coli culture was added to 0.15 ml of sterile glycerol (100%). The reaction tubes were vortexed to ensure even distribution of the bacterial cells and glycerol. Cells were frozen in liquid nitrogen and stored at -80°C. Duplicates were stored frozen at any time.

2.2.2 Protein related techniques

2.2.2.1 SDS-PAGE

Polyacrylamide gel electrophoresis under denaturing conditions in the presence of SDS (Sodium Dodecyl Sulfate) separates the proteins inversely proportional to the logarithm of their molecular mass (Laemmli, 1970). The presence of SDS molecules, mask the intrinsic charge of protein and create a relatively uniform negative charge distribution caused by the sulfate group on SDS. The reducing agent, β-mercaptoethanol aids in reducing the existing disulphide bonds and hence, in denaturing of the proteins. Protein samples were solubilized by boiling at 97°C for 3 minutes in 4X SDS loading buffer and the protein components were resolved electrophoretically. Stacking gel was discarded after electrophoresis, and the resolving gel was stained in Coomassie for 10 minutes at room temperature on a shaker. Proteins bands were visualized by the Coomassie brilliant blue (R-250) staining. The excess stain was removed with destaining solution (see material section) to visualize the protein bands.

2.2.2.2 Western Blot

Western Blot refers to the transfer of biological samples from a gel to a membrane and their

subsequent detection on the surface of the membrane. The first step in the western blotting procedure is to separate the macromolecules using gel electrophoresis. Following electrophoresis, the separated molecules were electrotransferred onto a nitrocellulose membrane. The proteins were electroblotted from Polyacrylamide gels onto nitrocellulose membrane. Blot transfer was carried out at 50V at +4°C and the durations were dependent on the size of protein to be transferred and the applied potential difference. The nitrocellulose membranes after blotting were stained with Ponceau-S and subsequently destained with PBS. Membrane was blocked for 1 hour at room temperature with 5% (w/v) nonfat dry milk (in PBS), on a shaker. For probing, the membrane was incubated overnight with primary antibody (depending upon antigen to be detected) at +4°C, on a shaker in appropriate dilutions (according to the manufacturer's instructions, see material section). The non-specifically membrane bound antibody was removed by washing thrice in PBS for 10 minutes each at room temperature. Secondary antibody incubation was carried out at room temperature for 1 hour on a shaker in appropriate dilutions (according to the manufacturer's instructions, see material section). Further, nonspecifically membrane bound antibody was removed by washing thrice in PBS for 10 minutes. The membrane was developed using ECL (see material section), chemiluminiscence signals were acquired using Quantity One (BioRad) software.

2.2.2.3 Stripping of nitrocellulose membranes

Nitrocellulose membranes were reprobed with different primary antibody for multiple purposes. The earlier signals were removed by stripping the blot with boiled 2% SDS (in 50mM Tris, pH 7.0 and 5mM of β-mercaptoethanol) in total volume of 20ml. The incubation was carried out at 55°C on a shaker for 20 mins with intermittent shaking. The excess stripping solution was removed by washing with PBS at room temperature for 20 minutes. The membrane was blocked as stated earlier (see section 2.2.2.2) and reprobed with the desired antibodies and the signals were detected as mentioned earlier (see section 2.2.2.2).

2.2.2.4 Determination of protein concentrations

In the acidic environment of the reagent, protein binds to the Coomassie dye. This results in a spectral shift from the reddish/brown form of the dye (absorbance at 465nm) to the blue form of the dye (absorbance maximum at 595 nm). Therefore, the absorbance at 595 nm gives fairly linear concentration dependence for most soluble proteins. The standard

calibration curve was routinely obtained by using duplicates of a known concentration of BSA, and the unknown concentration was determined (Bradford, 1976).

2.2.2.5 Recombinant Protein Expression

Recombinant proteins either GST or MBP and were routinely expressed in BL21 (DE3) and SNAP-TAG tagged fusion protein were expressed in BL21 T7 express. Bacterial fusion proteins were expressed in baffled shake flasks. For this purpose, isolated single colonies were inoculated, grown overnight in 100ml (in 200ml flask) LB medium containing 200µl ampicillin (100mg/ml) and 1% Glucose at 37°C, 220 rpm to obtain precultures. Main cultures were prepared using 500 ml of LB containing 1.0ml of ampicillin with addition of 15.0ml overnight grown preculture with 0.4% Glucose. The cells were grown at 37°C, 220 rpm till the $O.D._{600nm}$ reached 0.9-1.0. Once the O.D. was achieved cultures were induced with 0.1mM final concentration of IPTG for duration of 4 hours. The Induction temperature varied from one fusion protein either at R.T or 18°C. Cells were harvested by centrifugation at 3,500 rpm, +4°C for 30 minutes and washed thrice by resuspending in 50 ml cold PBS.

COS7 cells were used as second source for heterologous protein expression. On day 0, cells were splitted and plated with 50% confluency on 60mm dishes, in 3 ml DMEM medium (containing 10% FCS). After 48 hours of growth, COS7 cells were transfected with the eukaryotic expression construct (either EGFP- or mRFP tagged) indicated in the experiments, using DEAE Dextran method (Ishtchenko et al., 1995). Cells were washed twice with 5 ml of PBS and incubated with 3.3ml transfection cocktail (1650µl of 2X TBS, 1257µl of sterile double distilled water, 330µl of DEAE Dextran and 10µl of DNA) for 30 minutes at 37°C, 5% CO_2. Transfection cocktail was aspirated and incubated with fresh 5 ml medium containing 5µl of chloroquine (10mM stock) for 3 hours at 37°C, 5% CO_2. Chloroquine containing medium was aspirated and cells were washed twice with 5 ml of PBS. Cells were shocked for 2 minutes at room temperature with 2ml of 20% glycerol (prepared in DMEM medium). Glycerol containing medium was aspirated and cells were washed twice gently with 5 ml of PBS. Fresh DMEM medium (5ml) was added and cells were incubated for 48-60 hours at 37°C with 5% CO_2.

2.2.2.6 Purification of Recombinant Proteins

The expressed recombinant proteins were purified, before being used for experiments such as protein pull-downs and ribbon pull-down assays. Escherichia coli expressed GST and

MBP-tagged fusion proteins were purified on the basis of their affinity towards glutathione-agarose beads and amylose resin respectively. The 15ml cell resuspension (in PBS) was incubated with 500µl of lysozyme (10mg/ml) for 1 hour at +4°C on a shaker and subsequently sonicated for 20 seconds, 4 rounds with in between 20 seconds interval. Cell free supernatant was obtained by 2 rounds of centrifugation at 13,000 rpm, +4°C for 1 hour. Glutathione-agarose beads (200µl) or amylose resin (200µl) was washed thrice in 50 ml of cold PBS solution and sedimented at 1,500 rpm, +4°C for 1 minute. The cell free supernatant from earlier step was incubated overnight with the beads/resin. Non-specific binding was reduced by washing bound protein (to beads/resin) six times with cold PBS. The washings were carried out for 30 minutes at +4°C on shaker and beads/resin were sedimented at 1,500 rpm for 1 minute at +4°C.

2.2.3 Protein - Protein Interaction analyses:

2.2.3.1 Yeast Two-Hybrid assay

Yeast two-hybrid is an important system to analyze and characterize protein-protein interactions (Fields et al., 1989). In GAL4-based two-hybrid assay, a bait gene is expressed

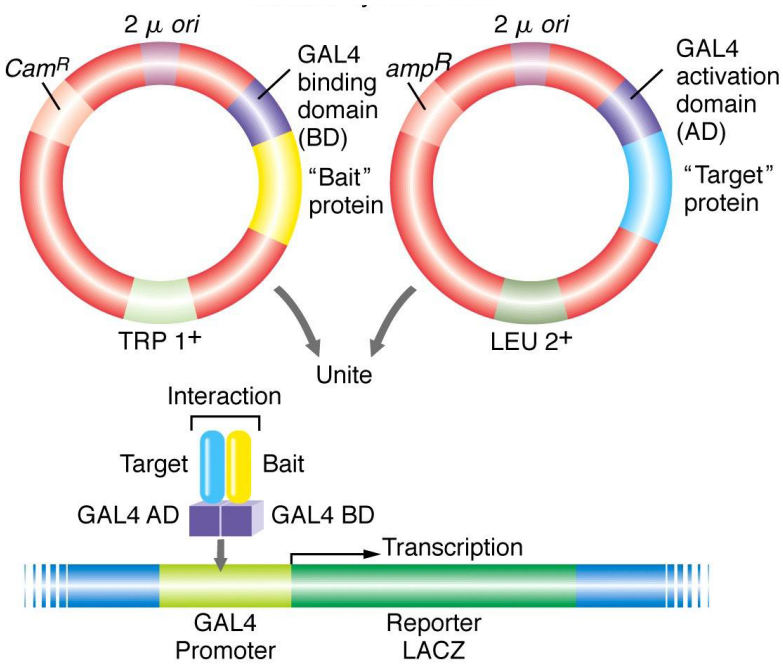

Figure 13: Principle of the Yeast two-hybrid system. Two physically discrete modular domains of eukaryotic transcriptional activators were constituted by the DNA-BD) (pGBKT7) and the (AD) activation domain (pACT2). The domains acts as independent modules: neither alone can activate transcription, but each domain continues to function when fused to other proteins. In the above case, protein of interest is expressed as a fusion to the DNA-BD. Another protein, or a cDNA library, is expressed as a fusion to the AD. If two proteins interact, the DNA-BD and AD are brought into close proximity and activate transcription of the reporter gene.

as a fusion to the GAL4 DNA-binding domain (DNA-BD), while another gene or cDNA is expressed as a fusion to the GAL4-activation domain (AD). Gal4 protein is a yeast transcription factor that normally controls genes responsible for galactose metabolism. Each Gal4- responsive gene contains a target site called an Upstream Activating Sequence, or UAS.

When Gal4 binds the UAS, transcription is activated from a downstream promoter. By linking the GAL UAS with other metabolic genes (e.g., ADE2, HIS3, MEL1 and lacZ) and by eliminating the wild-type GAL4 gene, yeast strains that change phenotype when Gal4 is activated are developed. The following schematic drawing elucidates principle of the Gal4-based Yeast two-hybrid (YTH) system.

2.2.3.1.1 Yeast mating

A single yeast colony was picked from both –L and –W selective plates. Colonies were resuspended in 1ml YPD broth (in 2 ml reaction tubes). -L and –W plates confers growth to the leucine synthesizing (pACT2) and tryptophan synthesizing (pGBKT7) colonies. The resuspended yeasts were incubated for 5 hours at 30°C on thermoshaker at 600 rpm. The mated yeasts were centrifuged at 3,000 rpm, +4°C for 5 minutes at the end of incubation. Yeast cell pellet was resuspended in 50-100µl of residual YPD broth. 50µl of the above suspension was spreaded each on –LW and –ALWH plates. –ALWH plates were spreaded with 100µl ATZ (10mM stock) and 60ng/ml of aureobasidin prior to use. The plates are incubated at 30°C and observed for growth. -LW plate confers growth, when both plasmids are present in a same cell (diploid) and indicates mating efficiency. Growth on –ALWH plates indicates protein-protein interaction. For the matings pSE111 and pSE1112 (Bai and Elledge, 1996) as well as the empty bait and prey vectors were used as negative controls.

2.2.3.1.2 β-Galactosidase assay

In yeast two-hybrid system host strains, integrated nutritional reporter genes provide an elegant and sensitive growth selection. The MATa reporter strain Y2H GOLD strain contains three reporters - HIS3, ADE2, and MEL1 (or lacZ) under the control of upstream activating sequences (UASs) and TATA boxes. These promoters yield strong and specific responses to GAL 4 may be used as mating partner for the MATα Y187. When two transformants cultures are mated to each other, diploid cells are formed which contain four reporter genes: HIS3, ADE2, MEL1, and lacZ. The GAL 4DNA-BD binds to the GAL-UAS and, the AD is brought into proximity to the reporter genes promoter, there by activating

transcription and permitting growth on selection medium and expression of α-galactosidase (MEL1 product) and β-galactosidase (lacZ product) providing a qualitative assessment (filter lift) of protein-protein interaction. Quantitatively, the interaction is measured by β-galactosidase liquid assay as described (Wang et al., 1997; Stahl et al., 1999).

For qualitative β-galactosidase filter test, yeast cells were streaked on –LW/-ALWH plates and incubated for 48-60 hours at 30°C. Whatmann filter paper cut to proportionate size, placed onto the yeast colonies to make a replica of the yeast on the filter paper. The impressions of summary plate on whatman filter paper were probed in β-galactosidase filter test. The yeast cells were cracked by dipping filter paper bound to colonies, in liquid nitrogen for 2 mins. and thawed for 5 seconds. The liquid nitrogen cracked filter paper (containing the replica of cells) was placed gently on a layer of filters, earlier soaked in an incubation solution (10 ml ´Z´ buffer + 350 µl X-gal + 150µl β- Mercaptoethanol). Reaction was carried out at room temperature in a petridish with a covered lid. Filter lifts for the positive yeast clones were observed for the appearance of blue color in contrast to the corresponding controls.

2.2.3.2 Protein pull-down assays

The Yeast two-hybrid findings were confirmed independently by protein pull-down assays. Recombinant proteins were expressed in bacteria with different fusion tags. The purification steps were described in section (2.2.2.6). The protein pull-down procedure is described below.

2.2.3.2.1 Recombinant protein pull-down assays

For fusion protein pull-down experiments, either GST-tagged or maltose-binding protein (MBP)-taged fusion proteins were used as immobilized bait proteins. If GST-tagged proteins were used as immobilized bait protein, the MBP-tagged protein was used as solubilized prey protein and vice versa. Bait and prey proteins were used in equimolar amounts (0.3µM in incubation buffer containing 100mM Tris, pH 8.0, 150mM NaCl, 1mM EDTA, 0.25% (w/v) Triton X-100 (Tx-100), and 1mM ß-mercaptoethanol (ßME) if not denoted otherwise). GST and MBP alone served as control proteins. Protein concentrations were determined using the Bradford method (Bradford, 1976). For pull-down experiments, fusion protein eluates were pre-cleared with 10ml of empty sepharose beads (per 1 ml of eluate) for 1hr at 4°C. Incubations were typically done in a volume of 500ml. After overnight incubation at 4°C,

immobilized beads were allowed to settle (20 mins, at 4°C). Samples were washed by repeated centrifugation of the beads (3000 rpm, 2mins, 4°C) and subsequent resuspension with binding buffer. This procedure was repeated three times. Afterward, the final pellets were boiled with SDS-sample buffer (96°C, 10mins) and subjected to SDS-PAGE and/or western blotting.

2.2.3.2.2 Effects of NADH and NAD^+ on ArfGAP3 (AGD) and RIBEYE(B) interaction.

Effect of NADH / NAD^+ on ArfGAP3 (AGD) and RIBEYE (B) interaction was studied using bacterial fusion protein. Full-length ArfGAP3 (AGD)-MBP was used as a bait to pulldown eluted prey F.L. RIBEYE (B)-GST fusion protein. This setup was studied in the absence and presence of ascending gradient of NADH/NAD^+ concentration. In a reaction volume of 500µl, 0.3 µM of bait- and prey- proteins were used. Beads with immobilized bait protein were earlier blocked in binding buffer (100mM Tris-HCl (pH 8.0), 150mM NaCl, 1mM EDTA & 0.5% Triton X-100). The effect of NADH/NAD+ on interaction was studied, by adding NADH / NAD^- concentration ranging from 0nM-1.0µM in a binding buffer while 1mM ßME in binding buffer was used a positive control to see maximym binding of ArfGAP3 (AGD) MBP to RIBEYE (B) GST. The incubation was carried out for ON at +4°C on a rotary wheel. The reaction tubes were allowed to settle down and 4°C for 20 mins and supernatant was carefully removed and beads were washed 3times with cold binding buffer by centrifugation. Last beads were boiled in 20µl of 4X sample buffer at 97°C for 3 minutes and the proteins were resolved on 10% SDS-PAGE, and processed for western blotting as described in section 2.2.2.2. The membrane was probed with Anti- MBP. Afterwards, the membrane was stripped (see section 2.2.2.3) and incubated with Anti-GST or Anti-RIBEYE (U2656) antibody to check the equal bait protein loading.

2.2.3.2.3 Co-immunoprecipitation assays using protein extracts from the bovine retina

For each immunoprecipitation, a single isolated bovine retina was incubated in 1ml lysis buffer, containing 100mM Tris-HCl, pH 8.0, 150mM NaCl, 1mM EDTA, and 1%Tx-100 for 45 min on vertical rotator at 4°C. The sample was mechanically cracked by forcefully ejecting the retinal lysate through a 20gauge needle (20times). The sample was sonicated (Bandelin, Sonoplus) at 1% output for 20 half-second pulse ON/OFF cycles on ice. Afterwards, the extract was centrifuged at 13,000 rpm for 30 min at 4°C. The supernatant was transferred into a new eppendorf tube. The centrifugation step was repeated one time to remove all cell debris. The resulting lysate was pre-cleared by the addition of 15ml of pre-

immune serum and 20ml of washed protein A-Sepharose beads (2hrs incubation at 4°C with an overhead rotator). Next, samples were centrifuged at 13,000rpm for 30mins at 4°C. The supernatant was split in two equal volumes, for the control and experimental assays. For negative control immunoprecipitations, 15ml of ArfGAP3-Cterm3 pre-immune serum was added; for the experimental immunoprecipitation, 15ml of ArfGAP3-Cterm3 immune serum was added. Samples were incubated overnight at 4°C using an overhead rotator. Afterwards, beads are allowed to settle (for 20mins, on ice). The supernatants were removed and saved; the bead pellets were resuspended in 1.0ml of lysis buffer and washed thrice by repeated centrifugation (3,000rpm, 1min, 4°C). The final pellet was boiled in 10ml SDS sample buffer, subjected to SDS-PAGE, and analyzed by Western blotting with the indicated antibodies.

2.2.3.3 Morphological analysis of protein-protein interactions

2.2.3.3.1 Heterologous expression of recombinant proteins in COS7 cells

Transfection of COS7 cells was done with perfectin kit, according to the manufacturer's instructions (peQLab, Germany). COS7 cells were splitted into six well plates one day before the time of transfection with each well having sterile coverslips of 24mm diameter The cells were transfected with 1-2µg DNA each either eGFP or mcherry (Perfectin kit). The transfection mixture was added to coverslips in the 6 well plates. COS7 cells were serum starved for atleast 4-5 hours after transfection to increase the uptake of lipid-DNA complex. Afterwards, the cells were washed once with PBS and were incubated in DMEM+10%FCS medium at 37°C, 5% CO_2 for 24-48 hours depending on the efficiency of transfection. The cells were fixed and visualized by indirect immunofluorescence microscopy. Indirect immunofluorescence microscopy on cells was performed largely as previously described (Schmitz et al., 1996; von Kriegstein et al., 1999). Cells were fixed with 1% PFA for 30 minutes and washed 3 times with 1X cold PBS for 5 minutes each. Cells were mounted in 60% glycerol in PBS that contained 1.5% n-propyl gallate in order to retard photobleaching. Control (untransfected cells) were also processed and analyzed in similar manner in parallel with transfected cells. Samples were analysed and documented with an Axiovert 200M microscope equipped with respective filter blocks. The fluorescence images were documented with an AxioCam MRm camera (Zeiss).

2.2.3.3.2 Immunolabelling of 0.5µm-thin retinal resin sections

Epon-embedded retinal samples were prepared as previously described (Wahl et al., 2013) From the tissue blocks, 0.5µm -thin sections were cut with a Reichert ultramicrotome. Epon was removed as described (Wahl et al., 2013). In brief, Epon was removed by incubating the sections in the following solutions: sodium methanolate (30% solution in methanol (MERCK) for 10mins); 1:1 mixture of xylol/methanol (10min); acetone (2x10min), H_2O (10min), PBS (10mins). Afterwards, sections were incubated with the respective primary and secondary antibodies as described (Schmitz et al., 2000; Alpadi et al., 2008; Wahl et al., 2013) using the antibodies indicated at the respective experiments that were used at the dilutions summarized above. Immunolabelled sections were either analyzed by conventional epifluorescence microscopy or by super-resolution structured illumination microscopy as indicated. The imunofluorescence data shown in Figs. 9-14 was obtained from mouse retinal sections. Qualitatitvely similar images were obtained from semithin sections of the bovine retina (data not shown).

2.2.3.3.2.1 Affinity-purification of antibodies

Antibodies were affinity-purified by the method of Olmsted (1981). In brief, ≈50µg of fusion protein was loaded on a 10% SDS-PAGE and transferred to nitrocellulose. The ArfGAP3Cterm-GST/ArfGAP3Cterm2 fusion protein bands at ≈35kDa were cut out with a scalpel blade. These fusion protein-loaded nitrocellulose strips were used for the subsequent affinity-purification of the antisera. The nitrocellulose strips were treated with 5% skim milk powder in PBS (for ≈30mins at RT) to block non-specific protein sites. Next, nitrocellulose strips were incubated with the respective antisera (diluted 1:10 in 5% skim milk dissolved in PBS) and incubated overnight at 4°C. The nitrocellulose strips were washed several times with PBS to remove serum components that do not bind to the immobilized fusion protein. Bound antibodies were eluted from the nitrocellulose strips with a minimal volume (typically 200ml) of 0.2M glycine pH 2.7 for 3-4 mins (at 4°C). The antibody eluate was neutralized by the addition of 50mµl of 1M Tris, pH 8.5. Protein concentration was measured at 280nm and antibody diluted to a concentration of 0.1mg/ml with PBS complemented with bovine serum albumin (BSA, 0.1mg/ml). NaN_3 was added to a concentration of 0.05% to prevent bacterial growth.

2.2.3.3.2.2 Pre-absorption experiments

Preabsorption experiments were performed exactly as previously described (Wahl et al., 2013) using 50mg of the respective GST-fusion protein was used for blocking. Pre-absorbed

ArfGAP3Cterm2 and ArfGAP3Cterm3 immunsera were used at a 1:20 dilution for immunofluorescence microscopy and at a 1:3,000 dilution for western blotting.

2.2.3.3.3 Super-resolution structured illumination microscopy (SR-SIM)

In order to further improve the spatial resolution of our immunolabelling analyses, I applied multicolour super-resolution (SR) 3D-SIM analyses (Schermelleh et al., 2008). The resolution of normal microscopy is limited to ≈200nm in lateral (XY) and ≈500nm in axial (Z) direction. Super-resolution microscopy gives the possibilty to exceed this diffraction limit. SR-SIM increases the normal lateral resolution by factor of two and 3D-super-resolution structured illumination microscopy (3D SR-SIM) provides the same increase in axial direction. Furthermore, SR-SIM allows us to use standard dyes and staining protocols (for review, see Schermelleh et al., 2010). Super-resolution structured illumination microscopy (SR-SIM) was performed exactly as previously described using the Elyra PS1 setup (Wahl et al., 2013). Images were taken with a 63x Plan-Apochromat objective (numerical aperture of 1.4) with excitation light wavelengths of 488nm, 561nm and 647nm, and then processed for super-resolution structured illumination microscopy to obtain higher resolutions (Gustafsson et al., 2008; for review, see Schermelleh et al., 2008, 2010). The employed ZEISS setup for SR-SIM was checked for chromatic aberration in X-, Y- and Z-direction using multicolour beads. For acquisition and processing, the Zen2010 software (Zeiss, Germany) was used.

2.2.3.3.4 Triple immunolabelling of 0.5µm thin retinal sections

Triple immunolabelling experiments were performed as previously described (Wahl et al., 2013). In brief, we used a directly labelled mouse monoclonal antibody against RIBEYE(B)-domain/CtBP2 (BD) conjugated with DyLight650, and two other primary antibodies (one from mouse, the second from rabbit [as indicated in the respective experiments]), which were not directly fluorophore-labelled. First, sections were incubated with the two unlabelled primary antibodies at the same time overnight (at the dilutions given above). On the next day, sections were washed 3 times with PBS and afterwards incubated with the respective secondary antibodies (donkey anti-rabbit Alexa568 and chicken anti-mouse Alexa488). After 1hr incubation, sections were washed again 3times with PBS and finally incubated with the directly DyLight647-labelled CtBP2 primary antibody (in the dilutions summarized above) overnight at 4^{o}C. After overnight incubation, sections were washed 3 times with PBS and embedded with anti-fade solution containing n-propyl gallate (NPG) as previously described (Schmitz et al., 2000).

2.2.3.4 Functional basis of protein-protein interaction

2.2.3.4.1 Preparation of retinas from the adult mouse for electroporation.

Retinas were isolated from adult mice within 5 min postmortem (in dim ambient light). The enucleated eyes were bisected at the equatorial plane and the posterior eye cup was transferred into ice-cold artificial CSF (ACSF) containing the following (in mM): 119 NaCl, 2.5 KCL, 2.5 $CaCl_2$, 1.3 $MgCl_2$, 1 NaH_2PO_4, 20 glucose, and 11 HEPES, pH 7.4, osmolarity ≈300 mOsm/L. ACSF was saturated with 5% CO_2/95% O_2 (carbogen) before use. From the posterior eyecup, the retina was gently peeled off from the pigment epithelium. Isolated retinas were transferred to black-gridded nitrocellulose filter membranes (Millipore, #HABG01300) with the ganglion cell side facing the nitrocellulose membrane. Thus, photoreceptors were facing the free surface and were in direct contact with the DNA plasmid solutions added to them in the electroporation experiments (see below). The filters with the attached retinas were transferred to sterile Petri dishes (3 cm diameter) containing ≈1.0 ml of AMES' medium, pH 7.4 (A1420, Sigma-Aldrich) pre-incubated at 37°C.

2.2.3.4.2 Electroporation of isolated mouse retinas and retinal explant culture.

Electroporation of adult mouse retinas was performed largely as previously described (Donovan and Dyer, 2006; Briggman and Euler, 2011; Vergara et al., 2013). Electroporation was performed with a square wave pulse electroporator and a tweezertrode electroporation device. Both electrodes of tweezertrode were dipped in ACSF buffer to obtain a good electrical connection. Excess of ACSF was removed with filter paper to avoid dilution of the DNA. Before electroporation, DNA was column purified. For each electroporation, 50ug of purified DNA was used. Immediately after isolation, the retina was placed in between the tweezertrode. The retina attached to the nitrocellulose was facing the positive electrode with the ganglion cell side while the plasmid DNA solution was added to the photoreceptor side at negative electrode in hanging drop manner. The distance between the two electrodes was optimized to approximately 3–4 mm. Electroporation was done at 20 V, 950 ms OFF, 20 ms ON (10 pulses). Electroporated retinas were transferred back to Petri dishes containing 1.0 ml of AMES' medium, pH 7.4. Retinas were transferred to open Petri dishes that were placed in an incubation chamber, as previously described (Morgan et al., 2011; Williams et al., 2013). Temperature was continuously maintained at 32°C using a feedback temperature controller and a transparent ITO heater attached to the incubation chamber. The incubation

chamber was filled with distilled H_2O to the lower edge of stage where the Petri dish with the retina was placed and continuously gassed with carbogen (5% CO_2/95% O_2). Retinas were incubated inside the light-protected incubation chamber typically for 18–24 h.

2.2.3.4.3 Loading of photoreceptors with FM1–43.

Isolated, electroporated retinas were incubated for 15 min in LCS containing 20µM FM1–43 at 37°C in the dark, similar to the procedure described by Rea et al. (2004). I used this method, because it favors specific FM1–43 uptakes in photoreceptor synaptic terminals (Rea et al., 2004). After labeling, the retinas were rinsed thrice with LCS and processed for the isolation of photoreceptor cells.

2.2.3.4.4 Dissociation of electroporated retinas and isolation of photoreceptors.

24hours after electroporation, photoreceptors were isolated from the retina with a papain digestion procedure, largely as described previously (Wahl et al., 2013). The enzyme solution containing 6 U/ml papain in low Ca^{2+}-containing saline solution (LCS solution; containing 132 mM NaCl, 3 mM KCl, 1 mM $MgCl_2$ X $6H_2O$, 0.5 mM $CaCl_2$, 10 mM sodium pyruvate, 10 mM glucose, and 10 mM HEPES, pH 7.4, ≈ 300 mOsm/L) was activated with 2.7 mM L-cysteine at 37°C for 20 min before the experiments. Isolated retinas were incubated in 1 ml of the cysteine-activated papain solution for 10 min at 25°C. LCS was saturated with 5% CO_2/95% O_2 before use. After removal of the papain solution, the retina was gently washed three times with 1ml of LCS solution containing 2% FCS and 0.01 mg/ml DNase (Sigma, #DN25-110MG). To dissociate photoreceptor cells, papain-treated retinas were very gently triturated (1–2 times) with a wide-bore plastic Pasteur pipette. The resulting cell suspension was plated on Concanavalin A coated coverslips. For coating of a 25 mm round coverslip, ≈200 µl of 1 mg/ml Concanavalin A (in LCS solution) was added to coverslips for 1 h at RT. Unbound Concanavalin A was removed by washing thrice with LCS before the addition of the dissociated cells. Cells were allowed to settle on the coverslips for 30 min at 37°C for tight attachment. Unbound retinal cells were removed by gentle washes with LCS. Photoreceptors were identified based on their typical morphology. Photoreceptors were fixed with 4% PFA in PBS for 15 min at RT. After several washes with PBS, cells were mounted with NPG antifade as previously described (Wahl et al., 2013, Dembla et al., 2014).

3 RESULTS:

3.1 ArfGAP3 binds to RIBEYE(B)-domain in the YTH system

Using RIBEYE(B) as a bait (Alpadi et al., 2008), I obtained full-length ArfGAP3 as a potential RIBEYE-interacting protein in the YTH system.

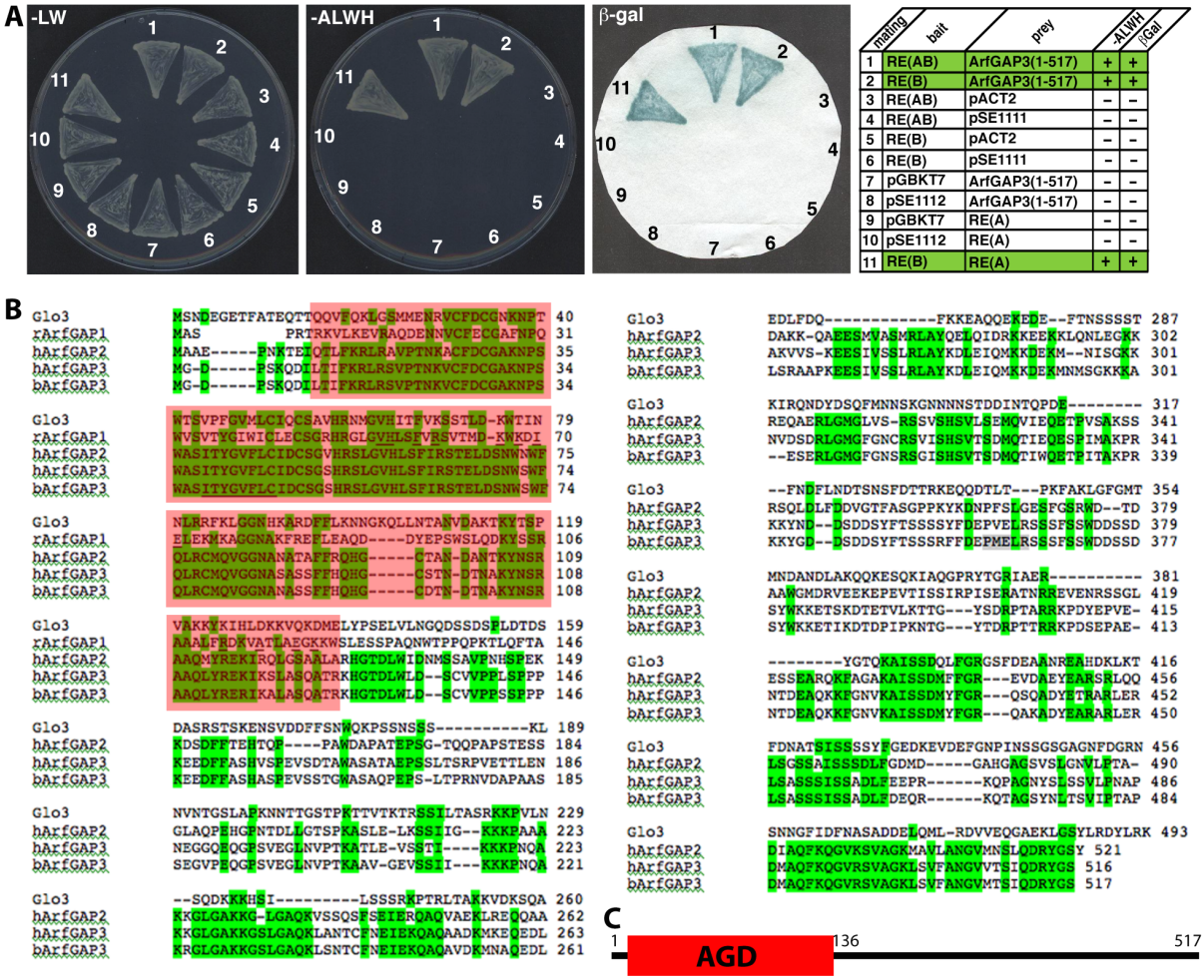

Figure 14: Interaction of RIBEYE(B) and RIBEYE(AB) with ArfGAP3 in the YTH system. RIBEYE(B) interacts with ArfGAP3 in YTH. Summary plates of YTH analyses obtained with the indicated bait and prey plasmids. For convenience, experimental bait-prey pairs are underlayered in color (green in case of interacting bait-prey pairs; yellow in case of non-interacting bait-prey-pairs; control matings are non-colored). RIBEYE(B) and also full-length RIBEYE (RIBEYE(AB) interact with ArfGAP3 in the YTH system (matings #1 and #2). Mating #11 in Fig. 1A denotes an unrelated positive control mating (Magupalli et al., 2008). pSE1111 is an irrelevant prey vector and pSE1112 an irrelevant bait vector (Tai et al., 1999; Magupalli et al., 2008). Control matings of both ArfGAP3 prey clones with empty bait clones (mating #7) or irrelevant bait clones (mating #8) demonstrate that the full-length ArfGAP3 clone is not auto-activating. The other matings represent control matings for the RIBEYE bait clones (matings #4-7) or RIBEYE prey clones (matings #9,10). (B) Amino acid sequence of bovine ArfGAP3 in comparison to the yeast parent ArfGAP glo3, rat ArfGAP1, human ArfGAP2 and human ArfGAP3. The catalytically active ArfGAP-domain (AGD) of ArfGAP3 is boxed in red. More than three identical amino acids in the alignment of the four sequences are denoted in green. The underligned 8 amino acids in the AGD of ArfGAP3 denote a deletion in the original ArfGAP3 clone that interacts with RIBEYE(B) (data not shown). The interaction between RIBEYE(B) and ArfGAP3 persists if a prey was used (from an EST clone; (accession number BC118087; IMAGE clone 8081904)) that does not possess this 8 amino acid deletion indicating that the interaction is real in the YTH system. Except for this 8 amino acid deletion in the AGD domain which is probably a cloning artefact the sequence is identical to the bovine ArfGAP3 sequence deposited at Genbank (accession number BC118087). (C) Schematic domain structures of ArfGAP3. The AGD domain is located in an aminoterminal position. The carboxyterminus of ArfGAP3 is heterogeneous and displays little similarity to other ArfGAPs, i.e. ArfGAP1.

The originally obtained full-length clone of ArfGAP3 from the YTH screen contained 8 amino acid-long deletion in the Zn-finger motif of the ArfGAP-domain of ArfGAP3 (Fig. 13B and data not shown). In order to exclude an artificial interaction of these two proteins in the YTH system, I cloned the full-length bovine ArfGAP3 cDNA (without an 8 amino acid deletion in the Zn-finger motif) from an IMAGE clone (BC118087; IMAGE clone 8081904 encoding full-length bovine ArfGAP3) into the pACT2 prey vector and re-tested this full-length ArfGAP3 prey construct for its interaction with RIBEYE(B) in the YTH system. Similary to the original prey clone, I obtained a strong interaction between RIBEYE(B) and full-length ArfGAP3, as judged by growth on –ALWH selective medium (supplemented with aminotriazole and aureobasidine for increased stringency) and expression of beta-galactosidase (Fig. 13A) indicating that the interaction between ArfGAP3 and RIBEYE(B) is real in the YTH system. Fig. 13C schematically summarizes the domain structure of ArfGAP3.

3.2 Mapping of RIBEYE-ArfGAP3 interaction in the YTH system: the NAD(H)-binding sub-domain RIBEYE(B) binds to the AGD-domain of ArfGAP3

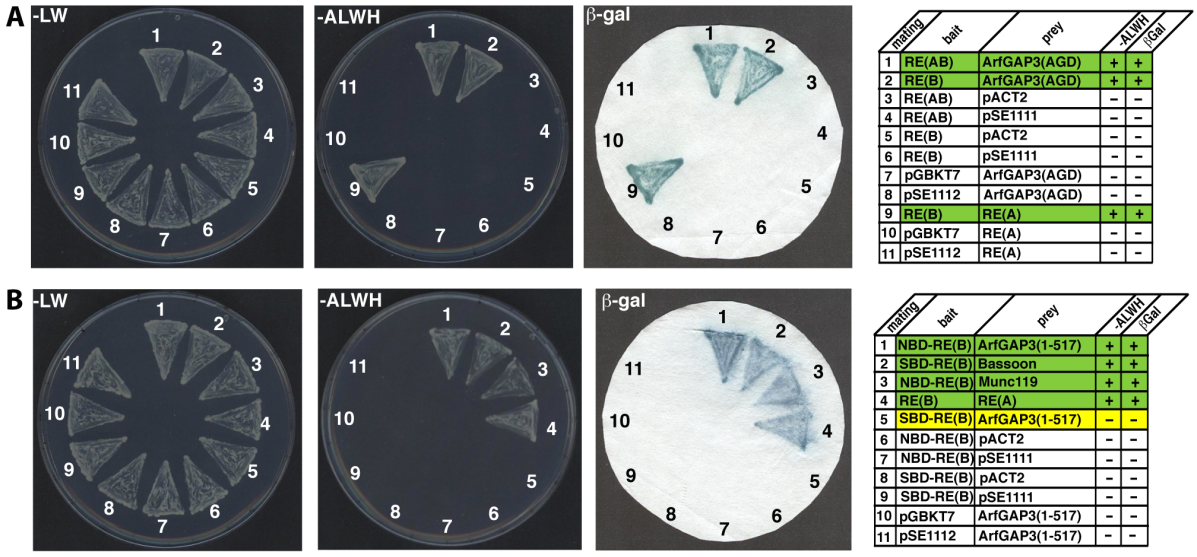

mating	bait	prey	-ALWH	βGal
1	RE(AB)	ArfGAP3(AGD)	+	+
2	RE(B)	ArfGAP3(AGD)	+	+
3	RE(AB)	pACT2	–	–
4	RE(AB)	pSE1111	–	–
5	RE(B)	pACT2	–	–
6	RE(B)	pSE1111	–	–
7	pGBKT7	ArfGAP3(AGD)	–	–
8	pSE1112	ArfGAP3(AGD)	–	–
9	RE(B)	RE(A)	+	+
10	pGBKT7	RE(A)	–	–
11	pSE1112	RE(A)	–	–

mating	bait	prey	-ALWH	βGal
1	NBD-RE(B)	ArfGAP3(1-517)	+	+
2	SBD-RE(B)	Bassoon	+	+
3	NBD-RE(B)	Munc119	+	+
4	RE(B)	RE(A)	+	+
5	SBD-RE(B)	ArfGAP3(1-517)	–	–
6	NBD-RE(B)	pACT2	–	–
7	NBD-RE(B)	pSE1111	–	–
8	SBD-RE(B)	pACT2	–	–
9	SBD-RE(B)	pSE1111	–	–
10	pGBKT7	ArfGAP3(1-517)	–	–
11	pSE1112	ArfGAP3(1-517)	–	–

Figure 15: Interaction of the NBD-domain of RIBEYE(B) with the AGD-domain of ArfGAP3 in the YTH system. (A) RIBEYE interacts with the ArfGAP-domain (AGD) of ArfGAP3. Summary plates of YTH analyses obtained with the indicated bait and prey plasmids. For convenience, experimental bait-prey pairs are underlayered in color (green in case of interacting bait-prey pairs; yellow in case of non-interacting bait-prey-pairs; control matings are non-colored). RIBEYE(B) and also full-length RIBEYE (RIBEYE(AB)) interact with ArfGAP-domain (AGD) of ArfGAP3 in the YTH system (matings #1 and #2). Mating #9 in Fig. 14A denote an unrelated positive control mating (Magupalli et al., 2008). The other matings are auto-activation control matings. None of the shown yeast constructs is auto-activating. (B) The NAD(H)-binding sub-domain of RIBEYE(B) interacts with ArfGAP3. Summary plates of YTH analyses obtained with the indicated bait and prey plasmids. For convenience, experimental bait-prey pairs are underlayered in color (green in case of interacting bait-prey pairs; yellow in case of non-interacting bait-prey-pairs; control matings are non-colored). The NAD(H)-binding sub-domain of RIBEYE(B), the NBD, interacts with ArfGAP3 (lane 1); but not the substrate-binding sub-domain of RIBEYE(B), the SBD (lane 5). Lanes #2-4 are positive control matings for the respective constructs (bassoon for SBD-RE(B) (tom Dieck et al., 2005); Munc119 for NBD-RE(B) (Alpadi et al., 2008); RE(A) for RE(B) (Magupalli et al., 2008); lanes 6-#11 are negative controls (auto-activation controls).

Next, I tested with the YTH system, which part of ArfGAP3 is relevant for the interaction with RIBEYE(B). I found that the AGD encoding aa1-aa136 of ArfGAP3 is responsible for the interaction with RIBEYE(B) (Fig. 14A). The C-terminus of ArfGAP3 did not interact with RIBEYE(B) (data not shown). RIBEYE(B) consists of an NADH-binding sub-domain (NBD) and a substrate-binding sub-domain (SBD) (Kumar et al., 2002; Nardini et al., 2003; for review, see Schmitz, 2009; Schmitz et al., 2012). YTH analyses were used to further map RIBEYE(B)/ArfGAP3 interaction. YTH-analyses demonstrated that the NBD interacts with ArfGAP3 (Fig. 14B, mating #1). The SBD did not promote ArfGAP3/RIBEYE(B) interaction in the YTH system (Fig. 14B, mating#5). The SBD domain interaction with bassoon validates its proper folding also confirms the negative interaction of SBD domain with AGD domain.

3.3 RIBEYE(B) interacts with ArfGAP3 in fusion protein pulldown assays

I used various independent approaches to verify the interaction between RIBEYE(B)-domain and the ArfGAP-domain (AGD) of ArfGAP3. First, I performed pulldown experiments using bacterially expressed and purified fusion protein (Fig. 15A,B). I used MBP-tagged fusion proteins (ArfGAP3 (AGD)-MBP and MBP alone) as immobilized bait proteins and GST-tagged proteins (RIBEYE(B)-GST and GST alone) as soluble prey proteins. For the pulldown experiments described in Fig. 15A,B, the buffer contained 1mM ß-mercaptoethanol (ßME; see Materials and Methods). ArfGAP3(AGD)-MBP (but not MBP alone) interacted with RIBEYE(B)-GST (but not with GST alone) as judged by protein pulldown analyses in SDS-PAGE (Fig. 15A,B). Specificity of interaction was consistently shown both by SDS-PAGE (Fig. 15A,B) and western blot analyses (Fig. 16; and data not shown). Identical results were obtained when tags were switched. Typically, ≥30% of the input fraction of the prey protein was bound to the immobilized bait fusion protein in these pull-down experiments.

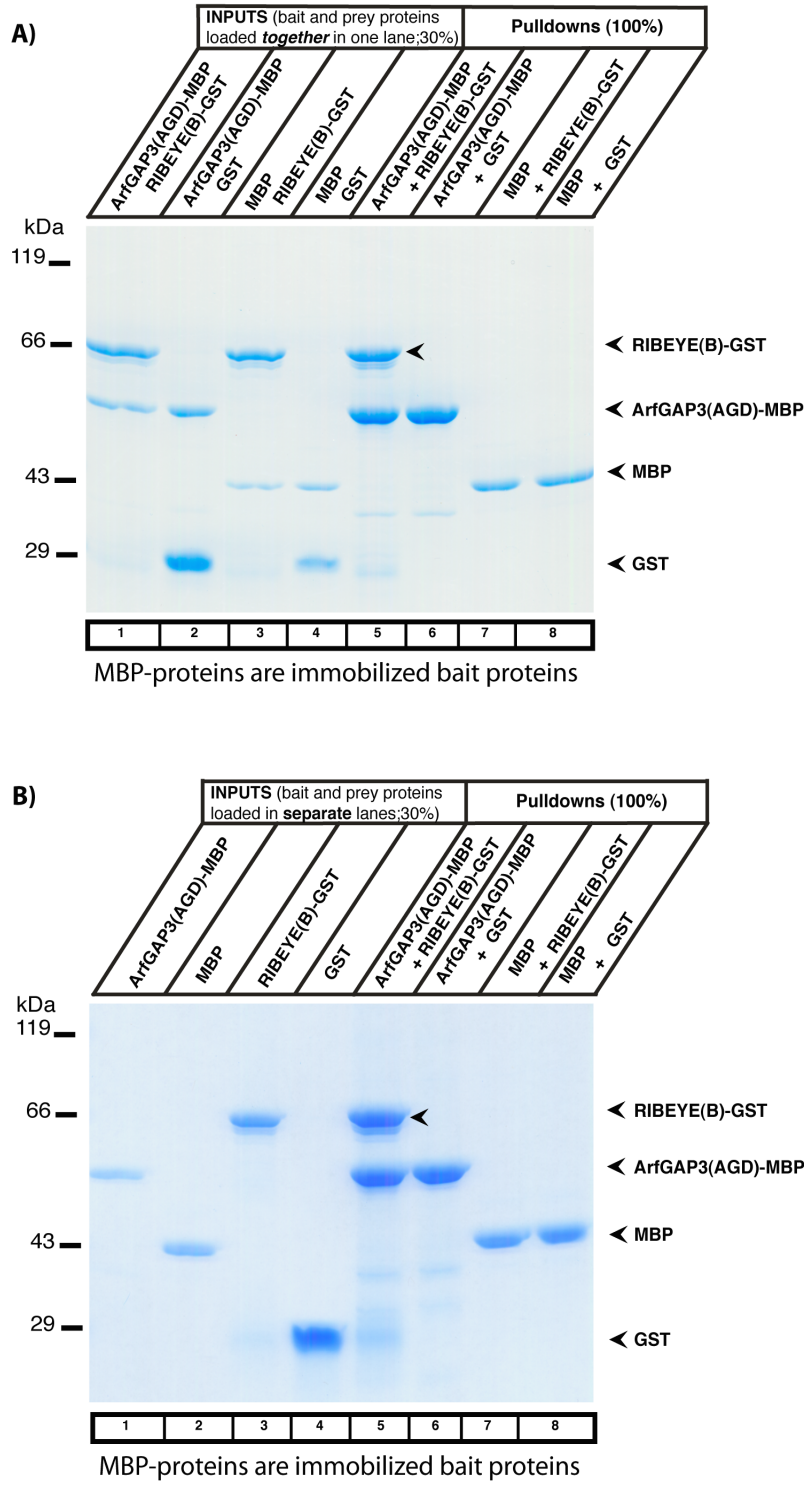

Figure16: RIBEYE(B) specifically interacts with ArfGAP3 in fusion protein pulldown assays (SDS-PAGE analyses). (A) Pulldown analyses of RIBEYE(B)/ArfGAP3 complexes using bacterially expressed fusion proteins. In Fig. 15, pulldown experiments were analyzed by Coomassie Blue-stained polyacrylamide gel after SDS-PAGE. Lanes 1-4 show the indicated purified fusion proteins (input fractions). Please note that due to limitations in lane numbers of the minigel system, both bait and prey input proteins were loaded in the same gel lane (30% of total input of both proteins). For documentation of binding experiments, in which the same experiments were done but with the single input proteins loaded in separate lanes, please see Fig. 15B. All input lanes, represent 30% of the input fraction. In lanes 5-8, 100% of the pulldown reactions were loaded. MBP-tagged fusion proteins were used as immobilized bait proteins and GST-tagged proteins as soluble prey proteins. Only ArfGAP3-MBP pulled-down RIBEYE(B)-GST (lane 5) but not MBP alone (lane 7). Neither MBP alone nor ArfGAP3-MBP pulled down GST alone (lanes 6,8). SDS-PAGE demonstrated that ArfGAP3-MBP pulled-down RIBEYE(B)-GST demonstrating interaction of the two proteins in this assay system. (B) The pulldown assay shown in (B) is identical to the one shown in (A) except that the input proteins were loaded in separate lanes. This was done to demonstrate that the input fusion proteins display only a single, main protein band.

3.4 RIBEYE(B) specific interaction with ArfGAP3 (AGD) confirmed by western blot assay using antibodies against fusion tag.

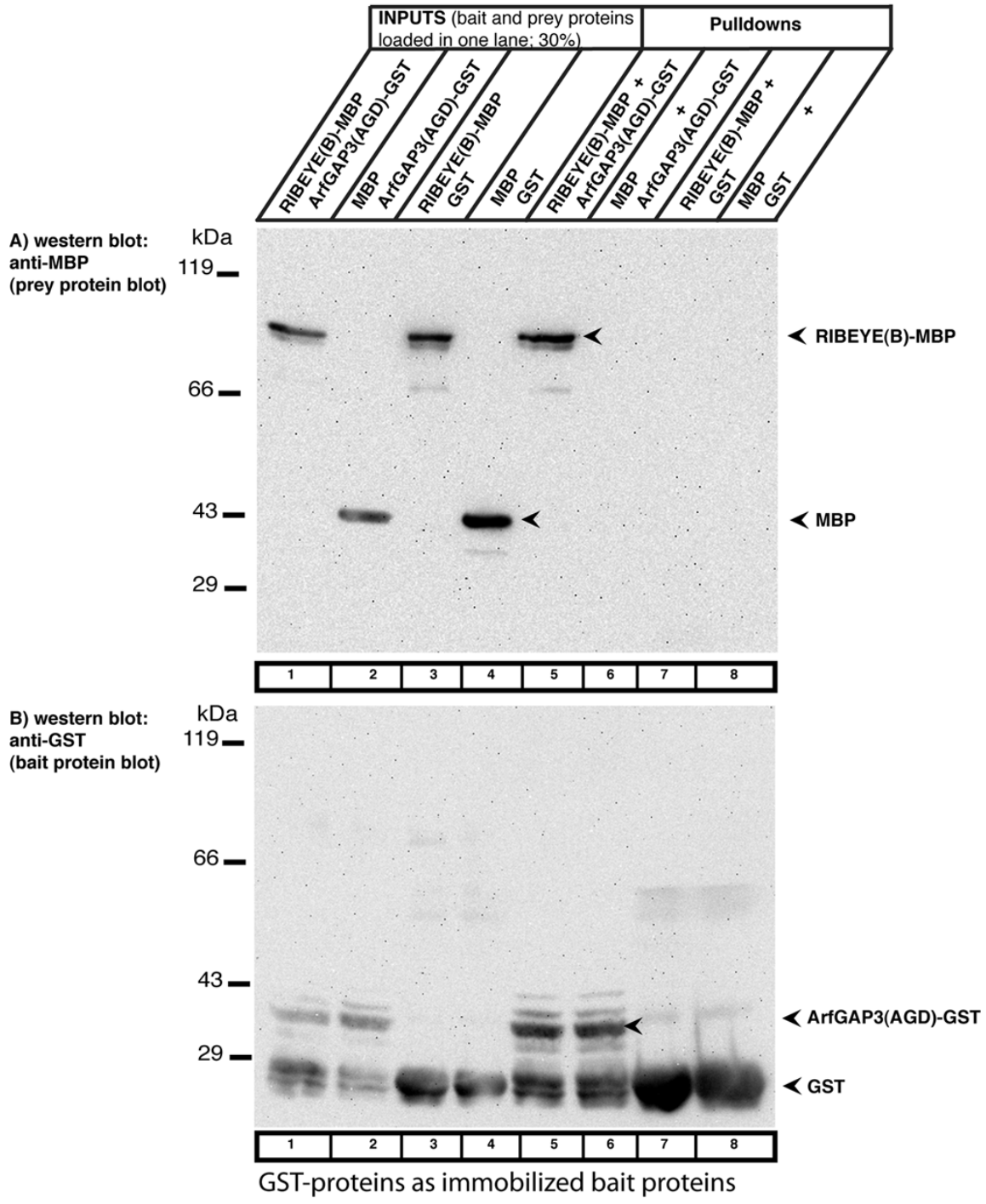

Figure17: RIBEYE(B) specifically interacts with ArfGAP3 in fusion protein pulldown assays (western blot analyses). In order to exclude that the tag has an importance for the pull-down results and to further exclude that any prey protein is unspecifically pulled-down by bait-GST I also analyzed the results of the pulldown assays by western blotting with anti-MBP and anti-GST antibodies. The reaction buffer used for these experiments contained 1 mM ß-mercaptoethanol (ßME). In the experiment shown in Fig. 16, GST-tagged fusion proteins were used as immobilized bait proteins and eluted MBP-proteins as soluble prey proteins. Similarly, to the experiments described in Fig. 15, only RE(B)-MBP (lane 5) but not MBP alone (lane 6) is pulled-down by the ArfGAP-domain-GST. GST alone does not pull-down RE(B)-MBP as well as MBP alone as shown by western blotting with antibodies against MBP (Fig. 16B) demonstrating the specificity of the interaction and completely confirming the results in Fig. 15. In Fig. 16B) same blot as analyzed in (Fig. 16A) was reprobed (after stripping) with antibodies against GST to show equal loading of the bait proteins. Abbreviations: RE(B)-MBP, RIBEYE(B)-MBP.

In Figure 16, RIBEYE(B) was tagged with MBP and ArfGAP3(AGD) with GST. Also with these switched tags, a strong interaction was observed between RIBEYE(B) and ArfGAP3. Typically, ≥30% of the input fraction of the RIBEYE(B) prey protein was bound to the immobilized ArfGAP3 bait fusion protein. Western blot was performed with antibodies against MBP and GST to confirm the specific interaction between ArfGAP3 and RIBEYE and no interference due to fusion tags MBP and GST.

3.5 Interaction between ArfGAP3 (AGD) and RIBEYE(B) is regulated by NAD(H) in a redox-sensitive manner

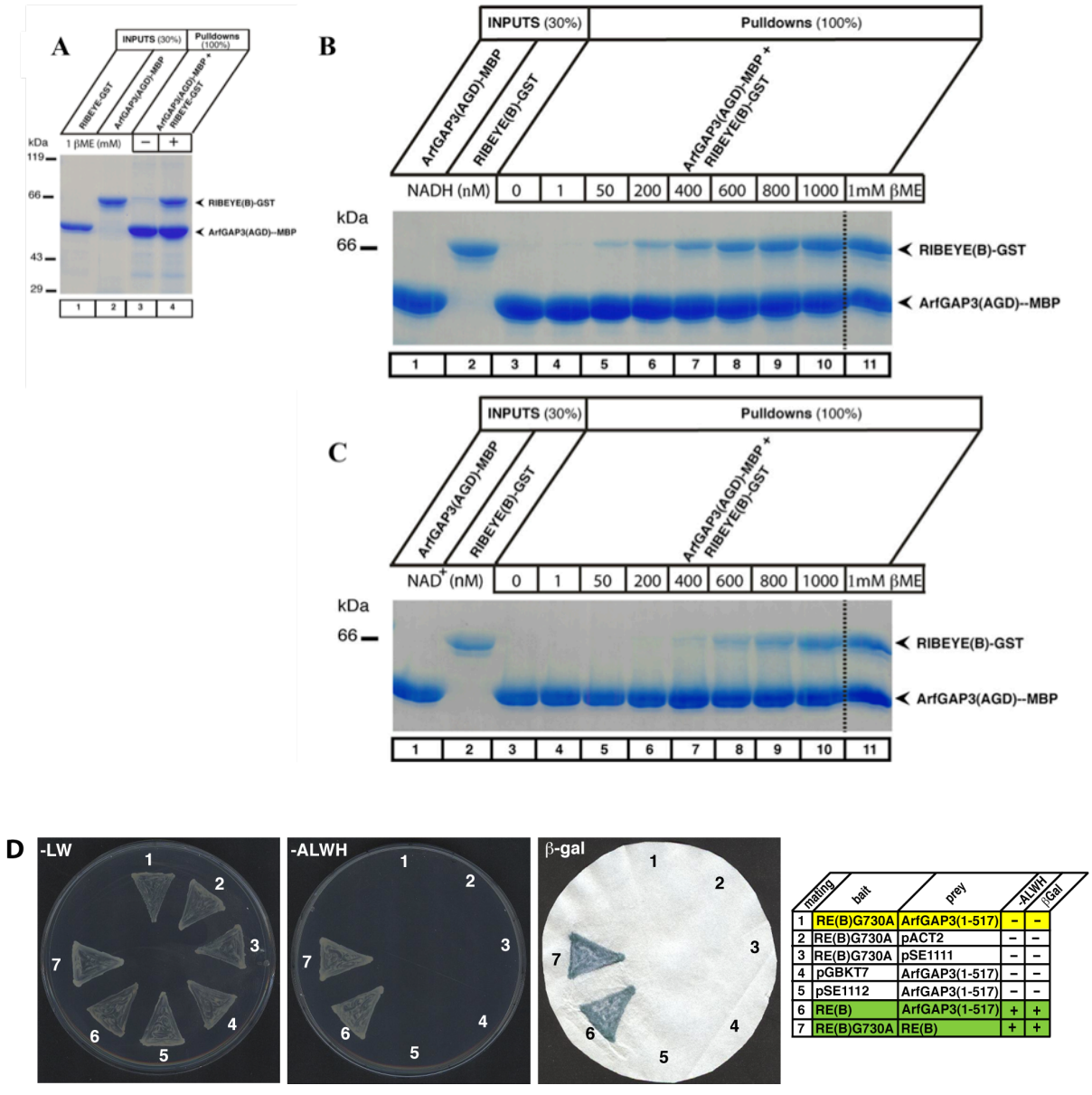

Figure 18: The binding between RIBEYE(B)-domain and the AGD of ArfGAP3 is stimulated by NAD(H). (A) Pulldown experiments were performed as in Fig. 15 in the absence (lane 3) or presence (lane 4) of 1mM ß-mercaptoethanol (ßME). ArfGAP3 binds to AGD of ArfGAP3 only in the presence (lane 4) but only in a very minor amount in the absence (lane 4) of 1 mM ß-mercaptoethanol (ßME). Lanes 1,2 are the respective input fractions (30% input). (B, C) Next, I tesed

whether addition of NAD^+ (B) or NADH(C) could substitute for the presence of 1mM ß-mercaptoethanol (ßME) in promoting ArfGAP3/RIBEYE(B) interaction. As a matter of fact, increasing concentrations of both NAD^+ (B) as well as NADH (C) could promote binding of RIBEYE(B)-GST to the AGD of ArfGAP3 even in the absence of 1mM ß-mercaptoethanol (ßME). Semiquantitative evaluation of the binding experiments demonstrated that ≈400nm for NADH and ≈600nm for NAD is promoting half-maximal binding of ArfGAP3 to RIBEYE(B) in our pulldown assays. (D) A NAD(H)-binding-deficient point mutant of RIBEYE(B), RIBEYE(B)G730A, no longer interacts with the ArfGAP-domain (AGD) of ArfGAP3 in the YTH system. Summary plates of YTH analyses obtained with the indicated bait and prey plasmids. For convenience, experimental bait-prey pairs are underlayered in color (green in case of interacting bait-prey pairs; yellow in case of non-interacting bait-prey-pairs; control matings are non-colored).

The fusion protein pulldown binding experiments shown above were done with buffer that contained 1mM ßME. If ßME was omitted, binding between ArfGAP3 and RIBEYE(B) was strongly diminished (Fig. 17A). Since YTH demonstrated that the NAD(H)-binding sub-domain of RIBEYE(B), the NBD, is responsible for the interaction with ArfGAP3 (see above), I tested whether the addition of NADH could replace ßME in promoting ArfGAP3/RIBEYE(B). As a matter of fact, NAD(H) was very efficient in promoting RIBEYE/ArfGAP3 interaction (Fig. 17B,C). Semiquantitative analysis showed binding half-maximal of ≈400nm for NADH and ≈600nm for NAD^+ for promoting interaction of ArfGAP3 to RIBEYE(B) in pull-down assays. Previously, it has been shown that 1mM ßME promotes a conformation of RIBEYE(B) that can be also induced by the addition of NAD(H) (Venkatesan et al., 2010). From the fusion protein experiments described above (Fig. 17B,C), I concluded that NAD(H) promotes RIBEYE(B)/ArfGAP3 interaction. In line with this proposal is our further finding, that an NAD(H)-binding deficient RIBEYE(B) point mutant, RIBEYE(B)G730A (Alpadi et al., 2008; Schwarz et al., 2011), did not interact with ArfGAP3(AGD) in the YTH system (Fig. 17D).

3.6 ArfGAP3 interacts with RIBEYE (B) in transfected COS cells

Next, I tested whether RIBEYE (B) and ArfGAP3 would interact with each other in transfected COS cells. When ArfGAP3 was transfected alone, ArfGAP3 (tagged with mCherry) was enriched at a perinuclear region that represents the Golgi apparatus (Fig. 18 A, B) similarly as previously described (Dogic et al., 1999; Eugster et al., 2000; Lewis et al., 2004; Watson et al., 2004; Frigerio et al., 2007; Kliouchnikov et al., 2009). When RIBEYE (B)-EGFP was transfected alone (Fig. 18C), it was largely diffusely distributed throughout the entire cell (as previously described; Schmitz et al., 2000). In contrast, when RIBEYE (B) was co-transfected with ArfGAP3 RIBEYE (B) was nearly completely recruited to the ArfGAP3-typical Golgi-like localization in the perinuclear region (Fig. 18 D1-3) indicating interaction of RIBEYE and ArfGAP3 also in transfected COS cells. These data demonstrate that ArfGAP3 also interacts with RIBEYE (B) in transfected COS cells.

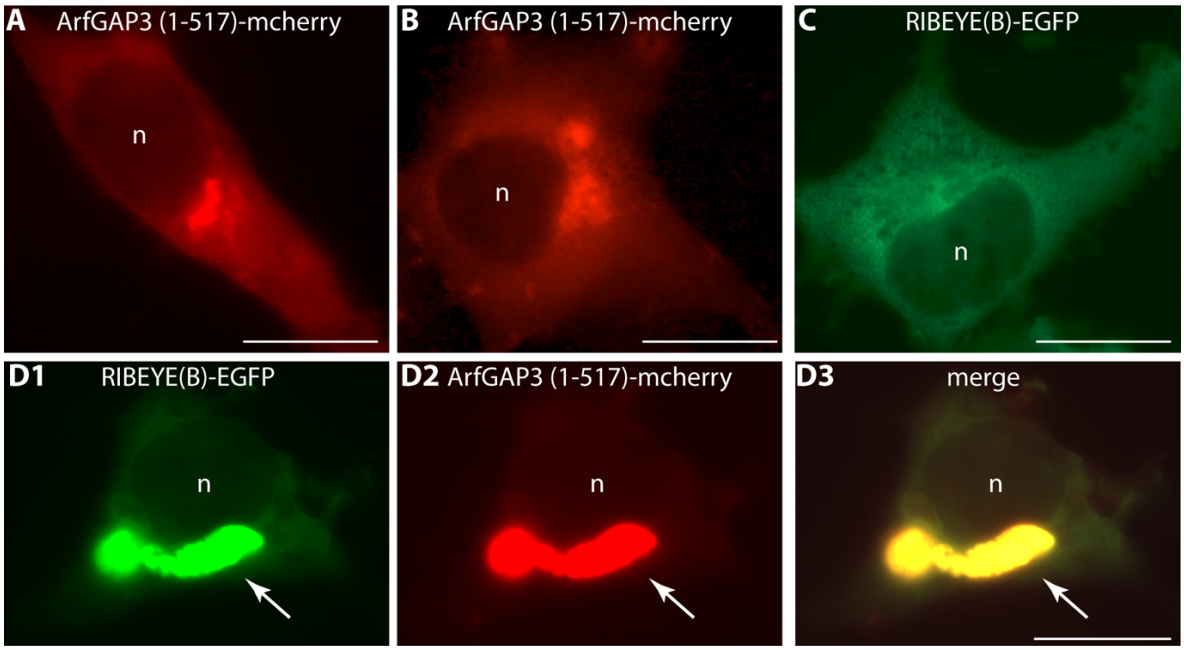

Figure 19: RIBEYE(B) is recruited by ArfGAP3 into a Golgi-like distribution. COS7 cells were transfected with the indicated mcherry-tagged ArfGAP3 or EGFP-tagged RIBEYE(B) constructs. Transfected cells were analyzed for the intracellular distribution of the respective proteins via direct epifluorescence microscopy. Cells transfected with ArfGAP3-mcherry alone show the typical enrichment at the Golgi apparatus in a perinuclear localization (Fig. 18 A, B), as already previously shown (Dogic et al., 1999; Eugster et al., 2000; Lewis et al., 2004; Watson et al., 2004; Frigerio et al., 2007; Kartberg et al., 2010; Yu et al., 2012). In contrast, RIBEYE(B) is diffusely distributed in single-transfected cells (Fig. 18C) (Schmitz et al., 2000). If RIBEYE(B)-EGFP is co-transfected with ArfGAP3-mcherry, RIBEYE(B) virtually completely redistributed from a diffuse distribution into the Golgi-like, perinuclear localization indicating interaction between RIBEYE(B) and ArfGAP3 also in transfected COS cells. Abbreviations: n, nucleus. The arrows in D-F point to the Golgi-like localization to which the RIBEYE(B)-EGFP signal is translocated in cells that were double-transfected with ArfGAP3-mCherry. Scale bars: 10µm (A-F).

3.7 Antibodies generated against cterm regions of Arfgap3 shows enrichment of ArfGAP3 in retina confirmed by western blot.

ArfGAP3Cterm2-pGEX and ArfGAP3Cterm3-pGEX fusion constructs were electroporated into BL21(DE3) and fusion proteins were expressed and purified as previously described (Schmitz et al., 2000). Antibody were generated by injecting fusion protein into rabbit and consecutive immune serum were collected and confirmed for its reactivity by western blot analysis against the fusion protein and also endogenous protein in retina lysate. Pre-absorption experiments were performed exactly as previously described (Wahl et al., 2013) using 50µg of the respective GST-fusion protein. Pre-absorbed ArfGAP3Cterm2 and ArfGAP3Cterm3 immunosera were used at a 1:3,000 dilution for Western blotting

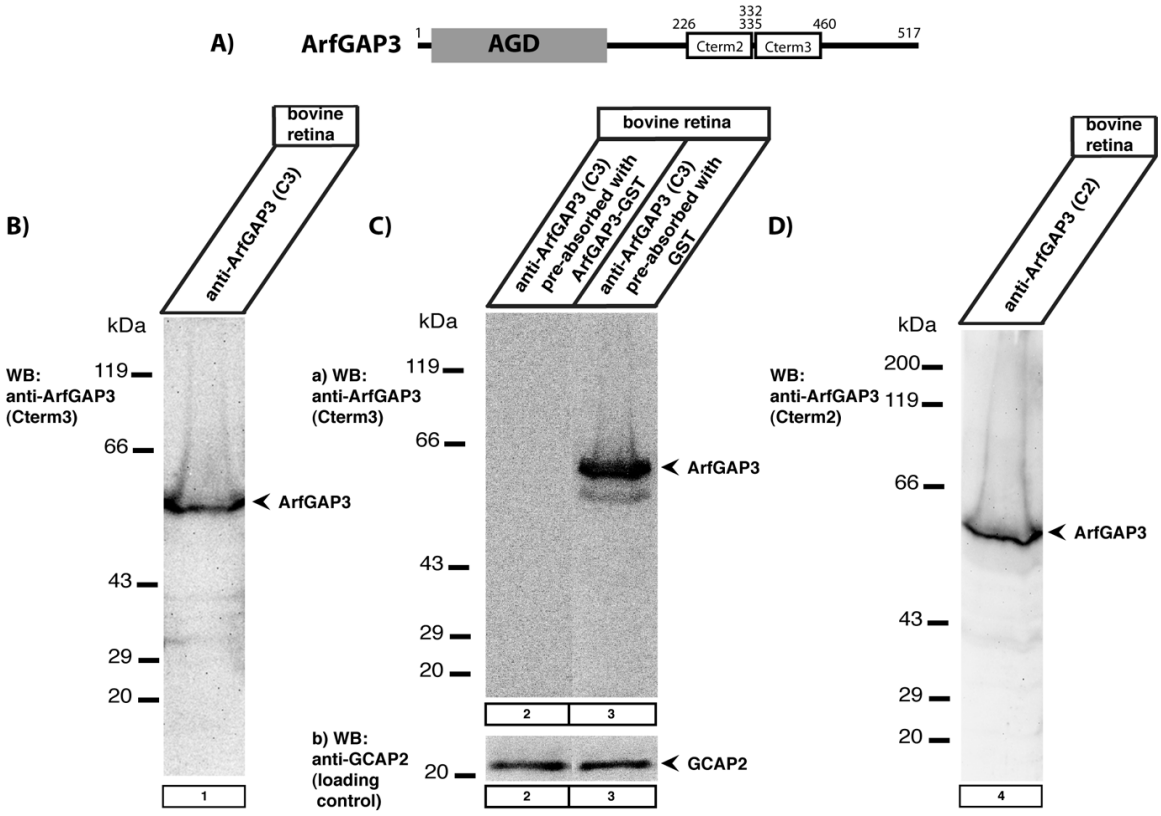

Figure 20: Western blots analyses of two antibodies that were generated against the carboxyterminus of ArfGAP3. A) The schematic drawing denotes the areas against which the two-poyclonal antibodies were generated. The antibody ArfGAP3 (Cterm2) was generated against a GST-fusion encoding aa226-aa335 or bovine ArfGAP3. The antibody ArfGAP3 (Cterm3) was generated against a GST fusion protein encoding aa332-460 of bovine ArfGAP3. (B-D) Both antibodies (Cterm2 and Cterm3 detected a single band at the expected running position of ArfGAP3 at 55kDa. This western blot band could be blocked by pre-absorption with the respective fusion protein (Fig 19C, and data not shown). Fig. 19Cb is a loading control (immunoblotting of the same blot as shown in a) after stripping of the blot and re-probing with an antibody against GCAP2 (Venkatesan et al., 2012) demonstrating equal protein loading.

3.8 ArfGAP3 can be co-immunoprecipitated with antibodies against RIBEYE from bovine retina

Next, I prepared extracts from bovine retina as described in Materials and Methods and tested whether antibodies against ArfGAP3 co-immunoprecipitated endogenous retinal RIBEYE. ArfGAP3 (Cterm3) immune serum (but not ArfGAP3 pre-immune serum) co-immunoprecipitated RIBEYE together with ArfGAP3 showing interaction of these proteins also in the retina *in-situ* (Fig. 20). Both RIBEYE and ArfGAP3 were strongly enriched in the experimental (Fig. 20, lane 3) but not in the control (Fig. 20, lane 2) immunoprecipitates

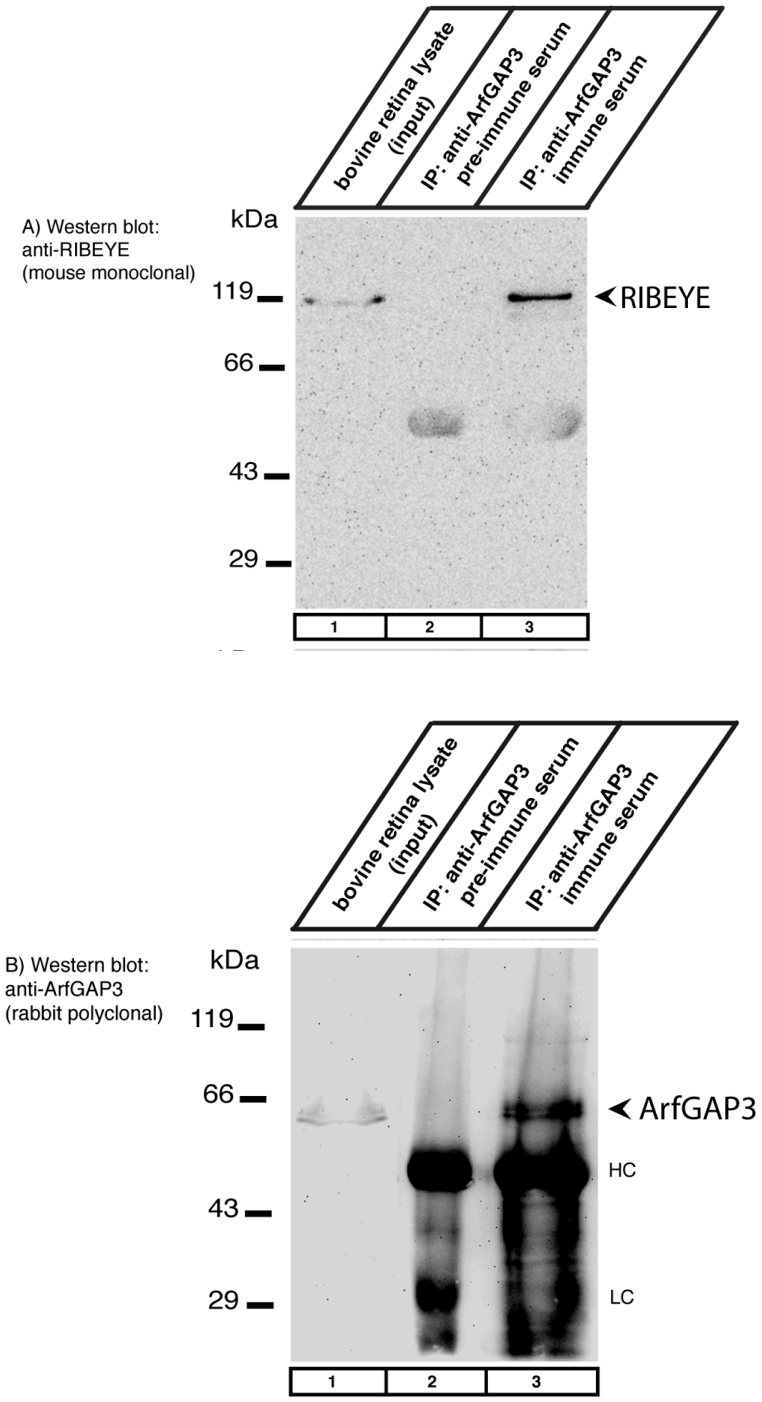

Figure 21: Co-immunprecipitation of RIBEYE and ArfGAP3 from the bovine retina. In A) ArfGAP3 immune serum and ArfGAP3 pre-immune serum were tested for their capability to co-immunoprecipitate RIBEYE from the bovine retina. RIBEYE is co-immunoprecipitated by ArfGAP3 immune serum (Cterm3 antiserum; lane 3, Fig 20a) but not by ArfGAP3 pre-immune serum (lane 2, Fig. 20a). Fig. 20a) shows the same blot as in Fig. 8b but reprobed with anti-ArfGAP3 antibodies. This blot shows the presence of ArfGAP3 precipitated by the immune serum (lane 3) but not by the pre-immune serume (lane 2). "HC" and "LC" indicate the immunoglobulin heavy and light chains respectively. Lane 1 shows the input fraction (1% of total input). Both ArfGAP3 as well as RIBEYE are strongly enriched in the experimental immunoprecipitate (lane 3, arrowhead) but not in the control immunoprecipitate (lane 2).

Since RIBEYE is exclusively present at synaptic ribbons in the mature retina (Schmitz et al., 2000) the co-immunoprecipitation experiments suggest that ArfGAP3 is a component of the synaptic ribbon complex *in-situ*.

3.9 ArfGAP3 is specifically enriched in close vicinity to the synaptic ribbon in the outer plexiform layer.

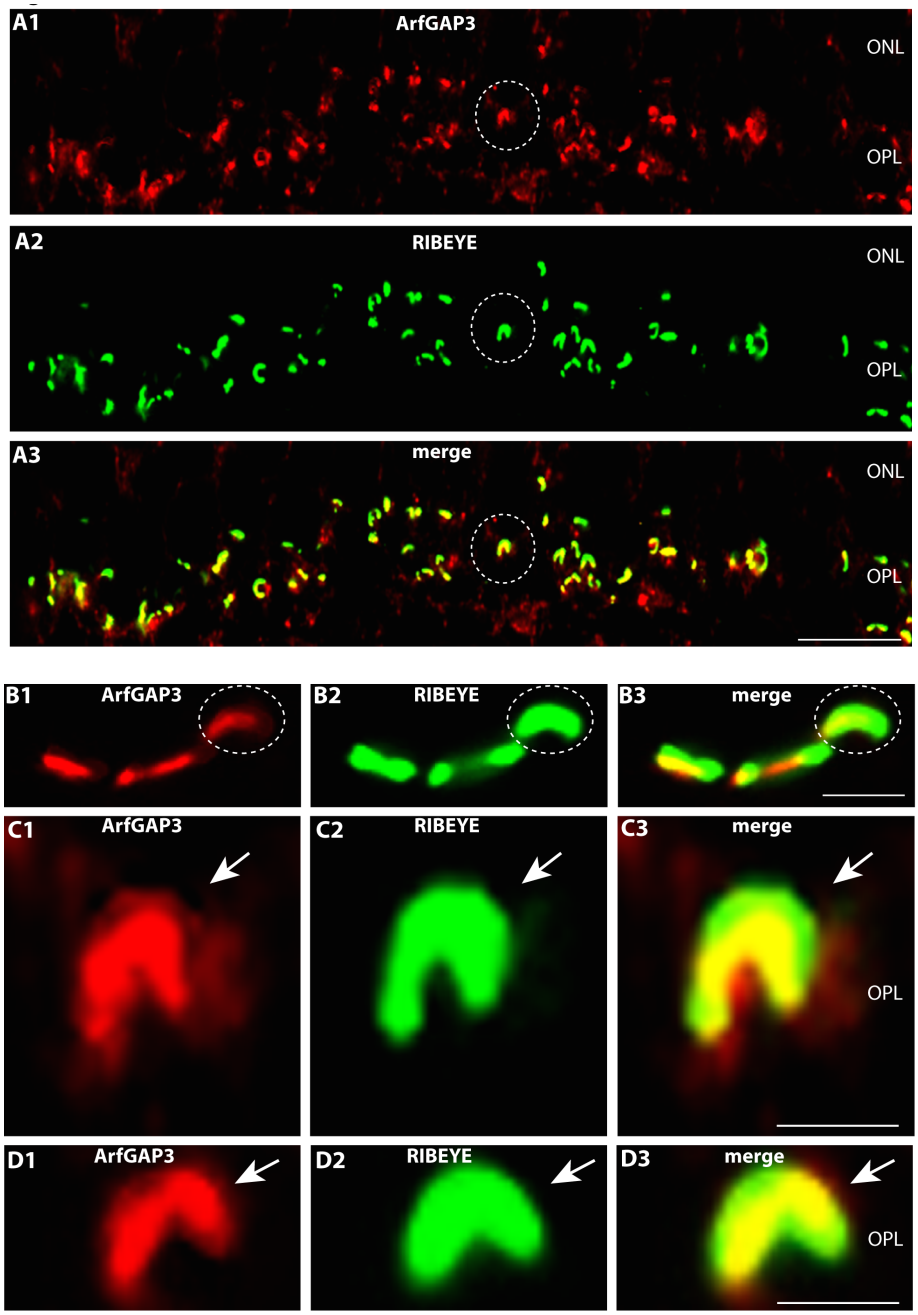

Figure 22: ArfGAP3 is strongly enriched at the synaptic ribbon of photoreceptor synapses *in-situ* (conventional imaging with ArfGAP3 Cterm3 antibody). ArfGAP3 colocalizes with synaptic ribbons. 0.5 µm-thin retinal sections double-immunolabelled with antibodies against ArfGAP3 (Cterm3 antibody) and monoclonal antibodies against RIBEYE(B)/CtBP2 (A-D). Strong ArfGAP3 immunosignals were found at the synaptic ribbons and in close vicinity to synaptic ribbons. The dashed circles in (A, B) denote single immunolabelled photoreceptor presynaptic terminals. Arrows in (C, D) point to immunolabelled single synaptic ribbons. (A-D) were obtained by conventional imaging Abbreviations: ONL, outer nuclear layer; OPL, outer plexiform layer. Scale bar: 10µm (A), 1µm (B-D).

To get further insights about the in situ localization of ArfGAP3 in the retina, I performed immunolabeling analyses with both ArfGAP3 antibodies (ArfGAP3 Cterm3 and ArfGAP3 Cterm2; Fig. 21). Both ArfGAP3 antibodies strongly labeled the outer plexiform layer (OPL) where photoreceptor ribbon synapses are localized (Fig. 21; data not shown).

Identical results were obtained independent of whether crude antisera or affinity-purified antibodies were used (compare Figs. 21, 22, 23). To define the relation between ArfGAP3 and synaptic ribbons, I performed double immunolabeling analyses with rabbit polyclonal antibodies against Arf-GAP3 and mouse monoclonal antibodies against RIBEYE(B)-domain/CtBP2 (Fig. 21). The ArfGAP3 immunosignals largely overlapped at the photoreceptor ribbon synapse with the RIBEYE immunosignals indicating that ArfGAP3 is strongly enriched at the synaptic ribbon complex (Fig. 21 A, B, C and D). Identical immunolabeling results were obtained with both ArfGAP3 antibodies (Fig.21)

3.10 ArfGAP3 colocalizes with active zone protein bassoon at photoreceptor cells ribbon synapse.

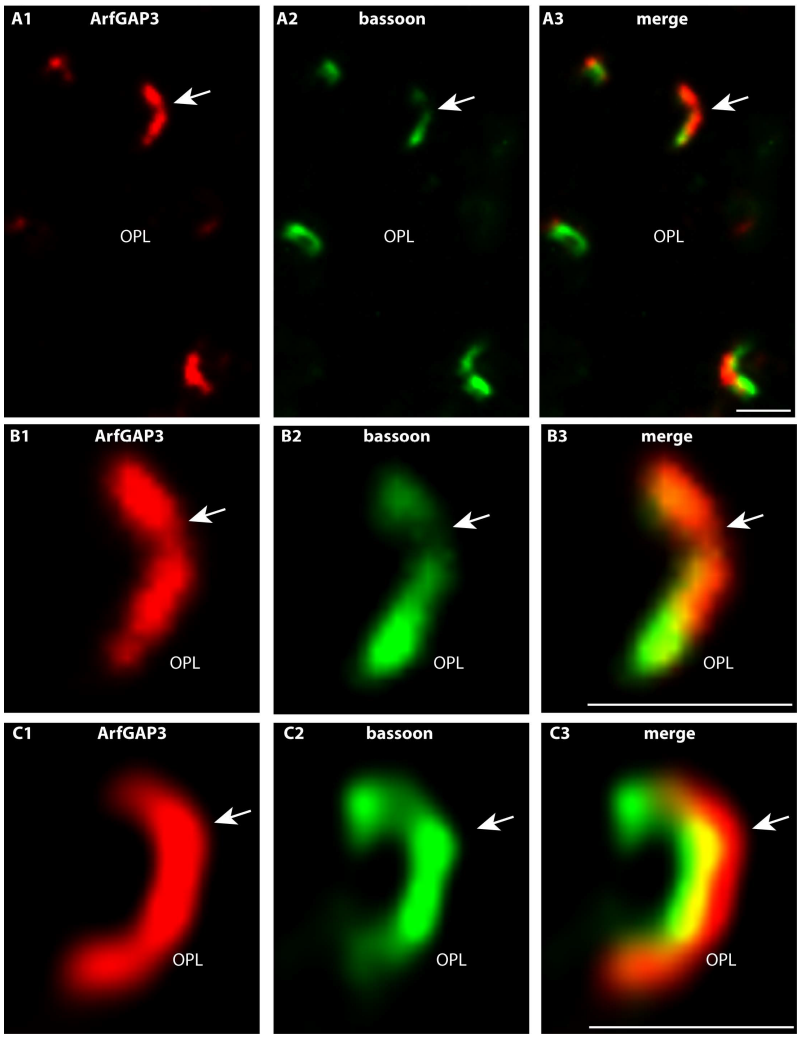

Figure 23: ArfGAP3 co-localizes with bassoon at photoreceptor synaptic ribbons. (A-C) 0.5 µm-thin retinal sections double-immunolabelled with affinity-purified rabbit antibodies against ArfGAP3 (Cterm3 antibody) and mouse monoclonal antibodies against Bassoon (A-C). Bassoon is known to be localized at the base of the synaptic ribbon (tom Dieck et al., 2005). Similar to the double-immunolabellings with RIBEYE(B)/CtBP2, there is a high degree of overlap between the two signals further confirming the strong enrichment of ArfGAP3 at the photoreceptor synaptic ribbon complex. (A,B) were obtained by conventional imaging; (C) is a micrograph obtained by SR-SIM imaging. Arrows in (A-C) point to immunolabelled single synaptic ribbons. Abbreviations: OPL, outer plexiform layer. Scale bars: 1µm.

The ArfGAP3 immunosignals also showed a strong colocalization with the active zone protein bassoon (Fig. 22 B). In the SR-SIM analyses, the ArfGAP3 immunosignal was slightly shifted toward the ONL compared with the bassoon immunosignal, also indicating ArfGAP3 localization in the basal portions at the synaptic ribbon (Fig. 22 B; see also discussion). Bassoon is localized to the arciform density and anchors the base of the synaptic ribbon (tom Dieck et al., 2005).

3.11 Pre-absorption experiment confirms the specificity of ArfGAP3 antibody.

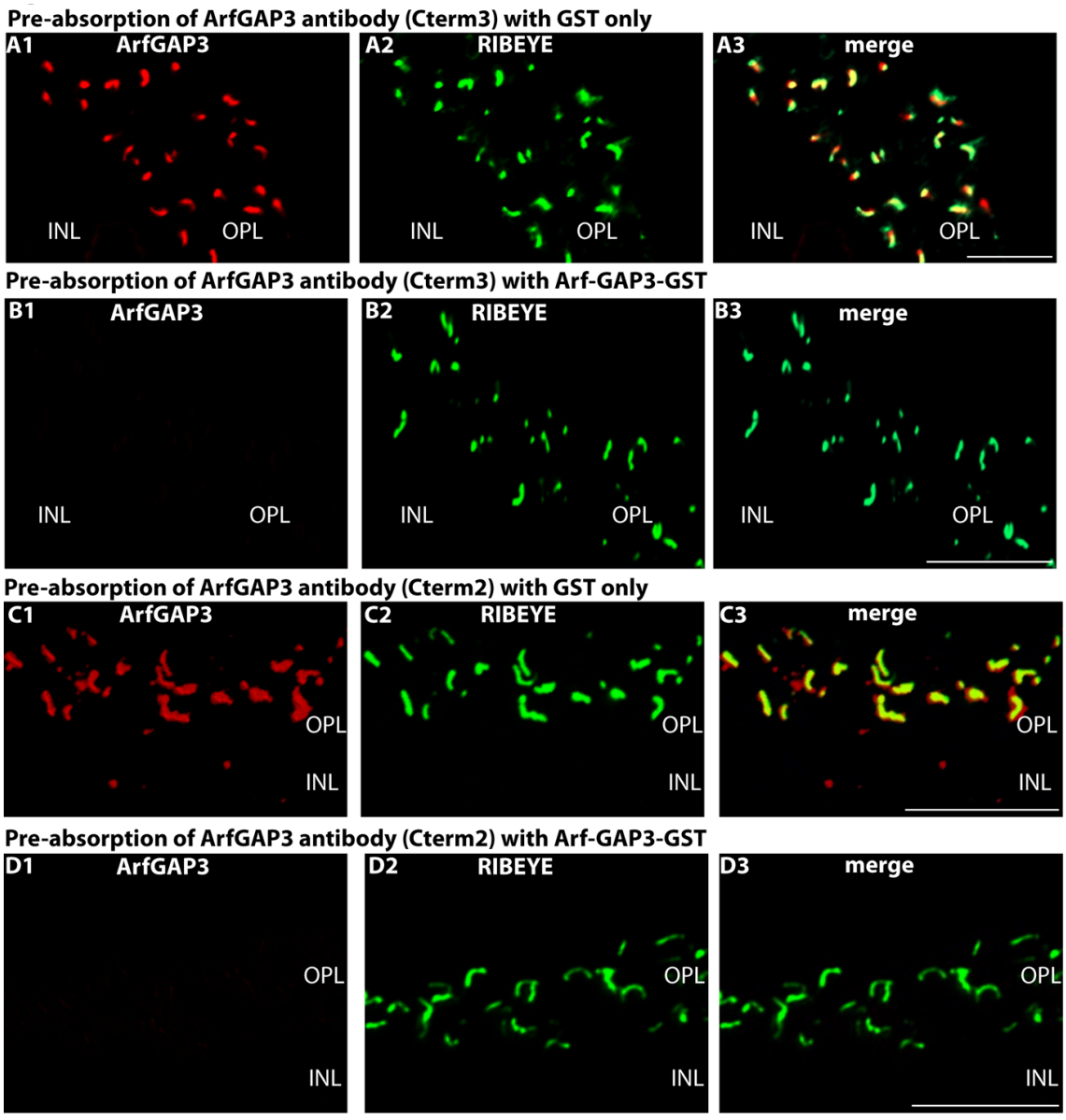

Figure 24: Pre-absorption control experiments for immunolabeling analyses experiments. (A,B) Double immunolabeling of 0.5µm-thin mouse retinal sections with ArfGAP3 (Cterm3) antibody pre-absorbed with either their specific ArfGAP3-GST-fusion protein used for immunization (B) or with GST alone (A). To visualize ribbon synapses, sections were coimmunolabeled with mouse monoclonal antibodies against RIBEYE(B)-domain/CtBP2. Pre-absorption with the specific fusion protein (but not with GST alone) completely blocked the respective immunosignals at the synaptic ribbon (B), whereas GST alone had no influence on the immunosignals (A), showing the specificity of the immunolabeling

results. (C,D) Pre-absorption control experiments for the immunolabeling analyses experiments shown in Fig. 21. (C,D) Double immunolabeling of 0.5µm-thin mouse retinal sections with ArfGAP3 (Cterm2) antibody pre-absorbed with either their specific ArfGAP3-GST-fusion protein used for immunization (D) or with GST alone (C). To visualize ribbon synapses, sections were co-immunolabeled with mouse monoclonal antibodies against RIBEYE(B)-domain/CtBP2. Pre-absorption with the specific fusion protein (but not with GST alone) completely blocked the respective immunosignals at the synaptic ribbon (D), whereas GST alone had no influence on the immunosignals (C), showing the specificity of the immunolabeling results. ONL, Outer nuclear layer; OPL, outer plexiform layer; INL, inner nuclear layer. Scale bars: 5µm.

The described ArfGAP3 immunosignals obtained with both ArfGAP3 antibodies could be specifically blocked by pre-absorption with the respective ArfGAP3-GST fusion protein but not by GST alone. Pre-absorption demonstrates that signals obtained in blots and immunolabeling are specific for ArfGAP3. The signals irrespective of which part of ArfGAP3 was used to make fusion construct to generate antibody are specific and are not blocked by GST, which was used to make tagged-Fusion protein (Fig. 23).

3.12 ArfGAP3 and RIBEYE are closely localized to each other at photoreceptor ribbon synapses as analyzed by Super resolution SIM-Microscopy.

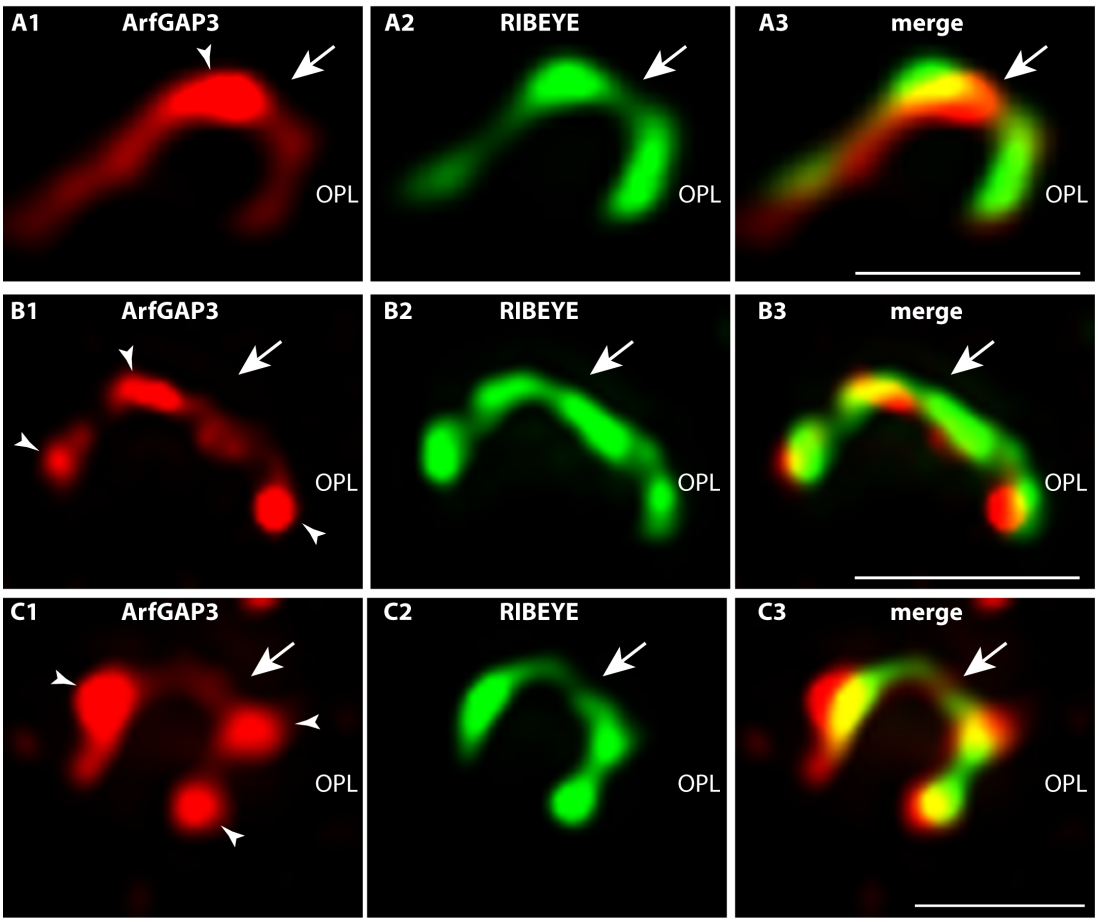

Figure 25. ArfGAP3 is strongly enriched at the synaptic ribbon of photoreceptor synapses *in-situ* (SR-SIM imaging with ArfGAP Cterm3 antibody). ArfGAP3 also co-localizes with synaptic ribbons as judged by super-resolution structured illumintion microscopy (SR-SIM). 0.5 µm-thin retinal sections double-immunolabelled with affinity-purified rabbit antiboies against ArfGAP3 (affinity-purified ArfGAP3 Cterm3 antibody) and mouse monoclonal antibodies against RIBEYE(B)/CtBP2 (A-C). Arrows in (A-C) point to immunolabelled single synaptic ribbons. Abbreviations: OPL, outer plexifor layer. Scale bars: 1µm (A-C).

We also performed SR-SIM of thin retinal sections double immunolabeled with affinity-purified rabbit polyclonal antibodies against ArfGAP3 and mouse monoclonal antibodies against RIBEYE(B)/CtBP2. Also, SR-SIM analyses demonstrated a strong enrichment of the ArfGAP3 immunosignals at the synaptic ribbons (Fig. 3.11). In the SR-SIM analyses, the ArfGAP3 antibody signal was slightly shifted toward inner nuclear layer (INL) compared with the RIBEYE immunosignal, which could indicate a localization of ArfGAP3 more toward the base of synaptic ribbon (Fig. 3.12 A3, B3 and C3) also supported by previously described SR-SIM analyses of ArfGAP3 and bassoon labeling (Fig 3.10)

3.13. Localization of ArfGAP3 in relation to other synaptic proteins of the presynaptic photoreceptor terminal.

Previously, we have shown that Dynamin is highly enriched at the presynaptic plasma membrane in close vicinity to the synaptic ribbon (Wahl et al., 2013). The Dynamin immunosignal surrounds the synaptic ribbon in a ring-like manner in a very short distance (Wahl et al., 2013).

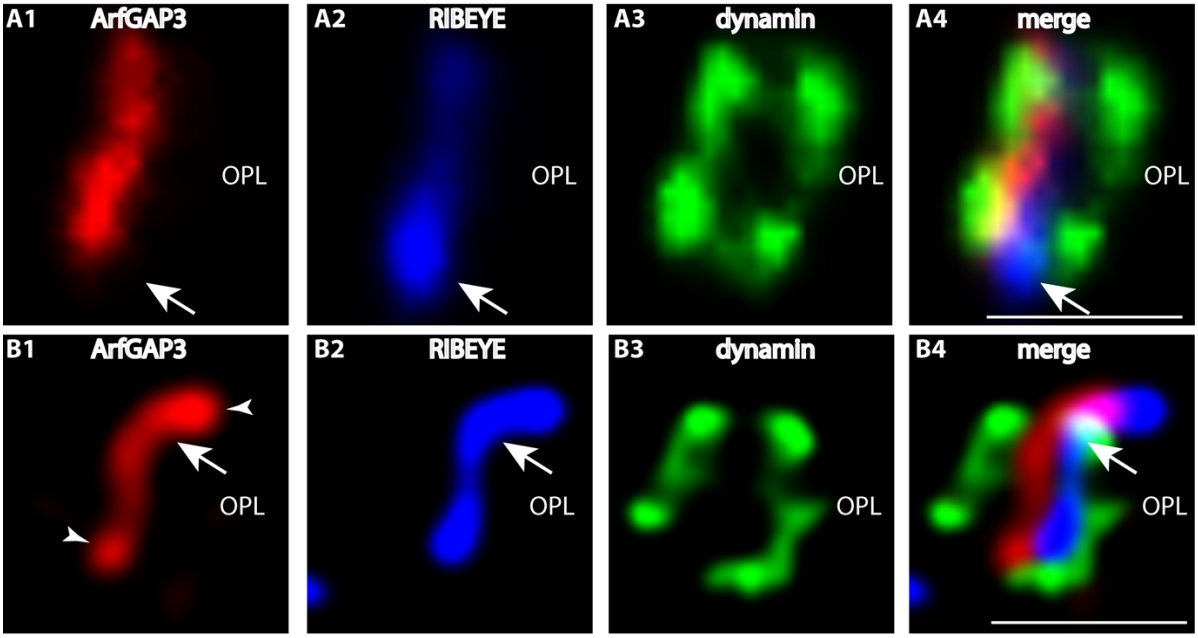

Figure 26: Localization of ArfGAP3 in relation to other synaptic proteins of the presynaptic photoreceptor terminal. (A-C) The 0.5µm-thin retinal sections were triple immunolabelled with affinity-purified rabbit polyclonal antibodies against ArfGAP3 (Cterm3), mouse monoclonal antibodies against dynamin (hudy-1) and DyLight 650-direct labeled primary antibodies against RIBEYE(B)/CtBP2. ArfGAP3 and RIBEYE are located very close to each other (A-C). The ArfGAP3 immunosignal is located within the ring-like dynamin immunosignal that demarcates the presynaptic plasma membrane of the periactive zone that surrounds the synaptic ribbon (Wahl et al., 2013). (A,B) was obtained by conventional imaging, (C) is a micrograph obtained by SR-SIM imaging. Arrows in (A-C) point to immunolabelled single synaptic ribbons. Abbreviations: OPL, outer plexiform layer. Scale bars, 1µm.

Immunogold electron microscopy previously demonstrated that this ring of Dynamin-1

immunoreactivity corresponded to the plasma membrane of the periactive zone (Wahl et al., 2013). We used Dynamin as a landmark protein to further define the localization of ArfGAP3 at the synaptic ribbon complex using high-resolution fluorescence microscopy. We performed triple immunolabeling analyses with rabbit polyclonal antibodies against ArfGAP3, mouse monoclonal antibodies against Dynamin (hudy-1), and Alexa 650 directly labeled primary mouse monoclonal antibodies against RIBEYE(B)-domain/ CtBP2 (Fig. 3.13). In these triple immunolabeling analyses, the ArfGAP3 immunosignals were located very close to the RIBEYE-labeled synaptic ribbon and within the ring-like Dynamin immunosignals that surrounded the synaptic ribbon (Fig.3.13)

3.14 Arf1, an effector of ArfGAP3, is enriched around the synaptic ribbon.

YTH analysis revealed specific interaction of ArfGAP3 with Arf1 as shown in Fig 26A ß-Gal assay and not with Arf6 (not shown). Western Blot analysis for Arf1 monoclonal antibody revealed strong enrichment of protein in retina as seen in Fig. 26D.

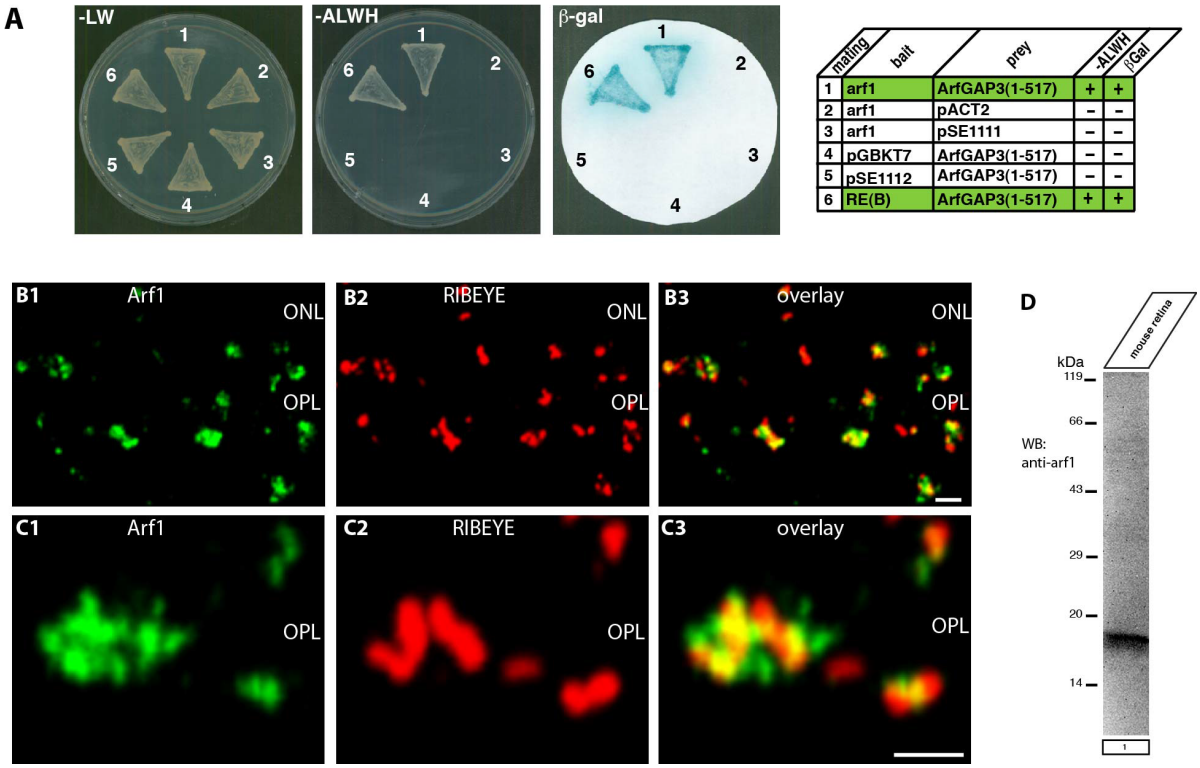

Figure 27: The ArfGAP3 effector Arf1 is enriched at synaptic ribbon complex of photoreceptor synapses. A, B, Double immunolabeling experiments of 0.5 µm thick retinal sections with mouse monoclonal antibodies against Arf1 and rabbit polyclonal antibodies against RIBEYE (U2656) demonstrated close enrichment of Arf1 around synaptic ribbon complex. ONL, outer nuclear layer; OPL, outer plexiform layer. Scale bars: 1µm. (C) Western blot analyses demonstrated that Arf1 is strongly expressed in the mouse retina.

Next step was to check the abundance of Arf1 at immunofluorescence level as shown in Fig. 26B1, C1. I found strong enrichment of signals at immunofluorescence levels, which also correlates to its abundance as judged by western blot. Arf1 is mostly seen in diffuse pattern

surrounding ribbons, as observed by co-labeling with RIBEYE. Presence of Arf1 in close vicinity to ribbons also correlates to its interaction with ArfGAP3 that colocalizes with RIBEYE as seen in Fig. 25, 26).

3.15 RIBEYE(B) competes with Arf1 for binding to ArfGAP3

To get functional insights into the importance of the ArfGAP3/ RIBEYE interaction I determined which Arf protein is interacting with ArfGAP3. In agreement with previous reports (Liu et al., 2001; Kartberg et al., 2010), I found that ArfGAP3 interacts with Arf1 (but not with Arf6; Fig. 25A, mating1; data not shown). Western blot analyses demonstrated that Arf1 is strongly expressed in the retina and immunofluorescence microscopy documented enrichment of Arf1 in close vicinity to the synaptic ribbon complex (Fig. 26B,C). Similar to RIBEYE(B), Arf1 also binds to ArfGAP-domain of ArfGAP3 (data not shown). Therefore, I tested whether Arf1 and RIBEYE(B) can bind simultaneously to ArfGAP3 or whether they compete with each other in binding to ArfGAP3 (Fig. 27). To address this question, I used fusion protein pull-down experiments. I tested whether increasing concentrations of Arf1 (Fig. 27A) added to a fixed concentration of immobilized ArfGAP3 (0.15µM) would inhibit binding of RIBEYE(B) to ArfGAP3. RIBEYE(B) was kept at a constant concentration in these experiments (0.15µM). Similarly, I also tested whether increasing concentrations of RIBEYE(B) (Fig. 27B) added to a fixed concentration of immobilized ArfGAP3 (0.15µM) would inhibit binding of Arf1 to ArfGAP3. Arf1 was kept at a constant concentration in these latter experiments (0.15µM). In both sets of experiments, I observed a competitive behavior between Arf1 and RIBEYE(B) in binding to ArfGAP3: if Arf1 was increased, binding of RIBEYE(B) to ArfGAP3 was diminished and, vice versa, increasing concentrations of RIBEYE(B) inhibit binding of Arf1 to ArfGAP3. These data demonstrate that RIBEYE(B) competes with Arf1 for binding to a common binding site on ArfGAP3, indicating that binding of RIBEYE(B) and Arf1 to ArfGAP3 is mutually exclusive.

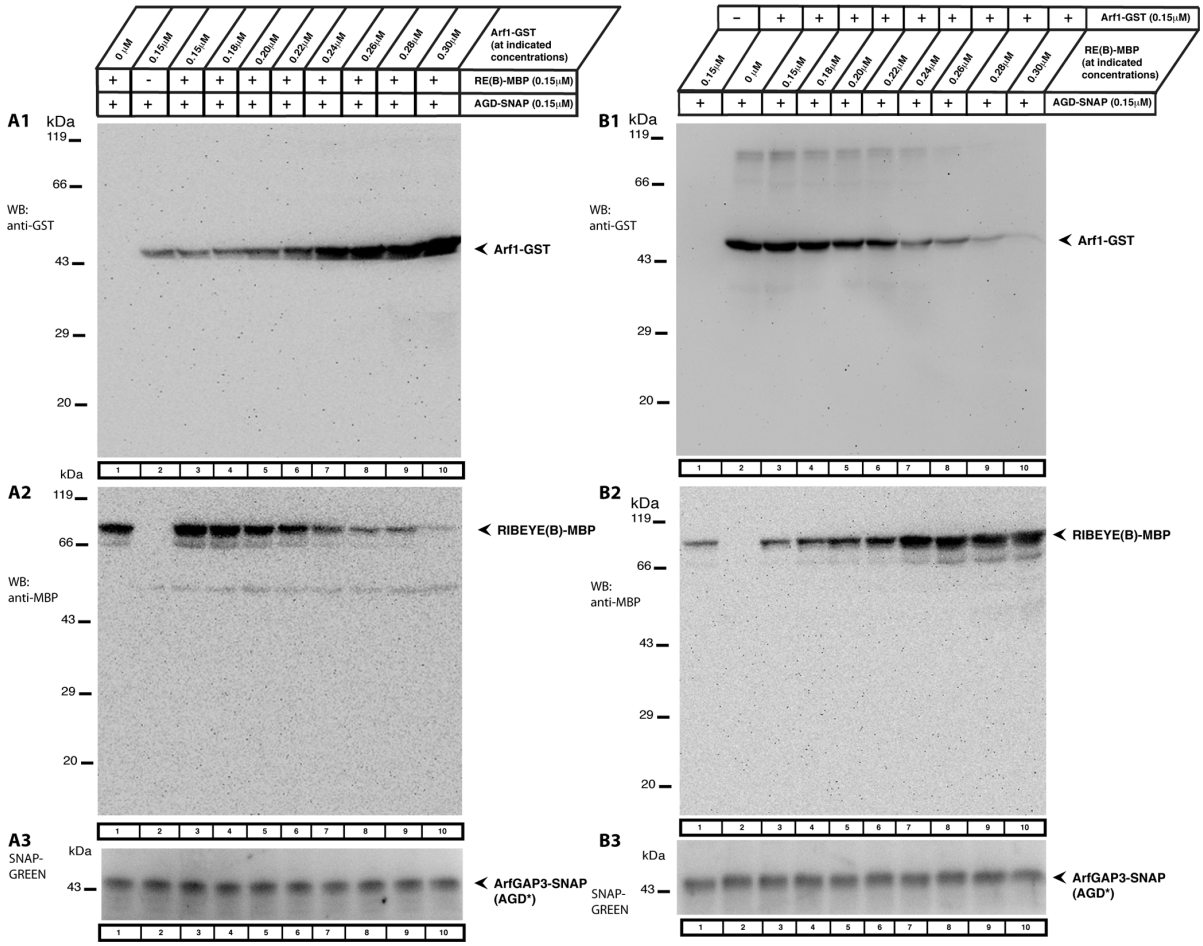

Figure 28: RIBEYE(B) and Arf1 compete with each other for binding to ArfGAP3. I tested in fusion protein pull-down experiments whether Arf1 and RIBEYE(B) can bind simultaneously to ArfGAP3 or whether they compete with each other for ArfGAP3-binding. A, B, Show representative Westerns blots incubated with the indicated antibodies to test for the binding of the respective fusion proteins. After detection of the GST-tagged protein (A1, B1), blots were stripped and re-incubated with antibodies against MBP (A2, B2). A3, B3, SNAP-tagged immobilized ArfGAP3 bait protein was visualized with SNAP-Vista Green (NEB). A, I tested whether increasing concentrations of Arf1 added to a fixed concentration of immobilized ArfGAP3 would inhibit binding of RIBEYE(B) to ArfGAP3. RIBEYE(B) was kept at a constant concentration in these experiments. B, I tested whether increasing concentrations of RIBEYE(B) added to a fixed concentration of immobilized ArfGAP3 would inhibit binding of Arf1 to ArfGAP3. Arf1 was kept at a constant concentration in these latter experiments. In both sets of experiments,weobserved a competitive behavior between Arf1 and RIBEYE(B) in binding to ArfGAP3. These data demonstrate that RIBEYE(B) competes with Arf1 for binding to ArfGAP3. indicating that binding of RIBEYE(B) and Arf1 to ArfGAP3 is mutually exclusive. Abbreviations: AGD*, extended ArfGAP-domain of ArfGAP3.

3.16 Over-expression of ArfGAP3 in photoreceptor cells inhibits the uptake of FM1-43.

Next, we wanted to find out for which synaptic process ArfGAP3is relevant at the synaptic ribbon. The synaptic ribbon is a site of intense membrane retrieval (Jackman et al., 2009; Snellman et al., 2011; Chen et al., 2013, Wahl et al., 2013). Therefore, we tested whether ArfGAP3 is involved in this process (Fig. 28). We added FM1–43 to the extracellular medium to compare endocytic uptake in photoreceptors that were either electroporated with ArfGAP3-mcherry or mcherry alone. In mcherry-electroporated photoreceptors, there was an intense uptake of FM1–43 (Fig. 28 A,B). The uptake of

FM1–43 in mcherry-transfected photoreceptors was similar to the FM1–43 uptake in nontransfected photoreceptors (data not shown). In contrast to mcherry-transfected photoreceptors, ArfGAP3-overexpressing transfected photoreceptors showed a very strong inhibition of FM1–43 uptake (Fig. 28 C,D) indicating that ArfGAP3 is essentially involved in endocytosis at the photoreceptor synapse

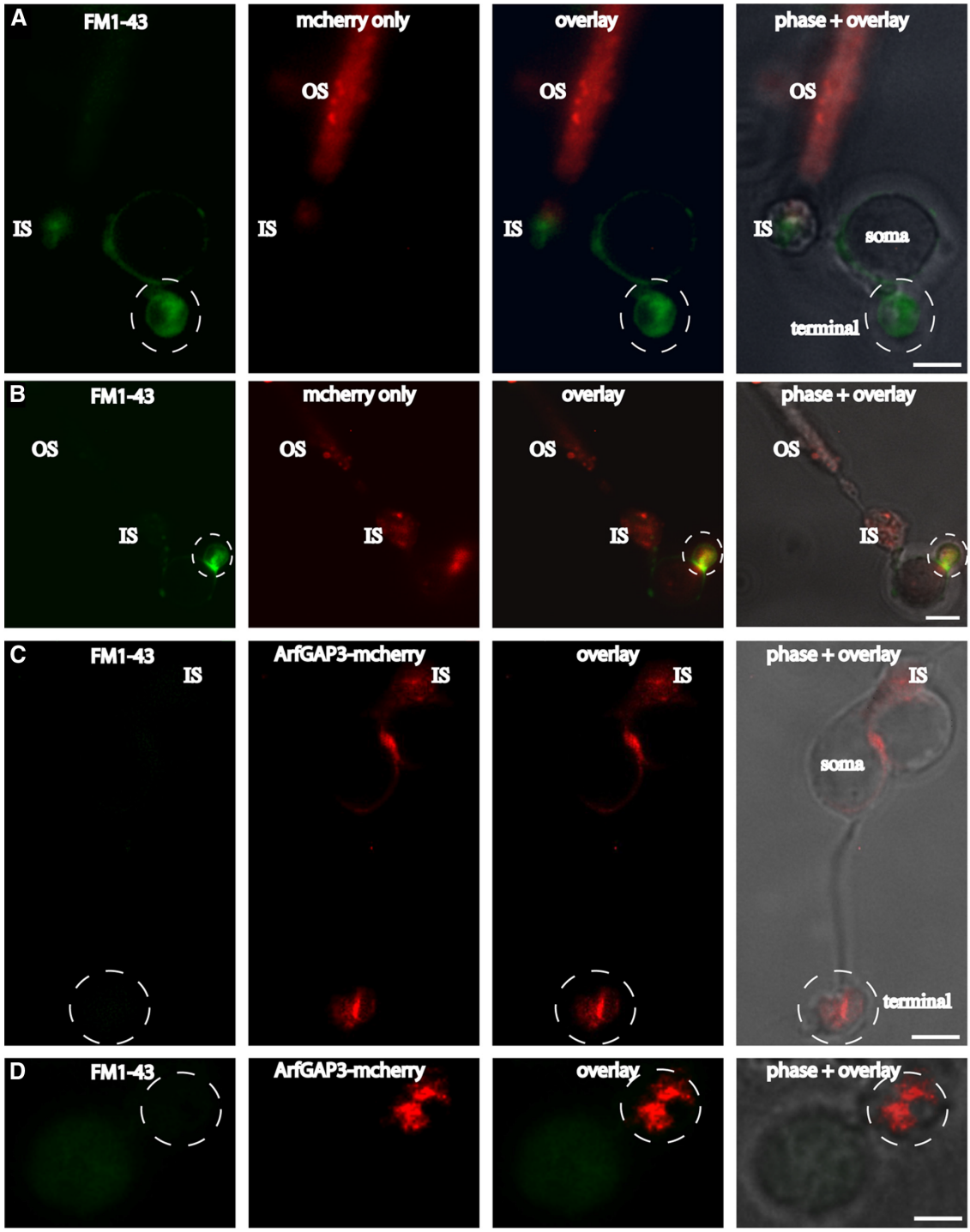

Figure 29: Overexpression of ArfGAP3 in mouse photoreceptors inhibits endocytic uptake of FM1-43. FM1-43 was used to compare endocytic uptake in photoreceptors that were either electroporated with mcherry alone (A, B) or ArfGAP3-mcherry (C, D). In mcherry-electroporated photoreceptors, there was an intense uptake of FM1–43 in the synaptic terminals (A, B). The uptake of FM1–43 in mcherry-transfected photoreceptor was similar to FM1–43 uptake in nontransfected photoreceptors (data not shown). In contrast to mcherry-transfected photoreceptors, ArfGAP3-mcherry overexpressing photoreceptors showed a strong inhibition of FM1–43 uptake in the synaptic terminals (C, D), indicating that ArfGAP3 is essential involved in endocytosis at the photoreceptor synapse. OS, Outer segment; IS, inner segment; Scale bars: A–C, 1µm; D, 0.75µm.

4. DISCUSSION:

In the present study, I demonstrated that the Arf-GTPase activating protein-3, ArfGAP3 interacts with RIBEYE and is a novel component of the photoreceptor synaptic ribbon complex using various independent assays. Conventional immunofluorescence microscopy as well as SR-SIM immunolabeling analyses on thin retinal resin sections demonstrated that Arf-GAP3 is highly enriched at the photoreceptor synaptic ribbon complex in-situ. ArfGAP3 is more weakly expressed in the IPL than in photoreceptor synapses of the OPL (data not shown). This is due to the fact that synaptic ribbons in the IPL are smaller than in photoreceptor synapses of the OPL and because the IPL is dominated by conventional, non ribbon-containing synapses. ArfGAP3 has been previously characterized as a component of the Golgi apparatus (for review, see Spang et al., 2010). At the Golgi apparatus, ArfGAP3 regulates vesicle trafficking in an Arf1-dependent manner (Dogic et al., 1999; Eugster et al., 2000; Lewis et al., 2004; Watson et al., 2004; Frigerio et al., 2007; Saitoh et al., 2009; Kartberg et al., 2010; Spang et al., 2010; Yu et al., 2012). The localization of ArfGAP3 at synaptic ribbon complex in-situ was confirmed by two different antibodies directed against different regions of the ArfGAP3 carboxy-terminus. Both antibodies showed the same enrichment of ArfGAP3 at the photoreceptor synaptic ribbon complex. In agreement with these morphological data, ArfGAP3 and RIBEYE were co-immunoprecipitated from bovine retina, further demonstrating enrichment of ArfGAP3 at the photoreceptor synaptic ribbon complex. We propose that the interaction with RIBEYE recruits ArfGAP3 in close proximity to synaptic ribbons where ArfGAP3 subsequently exerts its activity via its effectors molecules e.g. Arf1. YTH data demonstrated that the catalytically active, highly conserved ArfGAP-domain of ArfGAP3 is responsible for its binding to RIBEYE. The recruitment of ArfGAP3 to RIBEYE(B) is unlikely to require a functional catalytic activity of the AGD-domain because the initial ArfGAP3 prey clone obtained from our YTH screen that strongly interacted with RIBEYE(B) displayed a 8 a.a deletion in central Zn-finger motif of the AGD-domain (Goldberg, 1999; for review, see Gillingham and Munro, 2007; Kahn et al., 2008; Donaldson and Jackson, 2011). This finding does not exclude that ArfGAP3 exerts a catalytic activity at the synaptic ribbon. More likely, the ArfGAP3-RIBEYE complex is part of a larger catalytically active multiprotein complex that functions at the synaptic ribbon. In support of this proposal, the Arf GTP/GDP exchange factor IQ-ArfGEF BRAG1, which catalyzes exchange of GDP by GTP, has been shown to be associated with synaptic ribbons (Katsumata et al., 2009). Interestingly, the interaction

between RIBEYE(B) and ArfGAP3 is stimulated by NAD(H) in a redox-sensitive manner. NADH is more efficient than the oxidized NAD^+ in promoting RIBEYE(B)/ArfGAP3 interaction (≈400nm for NADH; ≈600nm for NAD). Such a metabolism-dependent interaction is also known for the nuclear co-repressor CtBP1, which regulates transcription in a redox-sensitive manner (Zhang et al., 2002, 2006; Fjeld et al., 2003; Ivanova et al., 2015). A main function of this redox-sensitive interaction in ribbon synapses appears to be controlling Arf1 function.

At the light microscopic level the small GTP-binding protein Arf1, an ArfGAP3 effector, is enriched at the synaptic ribbon complex. Arf1 is an important regulator of vesicle trafficking at various intracellular compartments, including the Golgi apparatus and endosomal compartments (Gillingham and Munro, 2007; Kahn et al., 2008; Donaldson and Jackson et al., 2011) and might perform a similar role at the photoreceptor synaptic ribbon complex. I demonstrated that Arf1 and RIBEYE cannot bind at the same time and also there is no interaction between these two partners in YTH system (data not shown). When RIBEYE is bound, e.g., at high levels of NADH, Arf1 can no longer bind to ArfGAP3. As a consequence, its GTPase activity will remain low and Arf1 will stay in its active, GTP-bound form that would hinder in Arf1's role in recycling vesicles. Immunofluorescence microscopic analyses confirmed the presence of Arf1 in close vicinity to synaptic ribbon but in diffuse pattern which implies its role is not only in close vicinity to synaptic ribbon but also at synaptically distinct periactive zone. Unfortunately, the antibodies against ArfGAP3 were not suitable for ultrastructural analyses. Knowing the exact position of ArfGAP3 at the Ultrastructural level is important expect to further elucidate its function at the synaptic ribbon in photoreceptor cells. Super-resolution immunofluorescence microscopy indicated a particularly high enrichment of ArfGAP3 at the base of synaptic ribbon complex. In support of this proposal, Arf-GAP3 was found close to bassoon (Fig. 22), which is located at the base of the ribbon, and within the ring-like dynamin signal that surrounds the synaptic ribbon in the periactive zone. Dynamin has been shown previously to be enriched at the presynaptic plasma membrane at the periactive zone (Wahl et al., 2013). Therefore, ArfGAP3 probably exerts its function at the base of the ribbon and in close proximity to the plasma membrane of the periactive zone where most of the endocytic proteins such as ampiphysin, endophilin and syndapin are localized (Wahl et al., 2013).

Clearly, future electron microscopic analyses need is required to demonstrate whether ArfGAP3-Arf1 function directly at the presynaptic plasma membrane or at an endosomal

compartment close to peri-active zone. Overexpression of ArfGAP3 in electroporated photoreceptors resulted in a strong inhibition of endocytic membrane retrieval as judged by an inhibition of uptake of FM1–43. Competitive inhibition assay by triple pull-down of ArfGAP3-RIBEYE(B)-Arf1 supports the over-expression experiment of ArfGAP3 in mouse retina, where over expression of ArfGAP3 leads to uncontrolled hydrolysis of Arf1 which leads to higher accumulation of Arf1-GDP thereby affecting the overall balance of endocytic machinery. Still the exact effector/s of Arf1 has to be elucidated by further biochemical experiments that will provide more detailed information of Arf-ArfGAP3 interaction in photoreceptor cells. Further, one of the early discoveries explaining the functions of GAP's showed cytosolic redistribution of ArfGAP's after BFA washout suggests that GAP is recruited back to Golgi through Arf1-Dependent manner (Cukierman et al., 1995) that suggests ArfGAP's role in vesicle recycling or even at earlier steps of vesicle biogenesis.

Recent finding of PIP5KIγ in close vicinity to ribbon synapses (Sakagami et al., 2014) is quite interesting in context to its ability to synthesize PIP2, an important phospholipid for intiating synaptic vesicle endocytosis. PIP5KIγ activity is regulated by various factors including ADP ribosylation factor (Arf) and Rho family GTPases, phosphatidic acid. Arf6 functions as a physiological upstream regulator of PIP5KIγ in neurons, which could be an important preliminary signal in very early stage of synaptic vesicle recycling. Also, RIBEYE(B) domain has been shown to have lysophosphatidic acid acyl transferase activity that generates phosphatidic acid (PA) at the synaptic ribbon (Schwarz et al., 2011). PA promotes negative membrane curvature that favors vesicle budding and fission (Jenkins and Frohman, 2005; Roth, 2008; Yang et al., 2008).

Therefore, I propose that the RIBEYE/ArfGAP3 complex is involved in endocytic membrane retrieval at the synaptic ribbon. Recent studies demonstrated that the synaptic ribbon complex is important for endocytic membrane traffic in the tonically active ribbon synapse (Spassova et al., 2004; Griesinger et al., 2005; Khimich et al., 2005; Jackman et al., 2009; Babai et al., 2010; Frank et al., 2010; Schnee et al., 2011; Snellman et al., 2011; Tian et al., 2012; Chen et al., 2013; Wahl et al., 2013). Still, the molecular details and mechanisms used to accomplish this remain to be elucidated. CtBP1/BARS, a close relative of RIBEYE(B)-domain/CtBP2 and component of the Golgi complex, is also localized to the synaptic ribbon complex (tom Dieck et al., 2005; for a review, see Corda et al., 2006). At the Golgi apparatus, CtBP1/BARS interacts with ArfGAP1 (Yang et al., 2005). This interaction has been proposed to be essential for vesicle formation and vesicle scission at the Golgi

complex (Yang et al., 2002, 2005, 2006; Corda et al., 2006). The function of CtBP1/BARS at the synaptic ribbon is still unclear (Vaithianathan et al., 2013). One of the difference between the CTBP's/ArfGAP's is their specific domain interactions. CtBP1/ArfGAP1 interaction at Golgi apparatus is mediated by the SBD domain of CtBP1, while the interaction between RIBEYE(B)domain and ArfGAP3 at synaptic ribbon is mediated by the NBD of RIBEYE(B)-domain.

The recruitment of ArfGAP3 to the synaptic ribbon via an inducible, redox-dependent manner provides the synaptic ribbon with the possibility to regulate endocytic vesicle trafficking. The catalytically active ArfGAP-domain could control Arf1 activity in a redox-switchable manner by a competitive interaction with RIBEYE. Increasing concentration either of ARF1 or RIBEYE inhibits the binding of subsequent partner to ArfGAP3. Even C-terminus of ArfGAP3 could be involved in different tasks, e.g., the cargo sorting and binding to SNARE. The C-terminus of ArfGAP3 has been shown to be involved in membrane-binding and cargo-binding/coat protein binding at the Golgi apparatus that could be also of prime importance for endocytic cargo selection close to synaptic ribbon in conjunction with diversity of proteins, which are found near ribbons. A similar function might also apply in the ribbon synapse and would provide the RIBEYE-ArfGAP3 complex a central position in the vesicle recycling machinery.

5. REFERENCES:

Alpadi K, Magupalli VG, Käppel S, Köblitz L, Schwarz K, Seigel GM, Sung CH, Schmitz F (2008) RIBEYE recruits a mammalian ortholog of the C. elegans protein unc119 to synaptic ribbons of photoreceptor synapses. J.Biol.Chem. 283:26461–26467.

Bai J, Wang CT, Richards DA, Jackson MB, Chapman ER (2004). Fusion pore dynamics are regulated by synaptotagmin/t-SNARE interactions. Neuron 41:929-942.

Babai N, Bartoletti TM, Thoreson WB (2010) Calcium regulates vesicle replenishment at the cone ribbon synapse. J. Neurosci. 30:15866-15877.

Bigay J, Casella JF, Drin G, Mesmin B, Antonny B (2005) ArfGAP1 responds to membrane curvature through the folding of a lipid packing sensor motif. EMBO. J. 24:2244-2253.

Bradford MM (1976) A rapid and sensitive method for the quantitation of microgram quantities of protein utilizing the principle of protein-dye binding. Anal. Biochem. 72:248-254.

Briggman KL, Euler T (2011) Bulk electroporation and population calcium imaging in the adult mammalian retina. J. Neurophysiol. 105:2601-2609.

Bowyer PW, Fivelman QL, Leber W, Skippen A, Cockcroft S (2009) A unique phosphatidylinositol 4-phosphate 5-kinase is activated by ADP-ribosylation factor in Plasmodium falciparum Int. J. Parasitol. 39:645-653.

Chen M, Van Hook MJ, Zenisek D, Thoreson WB (2013) Properties of ribbon and non-ribbon release from rod photoreceptors revealed by visualizing individual synaptic vesicles. J.Neurosci. 33:2071-2086.

Chinnadurai G (2009). The transcriptional corepressor CtBP: a foe of multiple tumor suppressors. Cancer. Res. 69:731-734.

Cooper B, Hemmerlein M, Ammermüller J, Imig C, Reim K, Lipstein N, Kalla S, Kawabe H, Brose N, Brandstätter JH, Varoqueaux F (2012) Munc13- independent vesicle priming at mouse photoreceptor ribbon synapses. J.Neurosci. 32:8040-8052.

Corda D, Colanzi A, Luini A (2006) The multiple activities of CtBP/BARS proteins: the Golgi view. Trends. Cell. Biol. 16:167-173.

Cukierman E, Huber I, Rotman M, Cassel D (1995) The Arf1 GTPase activating protein: zinc finger motif and Golgi complex localization. Science 270:1999-2002.

Curtis LB, Doneske B, Liu X, Thaller C, McNew JA, Janz R (2008) Syntaxin 3b is a t-SNARE specific for ribbon synapses of the retina. J. Comp. Neurol. 510:550-559.

Curtis L, Datta P, Liu X, Bogdanova N, Heidelberger R, Janz R (2010) Syntaxin 3B is essential for the for the exocytosis of synaptic vesicles in ribbon synapses of the retina. Neuroscience 166:832-841.

Deng L, Kaeser PS, Xu W, Südhof TC (2011) RIM proteins activate vesicle priming by reversing autoinhibitory homodimerization of Munc13. Neuron 69:317-331.

Dogic D, de Chassey B, Pick E, Cassel D, Lefkir Y, Hennecke S, Cosson P, Letourneur F (1999) The ADP-ribosylation factor GTPase-activating protein glo3p is involved in ER retrieval. Eur. J. Cell. Biol. 78:305-310.

Donaldson JG, Jackson CL (2011) Arf family G proteins and their regulators: roles in membrane transport, development and disease. Nat. Rev. Mol. Cell. Biol 12:36-2375.

Donovan SL, DyerMA (2006) Preparation and square wave electroporation of retinal explant cultures. Nat. Protoc. 1:2710 -2718.

Dubendorff JW, Studier FW (1991) Controlling basal expression in an inducible T7 expression system by blocking the target T7 promoter with lac repressor. J. Mol. Biol. 219:45–59

Eugster A, Frigerio G, Dale M, Duden R (2000) COP I domains required for coatomer integrity and novel interactions with Arf and ArfGAP. EMBO J. 19:3905-3917.

Fjeld CC, Birdsong WT, Goodman RH (2003) Differential binding of NAD and NADH allows the transcriptional corepressor C-terminal binding protein to serve as a metabolic sensor. Proc. Natl. Acad. Sci. U S A 100:9202-9207.

Frank T, Rutherford MA, Strenzke N, Neef A, Pangrsic T, Khimich D, Fejtova A, Gundelfinger ED, Liberman MC, Harke B, Bryan KE, Lee A, Egner A, Riedel D, Moser T (2010) Bassoon and the synaptic ribbon organize Ca^2-channels and vesicles to add release sites and promote refilling. Neuron 68:724 -738.

Frigerio G, Grimsey N, Dale M, Majoul I, Duden R (2007) Two human ArfGAPs associated with COP-I-coated vesicles. Traffic 8:1644-1655.

Ford MG, Pearse B.M., Higgins M.K., Vallis Y., Owen D.J., Gibson A., Hopkins C.R., Evans P.R., McMahon H.T. (2001) Simultaneous binding of PtdIns(4,5)P2 and clathrin by AP180 in the nucleation of clathrin lattices on membranes. Science 291:1051-1055.

Gaidarov I, Santini F, Warren RA, Keen JH (1999) Spatial control of coated-pit dynamics in living cells Nature. Cell. Biol. 1:1-7.

Gillingham AK, Munro S (2007) The small g proteins of the Arf family and their regulators. Annu. Rev. Cell. Dev. Biol. 23:579-611.

Gluzman Y (1981) SV40-transformed simian cells support the replication of early SV40 mutants. Cell 23:175-182.

Goldberg J (1999) Structural and functional analysis of the Arf1-Arfgap complex reveals a role for coatamer in GTP hydrolysis. Cell 96:893-902.

Grant SG, Jessee J, Bloom FR, Hanahan D. Differential plasmid rescue from transgenic mouse DNAs into Escherichia coli methylation-restriction mutants (1990) Proc. Natl. Acad. Sci. U S A. 12:4645-4649.

Grodberg, J., and Dunn, J. J. (1988). ompT Encodes the Escherichia coli Outer Membrane Protease that Cleaves T7 RNA Polymerase During Purification. J. Bacteriol. 170:1245-1253.

Griesinger CB, Richards CD, Ashmore JF (2005) Fast vesicle replenishment allows indefatigable ignaling at the first auditory synapse. Nature 435: 212-215.

Gustafsson MG, Shao L, Carlton PM, Wang CJ, Golubovskaya IN, Cande WZ, Agard DA, Sedat JW (2008) Three-dimensional resolution doubling in wide-field fluorescence microscopy by structured illumination. Biophys. J. 94:4957-4970.

Guan, C(1987) Vectors that facilitate the expression and purification of foreign peptides Escherichia coli by fusion to maltose-binding protein. Gene 67:21-30.

Harper JW, Adami GR, Wei N, Keyomarsi K, Elledge SJ (1993) The p21 Cdk-interacting protein Cip1 is a potent inhibitor of G1 cyclin-dependent kinases. Cell 75:805- 816.

Huang SP, Brown BM, Craft CM (2010) Visual Arrestin 1 acts as a modulator for N-ethylmaleimide-sensitive factor in the photoreceptor synapse. J. Neurosci. 30:9381-9391.

Inoue H, Randazzo PA (2007) Arf GAPs and their interacting proteins. Traffic 8:1465-1475.

Ivanova D, Dirks A, Montenegro-Venegas C, Schöne C, Altrock WD, Marini C, Frischknecht R, Schanze D, Zenker M, Gundelfinger ED, Fejtova A (2015) Synaptic activity controls localization and function of CtBP1 via binding to Bassoon and Piccolo. EMBO. J. 34:1056-1077

Jackman SL, Choi SY, Thoreson WB, Rabl K, Bartoletti TM, Kramer RH (2009) Role of the synaptic ribbon in transmitting the cone light response. Nat. Neurosci. 12:303-310.

James, D.J., C. Khodthong, J.A. Kowalchyk, and T.F.J. Martin. (2008) Phosphatidylinositol 4,5-bisphosphate regulates SNARE-dependent membrane fusion. J. Cell. Biol. 182:355-366.

Jeon CJ, Strettoi E, Masland RH (1998) The major cell populations of the mouse retina. J. Neurosci. 18:8936-8946.

Johnson RI, Sedgwick A, D'Souza-Schorey C, Cagan RL (2011) Role for a Cindr-Arf6 axis in patterning emerging epithelia. Mol. Biol. Cell. 23:4513-4526.

Kahn RA, Bruford E, Inoue H, Logsdon JM Jr, Nie Z, Premont RT, Randazzo PA, Satake M, Theibert AB, Zapp ML, Cassel D (2008) Consensus nomenclature of the human ArfGAP domain-containing proteins. J. Cell. Biol. 182:1039-1044.

Kartberg F, Asp L, Dejgaard SY, Smedh M, Fernandez-Rodriguez J, Nilsson T, Presley JF (2010) ArfGAP2 and ArfGAP3 are essential for COP I coat assembly on the Golgi membrane of living cells. J. Biol. Chem. 285:36709-36720.

Katsumata O, Ohara N, Tamaki H, Niimura T, Naganuma H, Watanabe M, SakagamiH (2009) IQ-ArfGEF/BRAG1 is associated with synaptic ribbons in the mouse retina. Eur. J. Neurosci. 30:1509-1516.

Khimich D, Nouvian R, Pujol R, Tom Dieck S, Egner A, Gundelfinger ED, Moser T (2005)

Hair cell synaptic ribbons are essential for synchronous auditory □ignaling. Nature 434:889-894.

Kliouchnikov L, Bigay J, Mesmin B, Parnis A, Rawet M, Goldfeder N, Antonny B, Cassel D (2009) Discrete determinants in ArfGAP23/3 conferring Golgi localization and regulation by the COPI coat. Mol. Biol. Cell. 20:859-869.

Kumar V, Carlson JE, Ohgi KA, Edwards TA, RoseDW, Escalante CR, Rosenfeld MG, Aggarwal AK (2002) Transcription corepressor CtBP is an NAD(H) regulated dehydrogenase. Mol. Cell. 10:857-869.

Koch M, Holt M (2012) Coupling exo- and endocytosis: an essential role for PIP(2) at the synapse. Biochim. Biophys. Acta. 1821:1114-1132.

Lewis SM, Poon PP, Singer RA, Johnston GC, Spang A (2004) The ArfGAP Glo3 is required for the generation of COP I vesicles. Mol. Biol. Cell 15: 4064-4072.

Liu X, Zhang C, Xing G, Chen Q, He F (2001) Functional characterization of novel human ArfGAP3. FEBS. Lett. 490:79-83.

Loyet KM, Kowalchyk JA, Chaudhary A, Chen J, Prestwich GD, Martin TF (1998) Specific binding of phosphatidylinositol 4,5-bisphosphate to calcium-dependent activator protein for secretion (CAPS), a potential phosphoinositide effector protein for regulated exocytosis.J Biol. Chem. 14:8337-8343.

Magupalli VG, Schwarz K, Alpadi K, Natarajan S, Seigel GM, Schmitz F (2008) Multiple RIBEYE-RIBEYE interactions create a dynamic scaffold for the formation of synaptic ribbons. J. Neurosci. 28:7954-7967.

Masland RH (2012) The neuronal organization of the retina. Neuron 2:266-80.

Martin TF. PI(4,5)P(2) regulation of surface membrane traffic (2001) Curr. Opin. Cell. Biol. 13:493-499

Morgan JL, Soto F, Wong RO, Kerschensteiner D (2011) Development of cell type-specific connectivity patterns of converging excitatory axons in the retina. Neuron 71:1014-1021.

Nouvian R, Beutner D, Parsons TD, Moser T (2006) Structure and function of the hair cell ribbon synapse. J. Membr. Biol. 209:153-165

Nardini M, Spano S, Cericola C, Pesce A, Massaro A, Millo E, Luini A, Corda D, BolognesiM (2003) CtBP/BARS: a dual-function protein involved in transcriptional corepression and Golgi membrane fission. EMBO. J. 22:3122-3130.

Nishimune H, Sanes JR, Carlson SS (2004 A synaptic laminin-calcium channel interaction organizes active zones in motor nerve terminals. Nature 432:580-587.

Nie Z, Randazzo PA (2006) Arf GAPs and membrane traffic. J. Cell. Sci. 119:1203-1211.

Schnapp BJ, Lyass A, Muresan V (1999) The kinesin motor KIF3A is a component of presynaptic ribbon in vertebrate photoreceptors. J. Neurosci. 19:1027-1037.

Olmsted JB (1981) Affinity purification of antibodies from diazotized paper blots of heterogeneous protein samples. J.Biol. Chem. 256:11955-11957.

Panda-Jonas S, JB Jonas, M Jakobczyk, U Schneider (1994) Retinal photoreceptor count, retinal surface area, and optic disc size in normal human eyes. Ophthalmology 101:519-523.

Paliwal S, Kovi RC, Nath B, Chen YW, Lewis BC, Grossman SR (2007) The alternative reading frame tumor suppressor antagonizes hypoxia-induced cancer cell migration via interaction with the COOH-terminal binding protein co-repressor. Cancer. Res. 67:9322-9329

Polyak SL (1941) The retina. Chicago: University of Chicago Press.

Purves, D., Augustine, G.J., Fitzpatrick, D., Katz, L.C., La Mantia, A.S., McNamara, J.O and Williams, SM (2001) Neuroscience. Second edition.

Rea R, Li J, Dharia A, Levitan ES, Sterling P, Kramer RH (2004) Streamlined synaptic vesicle cycle in cone photoreceptor terminals. Neuron 41:755-766.

Rein U, Andag U, Duden R, Schmitt HD, SpangA (2002) ArfGAP-mediated interaction between ER-Golgi v-SNAREs and the COP I coat. J. Cell. Biol. 157:395-404.

Reim K, Wegmeyer H, Brandstätter JH, Xue M, Rosenmund C, Dresbach T, Hofmann K, Brose N (2005) Structurally and functionally unique complexins at retinal ribbon synapses. J.Cell. Biol. 169:669-680.

Regus-Leidig H, Ott C, Löhner M, Atorf J, Fuchs M, Sedmak T, Kremers J, Fejtová A, Gundelfinger ED, Brandstätter JH (2013) Identification and immunocytochemical characterization of Piccolino, a novel Piccolo splice variant selectively expressed at sensory ribbon synapses of the eye and ear. PloS ONE 8:70373.

Saitoh A, Shin HW, Yamada A, Waguri S, Nakayama K (2009) Three homologous ArfGAPs participate in coat protein I-mediated transport. J. Biol. Chem. 284:13948-13957.

Schermelleh L, CarltonPM, Haase S, Shao L, Winoto L, Kner P, Burke B, Cardoso MC, AgardDA, GustafssonMG, Leonhardt H, SedatJW (2008) Subdiffraction multicolor imaging of the nuclear periphery with 3D structured illumination microscopy. Science 320:1332-1336.

Schermelleh L, Heintzmann R, Leonhardt H (2010) A guide to superresolution fluorescence microscopy. J. Cell. Biol. 190:165-175.

Schindler C, Spang A (2007) Interaction of SNAREs with ArfGAPs precedes recruitment of sec18p/NSF. Mol. Bio. Cell. 18:2852-2863.

Schindler C, Rodriguez F, Poon PP, Singer RA, Johnston GC, SpangA (2009) The GAP domain and the SNARE, coatomer and cargo interaction region of the ArfGAP2/3 glo3 are sufficient for glo3 function. Traffic 10:1362-1375.

Scholz R, Berberich S, Rathgeber L, Kolleker A, Kohr G, Kornau HC (2010) AMPA receptor signaling through BRAG2 and Arf6 critical for long-term synaptic depression. Neuron 66:768-780.

Schmitz F (2009) The making of synaptic ribbons: how they are built and what they do. Neuroscientist 15:611-624.

Schmitz F, Königstorfer A, Südhof TC (2000) RIBEYE, a component of ribbon synapses: a protein's journey through evolution provides insight into synaptic ribbon function. Neuron 28:857-872.

Schmitz F, Natarajan S, Venkatesan JK, Wahl S, Schwarz K, Grabner CP (2012) EF hand-mediated Ca and cGMP signaling in photoreceptor synaptic terminals. Front. Mol. Neurosci. 5:26.

Schnee ME, Santos-Sacchi J, Castellano-Mun˜oz M, Kong JH, Ricci AJ (2011) Calcium-dependent synaptic vesicle trafficking underlies indefatigable release of the hair cell afferent fiber synapse. Neuron 70:326-338.

Schwarz K, Natarajan S, Kassas N, Vitale N, Schmitz F (2011) The synaptic ribbon is a site of phosphatidic acid generation in ribbon synapses. J. Neurosci. 31:15996-16011.

Shin OH (2010) Munc13 C2B domain is an activity-dependent $Ca2^{+}$ regulator of synaptic exocytosis Nat. Struct. Mol. Biol. 17:280-288.

Sjöstrand, F.S (1953) Electron microscopy of mitochondria and cytoplasmic double membranes Nature 171:30-32.

Snellman J, Mehta B, Babai N, Bartoletti TM, Akmentin W, Francis A, Matthews G, Thoreson W, Zenisek D (2011) Acute destruction of the synaptic ribbon reveals a role for the ribbon in vesicle priming. Nat. Neurosci. 14:1135-1141.

Springer, S., A. Spang, and R. Schekman (1999) A primer on vesicle budding. Cell 97:145-148.

Sterling, P and Matthews, G (2005) Structure and function of ribbon synapses. Trends Neurosci. 28:20-29.

Spang A, Shiba Y, Randazzo PA (2010) ArfGAPs: gatekeepers of vesicle generation. FEBS. Lett. 584:2646-2651.

Spassova MA, Avissar M, Furman AC, Crumling MA, Saunders JC, Parsons TD (2004) Evidence that rapid replenishment of the synaptic ribbon mediates recovery from short-term adaptation at the hair cell afferent synapse. J. Assoc. Res. Otolaryngol. 5:376-390.

Tai AW, Chuang JZ, Bode C, Wolfrum U, Sung CH (1999) Rhodopsin's carboxyterminal cytoplasmic tail acts as a membrane receptor for cytoplasmic dynein by binding to the dynein light chain tctex-1. Cell 97:877-887.

Tian M, Xu CS, Montpetit R, KramerRH (2012) Rab3a mediates vesicle delivery at photoreceptor ribbon synapses. J. Neurosci. 32:6931-6936.

Tom Dieck S, Altrock WD, Kessels MM, Qualmann B, Regus H, Brauner D, Fejtova´ A, Bracko O, Gundelfinger ED, Brandstätter JH (2005) Molecular dissection of the photoreceptor ribbon synapse: physical interaction of Bassoon and RIBEYE is essential for the assembly of the ribbon complex. J. Cell. Biol. 168:825-836.

Tom Dieck S, Brandstätter JH (2006) Ribbon synapses of the retina. Cell. Tissue. Res. 326:339-346.

Vaithianathan T, Akmentin W, Henry D, Matthews G (2013) The ribbonassociatedprotein C-terminal-binding protein 1 is not essential for the structure and function of retinal ribbon synapses. Mol. Vis. 19:917-926.

Van Buren JM. The retinal ganglion cell layer (1963). Springfield (IL): Charles C. Thomas.

Venkatesan JK, Natarajan S, Schwarz K, Mayer SI, Alpadi K, Magupalli VG, Sung CH, Schmitz F (2010) Nicotinamide adenine dinucleotide dependent binding of the neuronal Ca^2-sensor protein GCAP2 to photoreceptor synaptic ribbons. J. Neurosci. 30:6559-6576.

Vergara MN, Gutierrez C, O'Brien DR, Canto-Soler MV (2013) Ex vivo electroporation of retinal cells: a novel, high efficiency method for functional studies in primary retinal cultures. Exp. Eye. Res. 109:40-50.

Wahl S, Katiyar R, Schmitz F (2013) A local, periactive zone endocytic machinery at photoreceptor synapses in close vicinity to photoreceptor synaptic ribbons. J. Neurosci. 33:10278-10300.

Wang Y, Okamoto M, Schmitz F, Hofmann, K, Südhof TC, (1997) Rim is a putative rab3 effector in regulating synaptic-vesicle fusion. Nature 388:593-598.

Watson PJ, Frigerio G, Collins BM, Duden R, Owen DJ (2004) gamma-COP appendage domain-structure and function. Traffic 5:79-88.

Williams PR, Morgan JL, Kerschensteiner D, Wong RO (2013) In vitro imaging of retinal whole mounts. Cold. Spring. Harb. Protoc. 2013(1).

Yang JS, Lee SY, Gao M, Bourgoin S, Randazzo PA, Premont RT, Hsu VW (2002) ArfGAP1 promotes the formation of COPI vesicles, suggesting function as a component of the coat. J. Cell. Biol. 159:69-78.

Yang JS, Lee SY, Spano S, Gad H, Zhang L, Nie Z, Bonazzi M, Corda D, Luini A, Hsu VW (2005) A role for BARS at the fission step of COP I vesicle formation from the Golgi membrane. EMBO. J. 24:4133-4143.

Yang JS, Zhang L, Lee SY, Gad H, Luini A, HsuVW (2006) Key components of the fission machinery are interchangeable. Nat. Cell. Biol. 8:1376-1382.

Yu X, Breitman M, Goldberg J (2012) A structure-based mechanism for Arf1-dependent recruitment of coatomer to membranes. Cell 148:530-542.

Zenisek D, Steyer JA, AlmersW (2000) Transport, capture and exocytosis of single synaptic vesicles at active zones. Nature 406:849-854.

Zhang Q, Piston DW, Goodman RH (2002) Regulation of co-repressor function by nuclear NADH. Science 295:1895-1897.

Zhang Q, Wang SY, Nottke AC, Rocheleau JV, Piston DW, Goodman RH (2006) Redox sensor CtBP mediates hypoxia-induced tumor cell migration. Proc. Natl. Acad. Sci. U S A 103:9029-9033.

LIST OF ABBREVIATIONS:

µg	Microgram
µl	microlitre
A	Adenine
A260 nm	Absorbance at 260 nm
A280 nm	Absorbance at 280 nm
aa	Amino acids
AD	Activation Domain
AGD	Arf GAP Domain
-ALWH	Drop out medium lacking Adenine, Leucine, Tryptophan and Histidine
Amp	Ampicillin
Arf's	ADP ribosylation factor
Arl's	ADP ribosylation factor like
BD	Binding Domain
bp	base pair
BSA	Bovine serum albumin
°C	Celsius
COS cells	CV-1 (simian) in Origin, carrying SV40 genetic material.
cDNA	Complementry DNA
CSF	Cerebral spinal fluid
CtBP2	C-terminal Binding Protein 2
ddH_2O	double distilled water
DMEM	Dulbecco´s Modified Eagle's Medium
DNA	Deoxyribonucleicacid
dNTP	deoxyribonucleotides
DTT	Dithiothreitol
ECL	Enhanced chemiluminiscence
E. coli	Escherichia coli
EGFP	Enhanced Green Fluorescent Protein
EDTA	Ethylenediaminetetrachloroacteic acid
f.l.	Full length
GAP-domain	GTPase activating domain
Gal	Galactose
GCAP2	guanylate cyclase-activating protein
GCL	Ganglion cell layer
GST	Glutathione S-transferase
H	Histidine
hc	Horizontal cell
INL	Inner nuclear layer
IPTG	Isopropyl-β-D-Thiogalactopyranoside
IPL	Inner plexiform layer
IS	Inner segments
I.S.	Immune serum
kb	Kilobases
kDa	kilo Dalton
-L	Yeast selection medium lacking Leucine

LB	Luria-Bertani medium
-LW	Yeast selection medium lacking Leucine and Tryptophan
MBP	Maltose binding protein
MCS	Multiple cloning site
min(s)	minute(s)
ml	millilitre
MW	Molecular weight
NAD^+	oxidized Nicotinamide adenine dinucleotide
NADH	reduced Nicotinamide adenine dinucleotide
NBD	NADH binding sub-domain
nm	nanometer
NLS	Nuclear localization signal
OD	Optical density
OLM	Outer Limiting Membrane
ONL	Outer nuclear layer
OPL	Outer plexiform layer
OS	Outer segments
p	Primer
PBS	Phosphate Buffered Saline
PCR	Polymerase Chain Reaction
PFA	Paraformaldehyde
RE(A)	RIBEYE(A)-Domain
RE(B)	RIBEYE(B)-Domain
rpm	revolutions per minute
RT	Room temperature
SBD	Substrate binding sub-domain
S	Synthetic Drop out medium
SDS	Sodiumdodecylsulfate
SNARE	Soluble NSF Attachment Protein receptor"
SDS-PAGE	SDS Polyacrylamide gel electrophoresis
TAE	Tris Acetate EDTA
TE	Tris EDTA
Tris	Trishydroxymethylaminomethane
U	Unit
V	Volts
-W	Yeast selection medium lacking Tryptophan
X-Gal	5-Bromo-4-chloro-3-indolyl-β-D-galactopyranoside
YPD	Yeast extract, peptone, and dextrose
YTH	Yeast two-hybrid

LIST OF FIGURES:

Curriculum Vitae

DEMBLA MAYUR HARISH

Postal address
Paracelsusstrasse 21,
Homburg 66424, Germany.
Date of Birth: *27 Dec'1982.*
Email*:m.dembla27@gmail.com*
Ph. no*: 004917660924109*

Academic experience

Oct'10-Sep'15	**PhD student at Universitat des Saarlandes**	**Homburg**
Aug'2003-05	**M.Sc Biotechnology**, (IASCA-ITM) from Jiwaji University with Distinction	**Gwalior**
July'2000-03	**B.Sc. Microbiology, B.P.** Baria Science Institute Navsari from VNSGU University with First Class	**Surat**

Professional experience

Dec'05-Oct'10	**Senior Research Officer at Span Diagnostics ltd, Department of Immunology**	**Surat**
Jan'2010	**Anna University, Biotech Dept.** Recombinant WbSxp-I protein expression in Baculovirus system	**Chennai**
Dec'2009	**Training at ICGEB. Malaria Lab.** culture, expression & purification of rHRP-II Protein for P Falciparum.	**New Delhi**
July'2007	**Training at South Campus, Delhi University** culture, expression and purification of rp17kDa, rp55kDa & rp66kDa Protein of HIV	**New Delhi**
May' 2007	**Training at IISC Bangalore:** culture, expression & purification of rPf LDH protein of P falciparum.	**Bangalore**
May' 2007	**Training at Anna University, Biotech Dept**	**Chennai**
Feb –June' 2005	**Master Thesis at Institute of Toxicological Research** Mechanistic toxicity study of cypermethrin using Drosophila melanogaster DNA repair mutants with use of comet assay technique.	**Lucknow**

Educational Qualification

March'1999-00	**Intermediate of Science (12th)** at C C Shah High School GSEB Board	**Surat**
March'1998-99	**Matriculation (10th)** at C C Shah High School, GSEB Board	**Surat**

Publications

2014 ArfGAP3 Is a Component of the Photoreceptor Synaptic Ribbon Complex and Forms an NAD(H)-Regulated, Redox-Sensitive Complex with RIBEYE That Is Important for Endocytosis. **Mayur Dembla**, Silke Wahl, Rashmi Katiyar, and Frank Schmitz. ***The Journal of Neuroscience*** 35: 5245-5260.

2015 The disease protein Tulp1 is essential for peri-active zone endocytosis in photoreceptor ribbon synapses. Silke Wahl, Venkat Giri Magupalli, **Mayur Dembla**, Rashmi Katiyar, Louise Köblitz, Karin Schwarz, Kannan Alpadi,

Elmar Krause, Jens Rettig, Ching-Hwa Sung, Andrew F.X. Goldberg, Frank Schmitz. ***The Journal of Neuroscience.*** (Under revision)

Technical Expertise

1. Yeast Two Hybrid Assays
2. Recombinant-DNA technology,
3. Bacterial and eurkaryotic proteins expression & purification
4. Site-directed Mutagenesis
5. Pull-down assay, Co-immunoprecipitation
6. Cell culture and Transfection methods
7. Immunohistochemistry
8. Organotypic culture of Retina
9. Fluorescence microscopy (Confocal & SR-SIM)
10. Electron microcopy related techniques

Reference:

Prof. Dr. Frank Schmitz
Institute of Anatomy and Cell Biology.
Building 61, Homburg 66421, Saarland,
Germany.
email: frank.schmitz@uniklinik-saarland.de.
Tel: +4968411626012
Fax: +4968411626112

Dr. H. C. Mody
Arlington Scientific, Inc.1840 N
Springville, UTAH 84663, USA.
Tel: 801489891
email: hcmody@gmail.com

Cellular/Molecular

ArfGAP3 Is a Component of the Photoreceptor Synaptic Ribbon Complex and Forms an NAD(H)-Regulated, Redox-Sensitive Complex with RIBEYE That Is Important for Endocytosis

Mayur Dembla, Silke Wahl,* Rashmi Katiyar,* and Frank Schmitz
Saarland University, Medical School, Department of Neuroanatomy, 66421 Homburg/Saar, Germany

Ribbon synapses are tonically active synapses in the retina and inner ear with intense vesicle traffic. How this traffic is organized and regulated is still unknown. Synaptic ribbons, large presynaptic structures associated with numerous synaptic vesicles, appear to be essential for this process. The base of the synaptic ribbon is anchored at the active zone and is a hotspot of exocytosis. The synaptic ribbon complex is also important for vesicle replenishment. RIBEYE is a unique and major component of synaptic ribbons. It consists of a unique A-domain and an NAD(H)-binding, C-terminal B-domain. In the present study, we show that the Arf-GTPase activating protein-3 (ArfGAP3), a well characterized regulator of vesicle formation at the Golgi apparatus, is also a component of the synaptic ribbon complex in photoreceptor synapses of the mouse retina and interacts with RIBEYE as shown by multiple, independent approaches. ArfGAP3 binds to RIBEYE(B)-domain in an NAD(H)-dependent manner. The interaction is redox sensitive because NADH is more efficient than the oxidized NAD^+ in promoting ArfGAP3-RIBEYE interaction. RIBEYE competes with the GTP-binding protein Arf1 for binding to ArfGAP3. Thus, binding of RIBEYE(B) to ArfGAP3 could prevent inactivation of Arf1 by ArfGAP3 and provides the synaptic ribbon with the possibility to control Arf1 function. The interaction is relevant for endocytic vesicle trafficking because overexpression of ArfGAP3 in photoreceptors strongly inhibited endocytotic uptake of FM1–43.

Key words: **ArfGAP3; endocytosis; photoreceptor synapse; ribbon synapse; RIBEYE; synaptic ribbon**

Introduction

Ribbon synapses, e.g., retinal photoreceptor synapses, are continuously active synapses with a high vesicle turnover. How this vesicle traffic is organized and regulated is still largely unknown. Synaptic ribbons, large presynaptic structures associated with numerous synaptic vesicles, appear to play a central role in this process. The basal end of the synaptic ribbon is anchored at the active zone where L-type voltage-gated channels are clustered. This site is a hotspot of exocytosis (Zenisek et al., 2000; Frank et al., 2010; Chen et al., 2013). The synaptic ribbon complex is also relevant for vesicle recycling (Spassova et al., 2004; Griesinger et al., 2005; Jackman et al., 2009; Babai et al., 2010; Frank et al., 2010; Schnee et al., 2011; Snellman et al., 2011; Tian et al., 2012; Wahl et al., 2013). In photoreceptor synapses, synaptic vesicle retrieval occurs in the periactive zone, in close proximity to the synaptic ribbon (Wahl et al., 2013). RIBEYE is a major and unique component of synaptic ribbons (Schmitz et al., 2000; for review, see Schmitz, 2009). It consists of an N-terminal A-domain and a C-terminal B-domain. The B-domain is largely identical with the protein CtBP2 and binds NAD(H) (for review, see Schmitz, 2009; Schmitz et al., 2012).

Small GTP-binding proteins of the Arf family are important regulators of intracellular membrane traffic (for review, see Gillingham and Munro, 2007). Arf proteins switch between a GTP-bound, active form and a GDP-bound, inactive form. Which nucleotide is bound is regulated by the activity of two classes of proteins, the ArfGEFs (Arf GTP-exchange factors) and the ArfGAPs (Arf-GTPase-activating proteins; for review, see Inoue and Randazzo, 2007; Kahn et al., 2008; Spang et al., 2010). ArfGAPs enhance the low intrinsic GTPase activity of Arfs. A large number of ArfGAPs have been identified in higher organisms. Conserved hallmark of ArfGAPs is an ~136 aa long, catalytically active GAP-domain (AGD) with a central Zn-finger motif that stimulates GTPase activity of the attached Arf (Cukierman et al., 1995; Goldberg, 1999). The regions outside of the

Received Sept. 8, 2013; revised Feb. 27, 2014; accepted March 7, 2014.

Author contributions: F.S. designed research; M.D., S.W., R.K., and F.S. performed research; M.D., S.W., R.K., and F.S. analyzed data; F.S. wrote the paper.

This work was supported by the German research community Deutsche Forschungsgemeinschaft (SFB894 and GRK1326). We thank Dr. Ching-Hwa Sung (Weill Medical College, Cornell University, New York) for the bovine retina YTH cDNA library, Dr. Rachel Wong (University of Washington, Seattle) for the kind gift of a retina incubation chamber and for her support and advice on retinal explant cultures, Dr. Andreas Beck (Saarland University, Department of Pharmacology) for advice for quantification of binding experiments, Dr. Kannan Alpadi for cloning of the bassoon-pGAD-T7 construct, Dr. Elmar Krause (platform project P1, SFB894) for help with the SIM microscope, and Dr. Jutta Schmitz-Kraemer for critically reading this manuscript.

*S.W. and R.K. contributed equally to this work.

The authors declare no competing financial interests.

Correspondence should be addressed to Dr. Frank Schmitz, Saarland University, Medical School, Institute of Anatomy and Cell Biology, Department of Neuroanatomy, 66421 Homburg/Saar, Germany. E-mail: frank.schmitz@uks.eu.

DOI:10.1523/JNEUROSCI.3837-13.2014

 0270-6474/14/345245-16$15.00/0

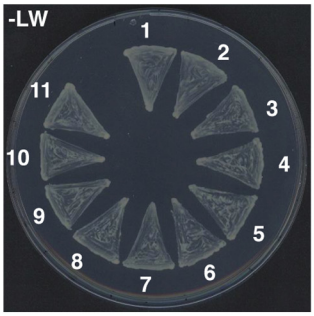

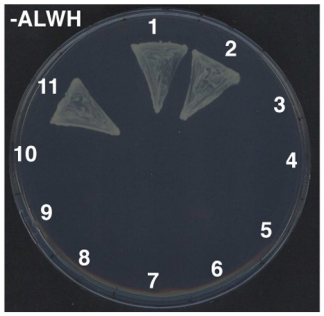

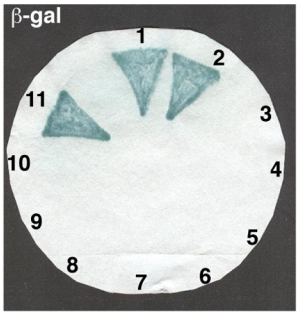

mating	bait	prey	-ALWH	βGal
1	RE(AB)	ArfGAP3(1-517)	+	+
2	RE(B)	ArfGAP3(1-517)	+	+
3	RE(AB)	pACT2	–	–
4	RE(AB)	pSE1111	–	–
5	RE(B)	pACT2	–	–
6	RE(B)	pSE1111	–	–
7	pGBKT7	ArfGAP3(1-517)	–	–
8	pSE1112	ArfGAP3(1-517)	–	–
9	pGBKT7	RE(A)	–	–
10	pSE1112	RE(A)	–	–
11	RE(B)	RE(A)	+	+

Figure 1. RIBEYE(B) and RIBEYE(AB) interact with ArfGAP3 in the YTH system. Summary plates of YTH analyses obtained with the indicated bait and prey plasmids. For convenience, experimental bait–prey pairs are underlayered in color (green in case of interacting bait–prey pairs; control matings are noncolored). RIBEYE(B) and also full-length RIBEYE [RIBEYE(AB)] interact with ArfGAP3 in the YTH system (matings 1 and 2). Mating 11 denotes an unrelated positive control (Magupalli et al., 2008). pSE1111 is an irrelevant prey vector and pSE1112 is an irrelevant bait vector (Tai et al., 1999; Magupalli et al., 2008). Negative control matings of the ArfGAP3 prey clone with empty bait clones (mating 7) or irrelevant bait clones (mating 8) demonstrate that the ArfGAP3 clone is not auto activating. The other matings represent negative control matings for the RIBEYE bait clones (matings 3–6) or RIBEYE prey clones (matings 9 and 10), demonstrating that these constructs are also not auto activating in the YTH system. RE(AB), full-length RIBEYE, containing both RIBEYE(A)- and RIBEYE(B)-domain; RE(A), RIBEYE(A)-domain; RE(B), RIBEYE(B)-domain; AGD, ArfGAP-domain of ArfGAP3.

AGD are divergent in different ArfGAPs. The prototypical yeast ArfGAPs gcs1p and glo3p possess mammalian orthologs in ArfGAP1 (for gcs1p) and ArfGAP2/ArfGAP3 (for glo3p). In these ArfGAPs, the conserved AGD is located at the N terminus. Both classes of ArfGAPs possess distinct motifs in their C terminus, which mediate membrane binding (Bigay et al., 2005; Kliouchnikov et al., 2009) as well as other functions (for review, see Spang et al., 2010).

In the present study, we identified ArfGAP3 as a new component of the synaptic ribbon complex in photoreceptor synapses of the mammalian retina. ArfGAP3 is a well known component of the Golgi apparatus where it regulates retrograde trafficking from the Golgi to the endoplasmic reticulum (for review, see Spang et al., 2010). We provide evidence that ArfGAP3 is important for controlling Arf1 activity at the synaptic ribbon complex and for regulating endocytic membrane traffic.

A

mating	bait	prey	-ALWH	β-gal
1	RE(AB)	ArfGAP3(AGD)	+	+
2	RE(B)	ArfGAP3(AGD)	+	+
3	RE(AB)	pACT2	-	-
4	RE(AB)	pSE1111	-	-
5	RE(B)	pACT2	-	-
6	RE(B)	pSE1111	-	-
7	pGBKT7	ArfGAP3(AGD)	-	-
8	pSE1112	ArfGAP3(AGD)	-	-
9	RE(B)	RE(A)	+	+
10	pGBKT7	RE(A)	-	-
11	pSE1112	RE(A)	-	-

B

mating	bait	prey	-ALWH	β-gal
1	NBD-RE(B)	ArfGAP3(1-517)	+	+
2	SBD-RE(B)	Bassoon	+	+
3	NBD-RE(B)	Munc119	+	+
4	RE(B)	RE(A)	+	+
5	SBD-RE(B)	ArfGAP3(1-517)	-	-
6	NBD-RE(B)	pACT2	-	-
7	NBD-RE(B)	pSE1111	-	-
8	SBD-RE(B)	pACT2	-	-
9	SBD-RE(B)	pSE1111	-	-
10	pGBKT7	ArfGAP3(1-517)	-	-
11	pSE1112	ArfGAP3(1-517)	-	-

C

D

mating	bait	prey	-ALWH	β-gal
1	RE(B)G730A	ArfGAP3(1-517)	-	-
2	RE(B)G730A	pACT2	-	-
3	RE(B)G730A	pSE1111	-	-
4	pGBKT7	ArfGAP3(1-517)	-	-
5	pSE1112	ArfGAP3(1-517)	-	-
6	RE(B)	ArfGAP3(1-517)	+	+
7	RE(B)G730A	RE(B)	+	+

E

mating	bait	prey	-ALWH	β-gal
1	Arf1	ArfGAP3(1-517)	+	+
2	Arf1	pACT2	-	-
3	Arf1	pSE1111	-	-
4	pGBKT7	ArfGAP3(1-517)	-	-
5	pSE1112	ArfGAP3(1-517)	-	-
6	RE(B)	ArfGAP3(1-517)	+	+

Figure 2. Summary tables of YTH matings. ***A***, RIBEYE interacts with the ArfGAP-domain (AGD) of ArfGAP3. RIBEYE(B) and also full-length RIBEYE [RIBEYE(AB)] interact with the ArfGAP-domain (AGD) of ArfGAP3 in the YTH system (matings 1 and 2). Mating 9 denotes an unrelated positive control (Magupalli et al., 2008). The other matings are auto-activation controls. None of the yeast constructs is auto activating. ***B***, The NAD(H)-binding subdomain of RIBEYE(B) interacts with ArfGAP3. The NAD(H)-binding subdomain of RIBEYE(B), the NBD, interacts with ArfGAP3 (mating 1), but not the substrate-binding subdomain of RIBEYE(B), the SBD (mating 5). Matings 2–4 are positive control matings–(Bassoon for SBD-RE(B); tom Dieck et al., 2005), Munc119 for NBD-RE(B) (Alpadi et al., 2008), RE(A) for RE(B) (Magupalli et al., 2008)–and matings 6–11 are negative controls (auto-activation controls). ***C***, Schematic domain structures of ArfGAP3. ***D***, An NAD(H)-binding-deficient mutant of RIBEYE(B), RE(B)G730A, does not interact with ArfGAP3 (mating 1), while wild-type RIBEYE does (mating 6). Mating 7 is a positive control mating for RE(B)G730A. ***E***, Arf1 interacts with ArfGAP3 (mating 1). All constructs are non-auto activating as demonstrated by the negative control matings (2–5); mating 6 is a positive control mating. RE(A), RIBEYE(A)-domain; RE(B), RIBEYE(B)-domain; RE(B)G730A, RIBEYE(B)G730A; GAP-dom, GAP-domain (AGD) of ArfGAP3; NBD, NAD(H)-binding subdomain of RIBEYE(B); SBD, substrate-binding subdomain of RIBEYE(B).

Materials and Methods

Plasmids

Bacterial expression constructs. These include *ArfGAP3(AGD)-pGEX-KG*, which encodes the ArfGAP-domain (AGD) (amino acids 1–136) of bovine ArfGAP3. The insert was excised from *GAP-dom(ArfGAP3)pACT2* with EcoRI and XhoI and cloned into the EcoRI/XhoI sites of pGEX-KG. *ArfGAP3(AGD)-pMal-C2*, encoding the ArfGAP-domain of bovine ArfGAP3. The insert was amplified from bovine ArfGAP3 cDNA (BC118087) using the following forward primer AAAAGAATTCA TGGGGGACCCCAG and reverse primer AAAAGTCGACGCTATCAAGCCAGAG and cloned into the EcoRI/SalI sites of pMal-C2. Also included is *ArfGAP3(AGD-extended)-pMal-C2*, which encodes the extended ArfGAP-domain (AGD extended, amino acids 1–225 of bovine ArfGAP3). The insert was amplified from bovine ArfGAP3 cDNA (BC118087) using forward primer AAAAGAATTCATG GGGGACCCCAG reverse primer AAACTCGAGAAGTCCT CTTTTAGC and cloned into the EcoRI/SalI sites of pMal-C2. *ArfGAP3(AGD extended)-pSNAPtagT7* encodes the extended ArfGAP-domain. The insert was amplified from bovine ArfGAP3 cDNA (BC118087) using forward primer AAAAGGATCCATGGGGGACCCCA and reverse primer AAACTCGAGAAGTCC TCTTTTAGC and cloned into the BamHI/XhoI sites of pSNAPtagT7 (NEB). *ArfGAP3Cterm2-pGEX-KG* encodes amino acids 226–335 of bovine ArfGAP3. The insert was amplified from bovine ArfGAP3 cDNA using forward primer AAAGAATTCGGGCCAAAAAAG GAAGT and reverse primer AAACTCGAGCGTGA TTGGTGTTTC and cloned into the EcoRI/XhoI sites of pGEX-KG. *ArfGAP3Cterm3-pGEX-KG* encodes amino acids 332–460 of bovine ArfGAP3. The insert was amplified from bovine ArfGAP3 cDNA using forward primer AAAGAATTCAAACACCAATCACG GCG and reverse primer AAACTCGAG AGCTGAGCTGATGGA and cloned into the EcoRI/XhoI sites of pGEX-KG. *RIBEYE(B)-MBP* (Magupalli et al., 2008). The plasmid *pMal-C2* corresponds to the commercially available pMal-C2 vector (NEB) to which multiple STOP codons have been added in all reading frames at the end of the multiple cloning site using standard methods.

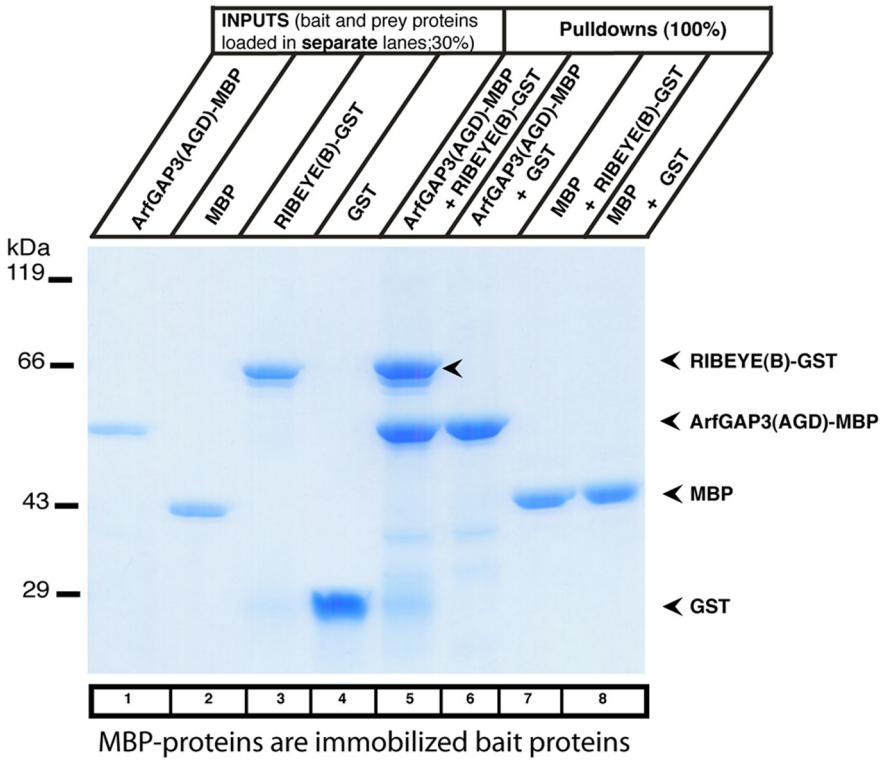

Figure 3. RIBEYE(B) specifically interacts with ArfGAP3 in fusion protein pull-down assays (SDS-PAGE analyses). Pull-down analyses of RIBEYE(B)/ArfGAP3 complexes were analyzed by Coomassie blue-stained polyacrylamide gel after SDS-PAGE. Lanes 1–4 show the indicated purified fusion proteins (input fractions). All input lanes represent 30% of the input fraction. Input proteins were loaded in separate lanes to demonstrate that the input fusion proteins display only a single, main protein band. In lanes 5–8, 100% of the pull-down reactions were loaded. MBP-tagged fusion proteins were used as immobilized bait proteins and GST-tagged proteins as soluble prey proteins. Only ArfGAP3-MBP pulled down RE(B)-GST (lane 5, arrowhead) but not MBP alone (lane 7). Neither MBP alone nor ArfGAP3-MBP pulled down GST alone (lanes 6 and 8). SDS-PAGE demonstrated that ArfGAP3-MBP specifically pulled down RIBEYE(B)-GST, demonstrating interaction of the two proteins in this assay system.

RE(B)pGEX-KG (Schmitz et al., 2000). *RE(B)G730ApGEX-KG* (Alpadi et al., 2008; Venkatesan et al., 2010). *Arf1-pGEX-KG*. The insert (~0.55 kb) was amplified from a bovine cDNA library using forward primer AAAACCATGGCGAATATCTTTGCAAAC and reverse primer AAAACTCGAGTCATTT CTGGTTC and cloned into the NcoI/XhoI sites of pGEX-KG. Plasmid constructs were verified by sequencing.

Eukaryotic expression constructs. ArfGAP3-mCherry encodes amino acids 1–517 of bovine ArfGAP3. Full-length ArfGAP3 was amplified by PCR using forward primer AAACTCGAGGCCACCATGGGGGA CCCCAGCAAG, reverse primer AAAGAATTCCGGAACCGTAG CGATC, and ArfGAP3 cDNA as template. The ~1.5 kb PCR product was cloned into the XhoI/EcoRI sites of pCherry-N1 (Alpadi et al., 2008). *RE(B)-EGFP* (Schmitz et al., 2000).

Yeast vectors

ArfGAP3-pACT2 encoding full-length bovine ArfGAP3 was obtained by yeast two-hybrid (YTH) screening with RIBEYE as bait construct. *ArfGAP3cDNA-pACT2*, encoding amino acids1–517 of bovine ArfGAP3, was amplified from the full-length ArfGAP3 IMAGE clone #8081904 (BC118087) using forward primer AAAGAATTCTGA TCATGGGGAC and reverse primer AAACTCGAGTTAGGAAC CGTAGCG and cloned into the EcoRI/XhoI sites of pACT2. *ArfGAP3(AGD)pACT2* encodes the ArfGAP-domain of ArfGAP3. The insert was amplified by PCR using forward primer AAAGAATTCTGAT CATGGGGAC, reverse primer AAACTCGAGTTAGCTATC AAGCCA, and bovine ArfGAP3 cDNA (BC118087) as a template. The PCR product was cloned into the EcoRI/XhoI sites of pACT2. *CtermArfGAP3pACT2*, encoding amino acids 127–517 of bovine ArfGAP3, was amplified from bovine ArfGAP3 cDNA (BC118087) using forward primer AAAGAATTCAGCACGGGCACTGAC and reverse primer AAACTCGAGTTAGGAACCGTAGC G and cloned into the EcoRI/XhoI sites of pACT2. The insert of *Arf1-pGBKT7* (~0.55 kb) was amplified from a bovine cDNA library (Alpadi et al., 2008) using forward primer AAAACCATGGCGAATATCTTTGCAAAC and reverse primer AAAACTCGAGTCATT TCTGGTTC and cloned into the NcoI/SalI sites of pGBKT7. *RE(AB)pGBK-T7* (Magupalli et al., 2008). *RE(B)pGBK-T7* (Magupalli et al., 2008). *RE(B)NBD-pGBK-T7* (Alpadi et al., 2008). *RE(B)SBD-pGBK-T7* (Alpadi et al., 2008). *RE(B)G730A-pGBK-T7* (Alpadi et al., 2008). *RE(A)pACT2* (Magupalli et al., 2008). *pGBK-T7* (empty bait plasmid) (Tai et al., 1999; Magupalli et al., 2008). *pSE1112* (control bait plasmid) (Tai et al., 1999; Magupalli et al., 2008). *pACT2* (empty prey plasmid) (Magupalli et al., 2008). *pSE1111* (control prey plasmid) (Tai et al., 1999; Magupalli et al., 2008). *Munc119pACT2* (Alpadi et al., 2008). Munc119 is known to interact with RIBEYE(B)-domain and was used as a positive control for yeast matings. *Bassoon pGAD-T7* (encoding amino acids1638–2081 of rat bassoon, NP062019.2) was cloned by reverse-transcriptase -PCR using cDNA isolated from rat R28 cells (Alpadi et al., 2008), forward primer TTTTCATATGTGC-CGGATCTCCTCTGTCCCT, and reverse primer TTTTGAATTCC TGGGCCAGGCTG-GCCTCCTG and cloned into the NdeI/EcoRI sites of pGADT7. Bassoon pGAD-T7 was used as a positive control mating for RIBEYE(B) (tom Dieck et al., 2005). Plasmid constructs were verified by sequencing.

Antibodies

Primary antibodies. The following primary antibodies were used in the present study: mouse monoclonal anti-GST (Sigma; Alpadi et al., 2008) used at 1:10,000 dilution for Western blotting; mouse monoclonal anti-MBP (NEB; Alpadi et al., 2008) used at 1:10,000 dilution for Western blotting; rabbit polyclonal anti-RIBEYE(B)-domain (U2656; Schmitz et al., 2000) used at 1:10,000 for Western blotting for immunofluorescence microscopy at a 1:1000 dilution; mouse monoclonal antibodies against RIBEYE(B)-domain/CtBP2 (BD Transduction Laboratories; Alpadi et al., 2008; Schwarz et al., 2011; Wahl et al., 2013) used at a 1:1000 dilution; mouse monoclonal anti-Bassoon (Stressgen, VAM-PS003) used at a 1:100 dilution for immunofluorescence microscopy (Wahl et al., 2013); mouse monoclonal antibody against Arf1 (ARFS 1A9/5; Santa Cruz Biotechnology, sc-53168) used at a 1:500 dilution; and anti-dynamin (hudy-1; Millipore) used at a 1:50 dilution. The DyLight 650 directly labeled mouse monoclonal antibody against RIBEYE(B)/CtBP2 was diluted 1:2.

We generated two different polyclonal antisera against two different regions in the C terminus of ArfGAP3 (Cterm2 and Cterm3; see Fig. 7*A*). ArfGAP3Cterm2-pGEX and ArfGAP3Cterm3-pGEX were electroporated into Bl21(DE3) and fusion proteins were expressed and purified as previously described (Schmitz et al., 2000). For antibody production, the purified fusion proteins were injected into rabbits multiple times. Immune sera were screened for reactivity against the fusion protein and the endogenous protein. Pre-immune serum was used as control serum. Both ArfGAP3 antibodies (named ArfGAP3Cterm2- and ArfGAP3Cterm3-antisera) were used for Western blotting in a 1:3000 dilution for immunofluorescence microscopy in a dilution of 1:20. Affinity-purified ArfGAP3 antibodies were used at a concentration of 10 μg/ml for immunofluorescence microscopy. ArfGAP3Cterm2 and ArfGAP3Cterm3 antibodies worked well for Western blotting and

immunofluorescence microscopy. Unfortunately, they did not work at the electron microscopic level, both in pre-embedding and postembedding procedures with immunogold- and immunoperoxidase-based techniques with the procedures available in our laboratory. Also the following commercially available antibodies did not work in postembedding immunogold electron microscopy: rabbit and goat polyclonal anti-ArfGAP3 antibodies (AAS68618C and ASA34060; Antibody Verify), rabbit polyclonal anti-ArfGAP3 (NBP1-18921; Novus Biologicals), rabbit polyclonal anti-ArfGAP3 (HPA000638; Sigma), and rabbit polyclonal anti-ArfGAP3 (A302-032A; Biomol).

Secondary antibodies (for immunofluorescence labeling). The following secondary antibodies were used: chicken anti-mouse Alexa 488, donkey anti-rabbit Alexa 568, goat anti-mouse Alexa 488. All fluorophore-conjugated secondary antibodies were purchased from Invitrogen and used at a 1:1000 dilution for 1 h at room temperature (RT) for immunolabeling experiments.

Methods

YTH analyses. YTH assays were performed largely as previously described (Alpadi et al., 2008; Magupalli et al., 2008). The Gal4-based Matchmaker Yeast Two-Hybrid System (Clontech) was used according to manufacturer's instructions. For the YTH screening we used a bovine retinal YTH cDNA library from the retina (Tai et al., 1999; Alpadi et al., 2008; Venkatesan et al., 2010). The cDNA of the respective bait proteins were cloned in frame with the Gal4-DNA-binding domain of pGBKT7. The cDNA of the indicated prey proteins were cloned in frame with the Gal4-activation domain of pACT2 or pGADT7. The bait and prey plasmids confer tryptophan (W) and leucine (L) prototrophy to the respective auxotrophic yeast strains. Two yeast strains, Y187 and Y2HGold (Clontech), were used that contain distinct auxotrophic marker genes. (1) Y2HGold (Clontech): MATa, trp1-901, leu2-3, 112, ura3-52, his3-200, gal4, gal80, LYS2::GAL1UAS–Gal1TATA–His3,GAL2UAS–Gal2TATA–Ade2,URA3::MEL1UAS–Mel1TATA, AU R1-C, MEL1. This strain contains distinct *ADE2*, *HIS3*, *MEL1*, and *AUR1-C* reporter constructs that are only expressed in the presence of GAL4-based protein interactions (Clontech). (2) Y187: MATα, ura3-52, his3-200, ade2-101, trp1-901, leu2-3,112, gal4, met, gal80, URA3::GAL1UASGAL1TATA-lacZ (Clontech) (Harper et al., 1993). Bait plasmids were electroporated into Y2HGold yeast and prey plasmids into Y187 yeast (Clontech). Preparation of electrocompetent yeasts and electroporation of yeasts were done as described previously (Magupalli et al., 2008). For identifying transformants, yeasts were plated on the respective selective plates to identify the resulting convertents to the respective prototrophy (dropout media; Clontech/ICN). For interaction analyses, Y2HGold yeasts containing the respective bait plasmid were mated with Y187 yeasts containing the respective prey plasmid. Mating was performed for 5 h at 30°C in 1 ml of YPD medium with heavy vortexing in a thermoshaker. For assessing mating efficiency, half of the mated sample was streaked on –LW plates, the other half was plated on –ALWH selective plates with 10 mM aminotriazole (3-amino 1,2,4-triazole) and 60 ng/ml aureobasidin. Growth of mated yeasts on –LW selective medium demonstrates presence of both bait and prey plasmids; growth on –ALWH selective medium [and expression of β-galactosidase (β-gal) activity] indicates interaction of bait and prey proteins taking place. For the matings, pSE1111 and pSE1112 that encode irrelevant proteins (Magupalli et al., 2008) as well as the empty bait and prey vectors were used as negative controls (autoactivation controls). Expression of β-gal marker gene activity was qualitatively analyzed by filter assays as described previously (Magupalli et al., 2008).

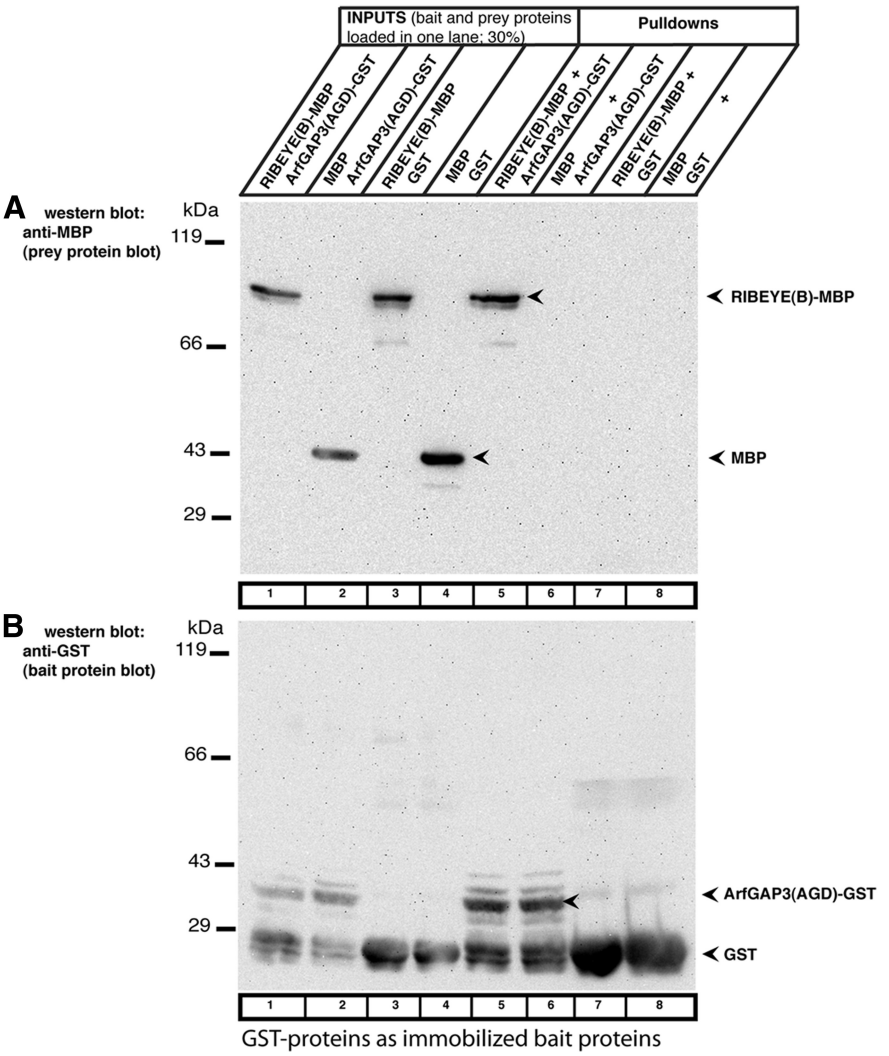

Figure 4. RIBEYE(B) specifically interacts with ArfGAP3 in fusion protein pull-down assays (Western blot analyses). To exclude that the tag has an importance for the pull-down results and to further exclude that any prey protein is unspecifically pulled down by bait-GST, we also analyzed the results of the pull-down assays by Western blotting with anti-MBP and anti-GST antibodies. The reaction buffer used for these experiments contained 1 mM βME. GST-tagged fusion proteins were used as immobilized bait proteins and eluted MBP-tagged proteins as soluble prey proteins. Similar to the experiments described in Figure 3, only RIBEYE(B)-MBP (lane 5) and not MBP alone (lane 6) is pulled down by the ArfGAP3(AGD)-GST. GST alone (lane 7) and MBP alone (lane 8) do not pull down RIBEYE(B)-MBP, as shown by Western blotting with antibodies against MBP (Fig. 4*A*), demonstrating the specificity of the interaction. The Western blot data fully confirm the results shown in Figure 3 that were obtained by SDS-PAGE analyses. In Figure 4*B*, the same blot as analyzed in Figure 4*A* was reprobed (after stripping of the blot) with antibodies against GST to show equal loading of the bait proteins. RE(B)-MBP, RIBEYE(B)-MBP; ArfGAP3(AGD)-MBP, MBP-tagged ArfGAP-domain (AGD) of ArfGAP3.

Fusion protein pull-down assay. For fusion protein pull-down experiments, either GST-tagged or maltose-binding protein (MBP)-tagged fusion proteins were used as immobilized bait proteins. If GST-tagged proteins were used as immobilized bait protein, the MBP-tagged protein was used as solubilized prey protein and vice versa. Bait and prey proteins were used in equimolar amounts [0.3 μM in incubation buffer containing 100 mM Tris, pH 8.0, 150 mM NaCl, 1 mM EDTA, 0.25% (w/v) Triton

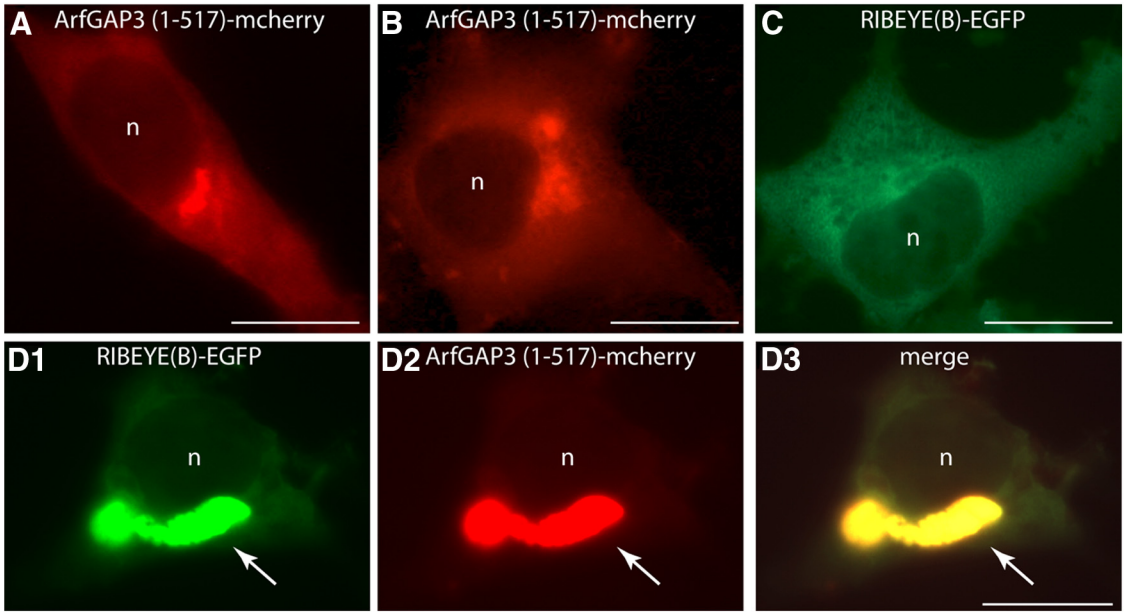

Figure 5. RIBEYE(B) is recruited by ArfGAP3 into a Golgi-like distribution in transfected COS cells. COS7 cells were transfected with the indicated mcherry-tagged ArfGAP3 or EGFP-tagged RIBEYE(B) constructs. Transfected cells were analyzed for the intracellular distribution of the respective proteins via direct epifluorescence microscopy. Cells transfected with ArfGAP3-mcherry alone show the typical enrichment at the Golgi apparatus in a perinuclear localization (***A***, ***B***), as already previously shown (Dogic et al., 1999; Eugster et al., 2000; Lewis et al., 2004; Watson et al., 2004; Frigerio et al., 2007; Kartberg et al., 2010; Yu et al., 2012). In contrast, RIBEYE(B) is diffusely distributed in single-transfected cells (***C***; Schmitz et al., 2000). If RIBEYE(B)-EGFP is cotransfected with ArfGAP3-mcherry, RIBEYE(B) virtually completely redistributed from a diffuse distribution into the Golgi-like, perinuclear localization indicating interaction between RIBEYE(B) and ArfGAP3 (***D***). n, nucleus. The arrow in ***D*** points to the Golgi-like localization to which the RIBEYE(B)-EGFP signal is translocated in ArfGAP3-mcherry-transfected cells. Scale bars: ***A–D***, 10 μm.

X-100 (Tx-100), and 1 mM β-mercaptoethanol (βME) if not denoted otherwise]. GST and MBP alone served as control proteins. Protein concentrations were determined using the Bradford method (Bradford, 1976). For pull-down experiments, fusion protein eluates were precleared with 10 μl of empty Sepharose beads (per 1 ml of eluate) for 1 h at 4°C. Incubations were typically done in a volume of 500 μl. After overnight incubation at 4°C, immobilized beads were allowed to settle (20 min, at 4°C). Samples were washed by repeated centrifugation of the beads (3000 rpm, 2 min, 4°C) and subsequent resuspension with binding buffer. This procedure was repeated three times. Afterward, the final pellets were boiled with SDS-sample buffer (96°C, 10 min) and subjected to SDS-PAGE and/or Western blotting.

Pre-absorption experiments. Pre-absorption experiments were performed exactly as previously described (Wahl et al., 2013) using 50 μg of the respective GST-fusion protein. Pre-absorbed ArfGAP3Cterm2 and ArfGAP3Cterm3 immunosera were used at a 1:20 dilution for immunofluorescence microscopy and at a 1:3000 dilution for Western blotting.

Affinity purification of antibodies. Antibodies were affinity purified by the method of Olmsted (1981). In brief, ~50 μg of fusion protein was loaded on a 10% SDS-PAGE and transferred to nitrocellulose. The ArfGAP3Cterm-GST/ArfGAP3Cterm2 fusion protein bands at ~35 kDa were cut out with a scalpel blade. These fusion protein-loaded nitrocellulose strips were used for affinity purification of the antisera and treated with 5% skim milk powder in PBS (for ~30 min at RT). Next, nitrocellulose strips were incubated with the respective antisera (diluted 1:10 in 5% skim milk dissolved in PBS) and incubated overnight at 4°C. The nitrocellulose strips were washed several times with PBS. Bound antibodies were eluted from the nitrocellulose strips with a minimal volume (typically 200 μl) of 0.2 M glycine, pH 2.7, for 3–4 min (at 4°C). The antibody eluate was neutralized by the addition of 50 μl of 1 M Tris, pH 8.5. Antibody was diluted to a concentration of 0.1 mg/ml and complemented with BSA (0.1 mg/ml) for stabilization.

Direct labeling of primary antibodies (mouse anti-RIBEYE(B)-domain/CtBP2) with fluorophores (DyLight 650). Direct labeling of mouse monoclonal antibodies against RIBEYE(B)/CtBP2 (BD) was performed exactly as previously described (Wahl et al., 2013) using the Thermo Scientific DyLight 650 Microscale Antibody Labeling Kit (Thermo Scientific #84536) according to the manufacturer's instructions.

Heterologous protein expression in eukaryotic cell lines. For heterologous expression, COS7 cells were used that were transfected with lipofection, as previously described (Magupalli et al., 2008; Schwarz et al., 2011). Transfected cells were typically analyzed 24 h after transfection.

Coimmunoprecipitation from bovine retina. For each immunoprecipitation, a single isolated bovine retina was incubated in 1 ml lysis buffer, containing 100 mM Tris-HCl, pH 8.0, 150 mM NaCl, 1 mM EDTA, and 1%Tx-100 for 45 min on vertical rotator at 4°C. The samples were mechanically cracked by forcefully ejecting the retinal lysates through a 20 gauge needle (20×). The samples were sonicated (Bandelin; Sonoplus) at 1% output for 20 half-second pulse ON/OFF cycles on ice. Afterward, the extracts were centrifuged at 13,000 rpm for 30 min at 4°C. The supernatants were transferred into new Eppendorf tubes. The centrifugation step was repeated one time to remove all cell debris. The resulting lysate was precleared by the addition of 15 μl of pre-immune serum and 20 μl of washed protein A-Sepharose beads (2 h incubation at 4°C with an overhead rotator). Next, samples were centrifuged at 13,000 rpm for 30 min at 4°C (Biofuge Fresco; Heraeus; ##3328 rotor). The supernatant was split in two equal volumes–for the control and experimental assays. For negative control immunoprecipitation, 15 μl of ArfGAP3-Cterm3 preimmune serum was added; for the experimental immunoprecipitation, 15 μl of ArfGAP3-Cterm3 immune serum was added. Samples were incubated overnight at 4°C using an overhead rotator. Afterward, beads were allowed to settle (for 20 min, on ice). The supernatants were removed and saved; the bead pellets were resuspended in 1.0 ml of lysis buffer and washed thrice by repeated centrifugation (3000 rpm, 1 min, 4°C). The final pellet was boiled in 10 μl of SDS sample buffer, subjected to SDS-PAGE, and analyzed by Western blotting with the indicated antibodies.

Immunofluorescence microscopy of transfected COS cells. Conventional fluorescence microscopy of transfected cells was done as previously described using a Zeiss Axiovert 200M equipped with the respective filter blocks (Schmitz et al., 2000; Magupalli et al., 2008; Wahl et al., 2013).

Immunolabeling of 0.5-μm-thick retinal resin sections. Epon-embedded samples of mouse and bovine retinas were prepared as previously described (Wahl et al., 2013). From the tissue blocks, 0.5-μm-thick sections were cut with a Reichert ultramicrotome. Epon was removed as described previously (Wahl et al., 2013). Afterward, sections were

incubated with the respective primary and secondary antibodies as described previously (Schmitz et al., 2000; Alpadi et al., 2008; Wahl et al., 2013). Immunolabeled sections were either analyzed by conventional epifluorescence microscopy or by super-resolution structured illumination microscopy (SR-SIM) as indicated. The immunofluorescence data shown in Figures 9–13 were obtained from incubations of mouse retinal sections. Qualitatively similar images were obtained from incubations of thin sections of the bovine retina (data not shown).

SR-SIM. To further improve the spatial resolution of our immunolabeling analyses, we applied multicolor SR-SIM analyses (Schermelleh et al., 2008, 2010; Wahl et al., 2013). SR-SIM was performed exactly as previously described using the Elyra PS1 setup (Wahl et al., 2013). Images were taken with a 63× Plan-Apochromat objective (NA 1.4) with excitation light wavelengths of 488, 561, and 650 nm, and then processed for SR-SIM to obtain higher resolutions (Gustafsson et al., 2008; for review, see Schermelleh et al., 2008, 2010), as previously described (Wahl et al., 2013). The Zeiss setup used for SR-SIM was checked for chromatic aberration in *X*-, *Y*-, and *Z*-direction using multicolor beads. For acquisition and processing, the Zen2010 software (Zeiss) was used.

Triple immunolabeling of thin retinal sections. Triple immunolabeling experiments were performed as previously described (Wahl et al., 2013). We used a directly labeled mouse monoclonal antibody against RIBEYE(B)-domain/CtBP2 (BD) conjugated with DyLight 650, and two other primary antibodies (one from mouse, the second from rabbit [as indicated in the respective experiments]), which were not directly fluorophore labeled. First, sections were incubated with the two unlabeled primary antibodies at the same time overnight (at the dilutions given above). On the next day, sections were washed three times with PBS and afterward incubated with the respective secondary antibodies (donkey anti-rabbit Alexa 568 and chicken anti-mouse Alexa 488). After 1 h incubation, sections were washed again three times with PBS and finally incubated with the directly DyLight 650-labeled CtBP2 primary antibody (in the dilutions summarized above) overnight at 4°C. After overnight incubation, sections were washed three times with PBS and embedded with anti-fade solution containing n-propyl gallate (NPG) as previously described (Schmitz et al., 2000).

Control incubation. Control incubations for immunolabeling experiments were done by omitting the primary antibody and only incubating with secondary antibody. No immunofluorescent signal was observed in photoreceptor synapses in these control incubations. In further control experiments, antibodies were pre-absorbed with the respective antigen as described below and processed for immunolabeling.

All experiments were done with mouse and bovine retinas of either sexes. Mice were killed in the early afternoon. Mouse eyes were collected at environmental daylight conditions (luminance of ~2 cd/m^2). Bovine eyes were obtained from a local slaughterhouse. Similar data as shown for the mouse retina were also obtained with the bovine retina (of either sexes; data not shown).

Preparation of retinas from the adult mouse for electroporation. Retinas were isolated from adult mice within 5 min postmortem (in dim ambient light). The enucleated eyes were bisected at the equatorial plane and the posterior eye cup was transferred into ice-cold artificial CSF (ACSF) containing the following (in mM): 119 NaCl, 2.5 KCL, 2.5 $CaCl_2$, 1.3 $MgCl_2$, 1 NaH_2PO_4, 20 glucose, and 11 HEPES, pH 7.4, osmolarity ~300 mOsm/L. ACSF was saturated with 5% CO_2/95% O_2 (carbogen) before use. From the posterior eyecup, the retina was gently peeled off from the pigment epithelium. Isolated retinas were transferred to black-gridded nitrocellulose filter membranes (Millipore, #HABG01300) with the ganglion cell side facing the nitrocellulose membrane. Thus, photoreceptors were facing the free surface and were in direct contact with the DNA plasmid solutions added to them in the electroporation experiments (see below). The filters with the attached retinas were transferred to sterile Petri dishes (3 cm diameter) containing ~1.0 ml of AMES' medium, pH 7.4 (A1420, Sigma-Aldrich) pre-incubated at 37°C.

Electroporation of isolated mouse retinas and retinal explant culture. Electroporation of adult mouse retinas was performed largely as previously described (Donovan and Dyer, 2006; Briggman and Euler, 2011; Vergara et al., 2013). Electroporation was performed with a square wave pulse electroporator (ECM 830; BTX) and a tweezertrode electroporation device (BTX; #45-0118, #45-0204). Both electrodes of tweezertrode were dipped in ACSF buffer to obtain a good electrical connection. Excess of ACSF was removed with filter paper to avoid dilution of the DNA. Before electroporation, DNA was column purified. For each electroporation, 50 μg of purified DNA was used. Immediately after isolation, the retina was placed in between the tweezertrode. The retina attached to the nitrocellulose was facing the positive electrode with the ganglion cell side

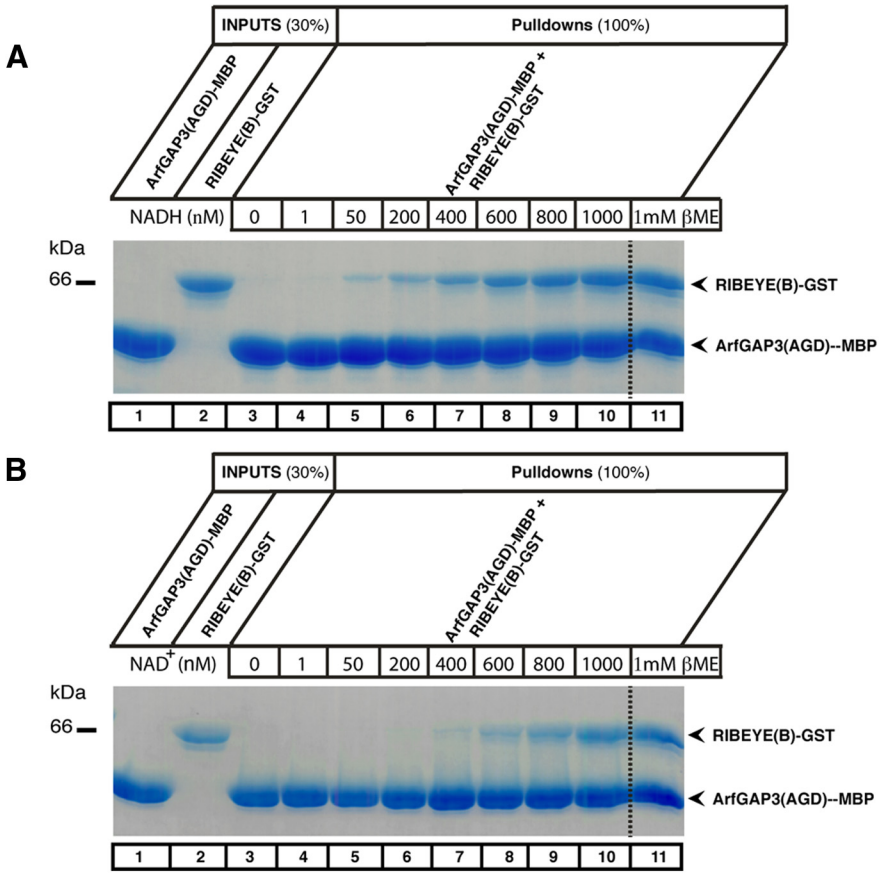

Figure 6. The binding between RIBEYE(B)-domain and the ArfGAP-domain (AGD) of ArfGAP3 is stimulated by NAD(H) in a redox-sensitive manner. ***A***, ***B***, Pull-down experiments were performed as in Figure 3 both in the absence (lanes 3—10; ***A***, ***B***) or presence (lane 11; ***A***, ***B***) of 1 mM βME. RIBEYE binds to the ArfGAP-domain (AGD) of ArfGAP3 only in the presence of 1 mM βME (lane 11; ***A***, ***B***) but not in the absence of 1 mM βME (lane 3; ***A***, ***B***). Lanes 1 and 2 show the respective input fractions (30% input). We tested whether addition of NADH (***A***) or NAD^+ (***B***) could substitute for the presence of 1 mM βME in promoting ArfGAP3/RIBEYE(B) interaction. As a matter of fact, increasing concentrations of both NADH (***A***) as well as NAD^+ (***B***) could promote binding of RIBEYE(B)-GST to the AGD of ArfGAP3 even in the absence of 1 mM βME (lanes 4—10; ***A***, ***B***). The reduced form of the dinucleotide, NADH (***A***), was more effective than the oxidized form, NAD^+ (***B***), to promote RIBEYE(B)/ArfGAP3 interaction. Semiquantitative evaluation of the binding experiments ($n = 4$) demonstrated that ~450 nM NADH and ~700 nM NAD^+ are promoting half-maximal binding of ArfGAP3 to RIBEYE(B) in the pull-down assays.

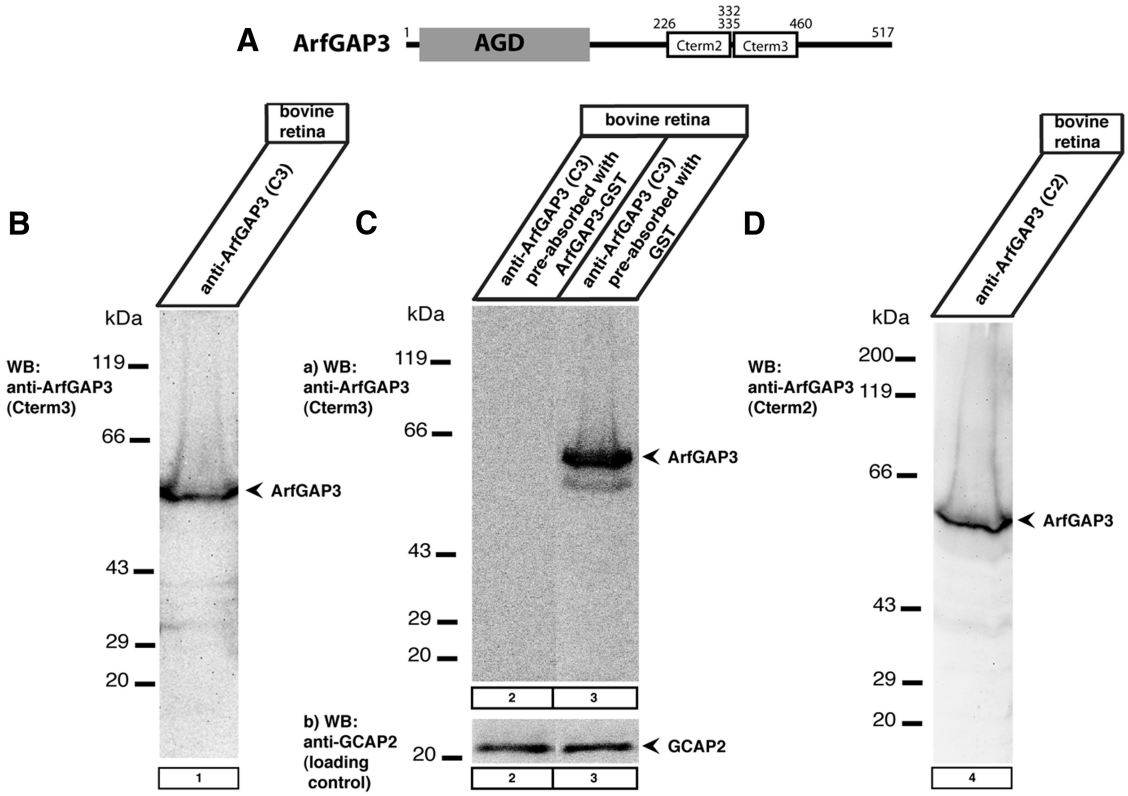

Figure 7. Western blot analyses of two antibodies that were generated against the C terminus of ArfGAP3. ***A***, Schematic drawing denotes the areas against which the two polyclonal ArfGAP3 antibodies (Cterm2 and Cterm3) were generated. ***B–D***, In Western blot analyses, both antibodies (Cterm2 and Cterm3) detected a single band at the expected running position of ArfGAP3 at ~55 kDa. This ArfGAP3 Western blot band could be blocked by pre-absorption of the antibody with the respective ArfGAP3-GST fusion protein (lane 2; *C*; data not shown) but not by pre-incubation with GST alone (***C***, lane 3; data not shown). ***Cb***, Loading control (immunoblotting of the same blot as shown in ***Ca***) after stripping of the blot and reprobing with an antibody against GCAP2 (Venkatesan et al., 2010), demonstrating equal protein loading.

while the plasmid DNA solution was added to the photoreceptor side at the negative electrode in hanging drop manner. The distance between the two electrodes was optimized to ~3–4 mm. Electroporation was done at 20 V, 950 ms OFF, 20 ms ON (10 pulses). Electroporated retinas were transferred back to Petri dishes containing 1.0 ml of AMES' medium, pH 7.4. Retinas were transferred to open Petri dishes that were placed in an incubation chamber, as previously described (Morgan et al., 2011; Williams et al., 2013). Temperature was continuously maintained at 32°C using a feedback temperature controller (TC324B; Warner Instruments) and a transparent ITO heater attached to the incubation chamber (HI-25Dp; MicroControls). The incubation chamber was filled with distilled H_2O to the lower edge of stage where the Petri dish with the retina was placed and continuously gassed with carbogen (5% CO_2/95% O_2). Retinas were incubated inside the light-protected incubation chamber typically for 18–24 h.

Loading of photoreceptors with FM1–43. Isolated, electroporated retinas were incubated for 15 min in LCS containing 20 μM FM1–43 (fixable FM1–43: FM1–43FX; Invitrogen, #F35355) at 37°C in the dark, similar to the procedure described by Rea et al. (2004). We used this method, because it favors specific FM1–43 uptake in photoreceptor synaptic terminals (Rea et al., 2004). After labeling, the retinas were rinsed thrice with LCS and processed for the isolation of photoreceptor cells (see below).

Dissociation of electroporated retinas and isolation of photoreceptors. Twenty-four hours after electroporation, photoreceptors were isolated from the retina with a papain digestion procedure, largely as previously described (Wahl et al., 2013). The papain solution containing 6 U/ml papain (Sigma, #76220-25G) in low Ca^{2+}-containing saline solution (LCS solution; containing 132 mM NaCl, 3 mM KCl, 1 mM $MgCl_2 \times 6H_2O$, 0.5 mM $CaCl_2$, 10 mM sodium pyruvate, 10 mM glucose, and 10 mM HEPES, pH 7.4, ~300 mOsm/L) was activated with 2.7 mM L-cysteine at 37°C for 20 min before the experiments. Isolated retinas were incubated in 1 ml of the cysteine-activated papain solution (containing 6 U papain/ml LCS) for 10 min at 25°C. LCS was saturated with 5% CO_2/95% O_2 before use. After removal of the papain solution, the retina was gently washed three times with 1ml of LCS solution containing 2% FCS and 0.01 mg/ml DNase (Sigma, #DN25-110MG). To dissociate photoreceptor cells, papain-treated retinas were very gently triturated (1–2 times) with a wide-bore plastic Pasteur pipette. The resulting cell suspension was plated on Concanavalin A (Sigma, #C7275-250 mg)-coated coverslips. For coating of a 25 mm round coverslip, ~200 μl of 1 mg/ml Concanavalin A (in LCS solution) was added for 1 h at RT. Unbound Concanavalin A was removed by three washes with LCS before the addition of the dissociated cells. Cells were allowed to settle on the coverslips for 30 min at 37°C for tight attachment. Unbound retinal cells were removed by gentle washes with LCS. Photoreceptors were identified based on their typical morphology. Photoreceptors were fixed with 4% PFA in PBS for 15 min at RT. After several washes with PBS, cells were mounted with NPG antifade as previously described (Wahl et al., 2013).

Miscellaneous procedures. SDS-PAGE and Western blotting were performed as previously described (Schmitz et al., 2000). Fusion proteins were expressed in BL21(DE3) bacteria for pGEX and pMal-C2 constructs as previously described (Schmitz et al., 2000). For expression of SNAP-tagged fusion proteins, *Escherichia coli* T7 Express bacteria (NEB; #C2566) were used. Expression and purification of SNAP-tagged fusion proteins were performed according to the manufacturer's instructions (NEB). SNAP-tagged fusion proteins were visualized SNAP-Vista Green (NEB; #S9147S) and covalently immobilized with SNAP-capture pull-down resin according to the manufacturer's instructions. Conventional immunofluorescence microscopy was performed as previously described (Schmitz et al., 2000) using a Zeiss Axiovert 200M equipped with the respective filter blocks.

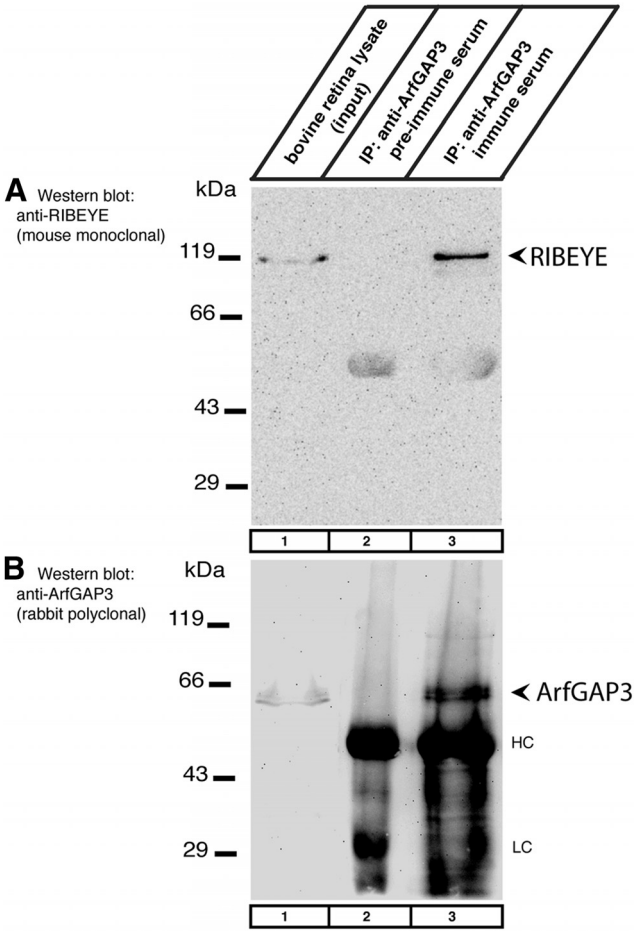

Figure 8. Coimmunoprecipitation of RIBEYE and ArfGAP3 from the bovine retina (Western blot analyses). ***A***, ArfGAP3 immune serum (lane 3) and ArfGAP3 pre-immune serum (lane 2) were tested for their capability to coimmunoprecipitate RIBEYE from the bovine retina. Lane 1 shows the input fraction (1% of total input). RIBEYE is coimmunoprecipitated by ArfGAP3 immune serum (Cterm3 antiserum; lane 3) but not by ArfGAP3 pre-immune serum (lane 2). ***B***, Shows the same blot as in ***A*** but reprobed with anti-ArfGAP3 antibodies (after stripping of the blot). This blot shows that ArfGAP3 was successfully immunoprecipitated by the immune serum (lane 3) but not by the control pre-immune serum (lane 2). HC and LC indicate the Ig heavy and light chains, respectively.

Results

ArfGAP3 binds to RIBEYE(B)-domain in the YTH system

Using RIBEYE(B) as bait, we obtained full-length ArfGAP3 as a RIBEYE-interacting YTH prey clone. The original ArfGAP3 prey clone contained a deletion of 8 aa in the Zn-finger motif of the ArfGAP-domain (data not shown). To exclude an artificial interaction of these proteins in the YTH system, we recloned full-length ArfGAP3 cDNA from an IMAGE clone (IMAGE #8081904, BC118087; encoding full-length bovine ArfGAP3 with no deletion in the Zn-finger) into the pACT2 prey vector. Then, we retested whether this entirely full-length ArfGAP3 prey interacts with RIBEYE(B) in the YTH system. Similar as observed for the original ArfGAP3 prey clone, we obtained a strong interaction between RIBEYE(B) and the recloned full-length ArfGAP3, as judged by growth on –ALWH selective medium and expression of β-gal activity (Fig. 1, matings 1 and 2) indicating that the interaction between ArfGAP3 and RIBEYE(B) is real in the YTH system. Negative control matings (Fig. 1, matings 3–10) demonstrated that ArfGAP3/RIBEYE interaction is not due to auto activation.

Mapping of RIBEYE-ArfGAP3 interaction in the YTH system: the NAD(H)-binding subdomain RIBEYE(B) binds to the AGD-domain of ArfGAP3

Next, we tested with the YTH system which part of ArfGAP3 mediates the interaction with RIBEYE(B). We found that the AGD encoding amino acids 1–136 of ArfGAP3 is responsible for the interaction with RIBEYE(B) (Fig. 2*A*, matings 1 and 2). The C terminus of ArfGAP3 did not interact with RIBEYE(B) (data not shown). RIBEYE(B) consists of an NADH-binding subdomain (NBD) and a substrate-binding subdomain (SBD; Kumar et al., 2002; Nardini et al., 2003; for review, see Schmitz, 2009; Schmitz et al., 2012). Further YTH analyses demonstrated that the NBD of RIBEYE(B) interacts with ArfGAP3 (Fig. 2*B*, mating 1). The SBD did not promote ArfGAP3/RIBEYE(B) interaction in the YTH system (Fig. 2*B*, mating 5). Negative control matings (Fig. 2*A*, matings 3–8, 10, and 11; *B*, matings 6–11) demonstrated that bait and prey clones were not auto activating.

RIBEYE(B) interacts with ArfGAP3 in fusion protein pull-down assays

We used various independent approaches to verify the interaction between RIBEYE(B)-domain and the ArfGAP-domain (AGD) of ArfGAP3. First, we performed pull-down experiments using bacterially expressed and purified fusion protein (Fig. 3). We used MBP-tagged fusion proteins (ArfGAP3(AGD)-MBP and MBP alone) as immobilized bait proteins and GST-tagged proteins (RIBEYE(B)-GST and GST alone) as soluble prey proteins. For the pull-down experiments demonstrated in Figures 3 and 4, the buffer contained 1 mM βME (see Materials and Methods). ArfGAP3(AGD)-MBP (lane 5; but not MBP alone, lane 7) interacted with RIBEYE(B)-GST (but not with GST alone, lanes 6 and 8) as judged by protein pull-down analyses in SDS-PAGE (Fig. 3). Specificity of interaction was consistently shown both by SDS-PAGE (Fig. 3) and by Western blot analyses (Fig. 4; and data not shown). Identical results were obtained when tags were switched. In Figure 4, RIBEYE(B) was tagged with MBP and ArfGAP3(AGD) with GST. Also with these switched tags, a strong interaction was observed between RIBEYE(B) and ArfGAP3. Typically, $>\sim$30% of the input fraction of the RIBEYE(B) prey protein was bound to the immobilized ArfGAP3 bait fusion protein.

ArfGAP3 interacts with RIBEYE(B) in transfected COS cells

Next, we tested whether RIBEYE(B) and ArfGAP3 would interact with each other in transfected COS cells (Fig. 5). ArfGAP3 and RIBEYE(B) were tagged with different fluorescent proteins, i.e., ArfGAP3 with mCherry and RIBEYE(B) with EGFP. When ArfGAP3 was transfected alone, ArfGAP3 was enriched at a perinuclear region that represents the Golgi apparatus (Fig. 5*A*,*B*) similarly as previously described (Dogic et al., 1999; Eugster et al., 2000; Lewis et al., 2004; Watson et al., 2004; Frigerio et al., 2007; Kliouchnikov et al., 2009). When RIBEYE(B)-EGFP was transfected alone (Fig. 5*C*), it was largely diffusely distributed throughout the entire cell (as previously described; Schmitz et al., 2000). In contrast, when RIBEYE(B) was cotransfected with ArfGAP3, RIBEYE(B) was nearly completely recruited to the ArfGAP3-typical Golgi-like perinuclear localization (Fig. 5*D*) indicating interaction of RIBEYE(B) and ArfGAP3 in cotransfected COS cells.

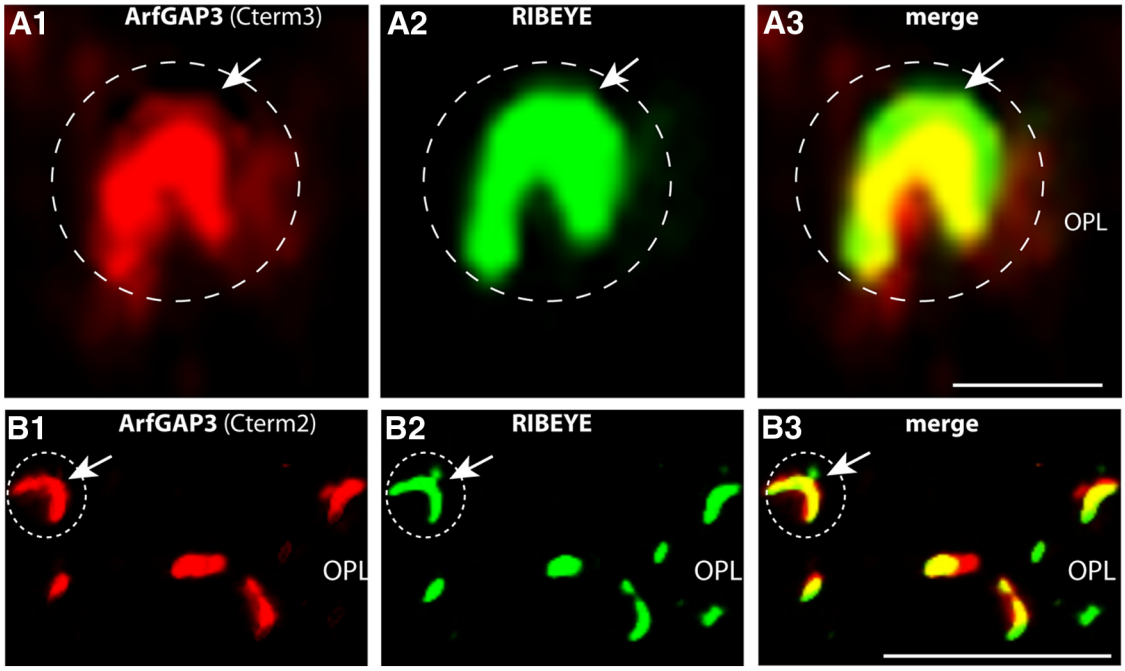

Figure 9. ArfGAP3 is strongly enriched at synaptic ribbons of photoreceptor synapses *in situ* (conventional imaging). ArfGAP3 colocalizes with synaptic ribbons. The 0.5-μm-thick retinal sections are double immunolabeled with antibodies against ArfGAP3 and monoclonal antibodies against RIBEYE(B)/CtBP2 (***A***, ***B***). ArfGAP3 Cterm3-antibody was used in ***A***, and ArfGAP3 Cterm2 was used for immunolabeling of ArfGAP3 in ***B***. Strong ArfGAP3 immunosignals were found in an identical manner with both ArfGAP3 antibodies at the RIBEYE-immunolabeled synaptic ribbons and in close vicinity to synaptic ribbons. The dashed circles denote single immunolabeled photoreceptor presynaptic terminals. Arrows in ***B*** and ***C*** point to single immunolabeled synaptic ribbons. No immunosignals were observed in the presynaptic terminals if pre-immune serum was used (data not shown). ***A*** and ***B*** were obtained by conventional imaging. OPL, Outer plexiform layer. Scale bars: ***A***, 1 μm; ***B***, 5 μm.

Interaction between ArfGAP3(AGD) and RIBEYE(B) is regulated by NAD(H) in a redox-sensitive manner

The fusion protein pull-down binding experiments shown above in Figures 3 and 4 were done with buffer that contained 1 mM βME. If βME was omitted, there was no binding between ArfGAP3 and RIBEYE(B) (Fig. 6*A*,*B*, compare lane 3 with lane 11). Previously, it has been shown that 1 mM βME promotes a conformation of RIBEYE(B) that can be also induced by the addition of NAD(H) (Venkatesan et al., 2010). Furthermore, we demonstrated that the NAD(H)-binding subdomain of RIBEYE(B), the NBD, is responsible for the interaction with ArfGAP3 (see above). Therefore, we tested whether the addition of NAD(H) could replace βME in promoting ArfGAP3/RIBEYE(B) interaction. Indeed, NAD(H) was very efficient in promoting RIBEYE(B)/ArfGAP3 interaction (Fig. 6*A*). The reduced form, NADH, was more efficient in promoting RIBEYE(B)/ArfGAP3 interaction in the absence of βME than its oxidized form, NAD^+ (Fig. 6*A*,*B*; K_d ~450 nM for NADH; K_d ~700 nM for NAD^+). From these experiments we concluded that NAD(H), particularly the reduced NADH, promotes RIBEYE(B)/ArfGAP3 interaction. In line with this proposal is our finding that an NAD(H)-binding-deficient RIBEYE(B) point mutant, RIBEYE(B) G730A (Alpadi et al., 2008; Schwarz et al., 2011), did not interact with ArfGAP3(AGD) in the YTH system (Fig. 2*D*, mating 1).

ArfGAP3 can be coimmunoprecipitated with RIBEYE from the bovine retina

We generated two different polyclonal antibodies against ArfGAP3 to analyze the relation between RIBEYE and ArfGAP3 *in situ*. The two different antibodies against ArfGAP3 were directed against two different portions in the divergent C terminus of ArfGAP3 (ArfGAP Cterm2 and ArfGAP Cterm3; see Fig. 7*A*). Both antibodies immunodetected a typical single, major band at ~55 kDa in crude bovine retinal homogenates in Western blot analyses (Fig. 7; data not shown) that was absent in the pre-immune serum and that could be specifically blocked by the respective ArfGAP3-GST fusion protein but not by GST alone (Fig. 7*C*; data not shown).

Next, we tested whether antibodies against ArfGAP3 coimmunoprecipitated endogenous retinal RIBEYE. ArfGAP3 (Cterm3) immune serum (lane 3, but not ArfGAP3 pre-immune serum, lane 2) coimmunoprecipitated RIBEYE (Fig. 8*A*) together with ArfGAP3 (Fig. 8*B*), showing interaction of these proteins also in the retina *in situ* (Fig. 8). Both RIBEYE and ArfGAP3 were strongly enriched in the experimental (Fig. 8, lane 3) but not in the control (Fig. 8, lane 2) immunoprecipitates. Since RIBEYE is exclusively present at synaptic ribbons in the mature retina (Schmitz et al., 2000), the coimmunoprecipitation experiments suggested that ArfGAP3 is a component of the synaptic ribbon complex *in situ*.

ArfGAP3 is present at the photoreceptor synaptic ribbon complex

To get further insights about the *in situ* localization of ArfGAP3 in the retina, we performed immunolabeling analyses with both ArfGAP3 antibodies (ArfGAP3 Cterm3 and ArfGAP Cterm2; Fig. 9). Both ArfGAP3 antibodies strongly labeled the outer plexiform layer (OPL) where photoreceptor ribbon synapses are localized (Fig. 9; data not shown). Identical results were obtained independent of whether crude antisera or affinity-purified antibodies were used (compare Figs. 9, 11, 12). To define the relation between ArfGAP3 and synaptic ribbons, we performed double immunolabelings with rabbit polyclonal antibodies against ArfGAP3 and mouse monoclonal antibodies against RIBEYE(B)-domain/CtBP2 (Fig. 9). The ArfGAP3 immunosignals largely

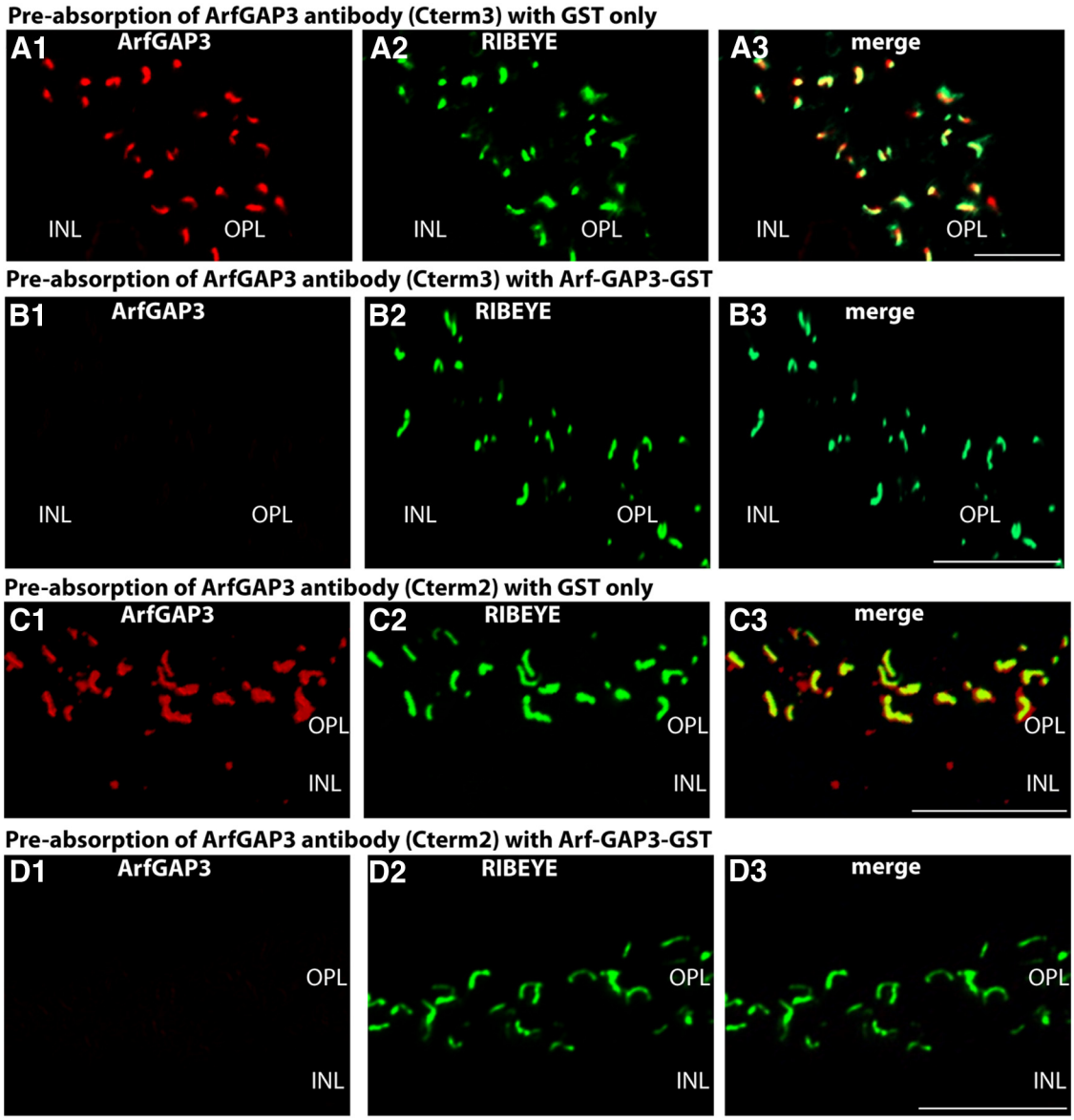

Figure 10. ***A***, ***B***, Pre-absorption control experiments for the immunolabeling analyses shown in Figure 9*A*. Double immunolabeling of 0.5-μm-thick mouse retinal sections with ArfGAP3 (Cterm3) antibody pre-absorbed either with ArfGAP3-GST-fusion protein (***B***) or with GST alone (***A***). To visualize ribbon synapses, sections were coimmunolabeled with mouse monoclonal antibodies against RIBEYE(B)-domain/CtBP2. Pre-absorption with ArfGAP3Cterm3-GST fusion protein completely blocked the ArfGAP3 immunosignals at the synaptic ribbon (***B***), whereas GST alone had no influence on the ArfGAP3 immunosignals (***A***), demonstrating the specificity of the previous immunolabeling results. ***C***, ***D***, Pre-absorption control experiments for the immunolabeling analyses shown in Figure 9*B*. Double immunolabeling of 0.5-μm-thick mouse retinal sections with ArfGAP3 (Cterm2) antibody pre-absorbed with either ArfGAP3Cterm2-GST-fusion protein (***D***) or with GST alone (***C***). Synaptic ribbons were coimmunolabeled with mouse monoclonal antibodies against RIBEYE(B)-domain/CtBP2. Pre-absorption with the specific fusion protein completely blocked the ArfGAP3 immunosignals at the synaptic ribbon (***D***), whereas GST alone had no influence on the ArfGAP3 immunosignals (***C***), demonstrating the specificity of the previous immunolabeling results. ***A–D*** were obtained by conventional imaging. OPL, Outer plexiform layer; INL, inner nuclear layer. Scale bars: ***A–D***, 5 μm.

overlapped at the photoreceptor ribbon synapse with the RIBEYE immunosignals indicating that ArfGAP3 is strongly enriched at the synaptic ribbon complex (Fig. 9*A*,*B*). Identical immunolabeling results were obtained with both ArfGAP3 antibodies (Fig. 9), further demonstrating that the immunoreactivity at the RIBEYE-immunolabeled synaptic ribbon is due to ArfGAP3 and not due to an unrelated protein. The described ArfGAP3 immunosignals obtained with both ArfGAP3 antibodies could be specifically blocked by pre-absorption with the respective ArfGAP3-GST fusion protein but not by GST alone, demonstrating the specificity of the immunolabeling results (Fig. 10). To further corroborate these findings, we performed SR-SIM of thin retinal sections double immunolabeled with affinity-purified rabbit polyclonal antibodies against ArfGAP3 and mouse monoclonal antibodies against RIBEYE(B)/CtBP2 (Fig. 11). Also, SR-SIM analyses demonstrated a strong enrichment of the ArfGAP3 immunosignals at the synaptic ribbons (Fig. 11). In the SR-SIM analyses, the ArfGAP3 immunosignal was slightly shifted toward the inner nuclear layer (INL) compared with the RIBEYE immunosignal, which could indicate a localization of ArfGAP3 more toward the base of the synaptic ribbon (Fig. 11*A*; see also discussion). The ArfGAP3 immunosignals also showed a strong colocalization with the active zone protein bassoon (Fig. 11*B*). In the SR-SIM analyses, the ArfGAP3 immunosignal was slightly shifted toward the ONL compared with the bassoon immunosignal, also indicating an ArfGAP3 localization in the basal portions at the

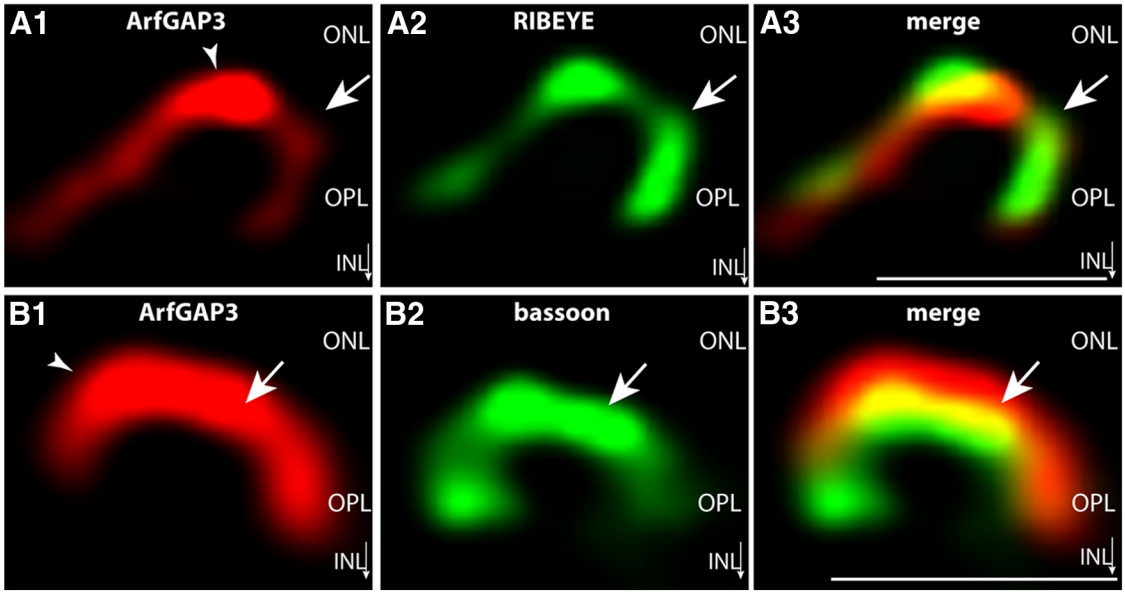

Figure 11. ArfGAP3 is strongly enriched at the synaptic ribbon of photoreceptor synapses *in situ* (SR-SIM imaging with ArfGAP3 Cterm3 antibody). ***A***, 0.5-μm-thick retinal sections double immunolabeled with affinity-purified rabbit antibodies against ArfGAP3 (ArfGAP3 Cterm3 antibody) and mouse monoclonal antibodies against RIBEYE(B)/CtBP2. ***B***, Shows 0.5-μm-thick retinal sections double immunolabeled with affinity-purified rabbit antibodies against ArfGAP3 (Cterm3 antibody) and mouse monoclonal antibodies against the active zone protein bassoon. Arrows in ***A*** and ***B*** point to single immunolabeled synaptic ribbons. Arrowheads denote ArfGAP3 immunoreactivity at the synaptic ribbon. ***A*** and ***B*** were obtained by SR-SIM imaging. ONL, Outer nuclear layer; OPL, outer plexiform layer; INL, inner nuclear layer. Scale bars: ***A***, ***B***, 1 μm.

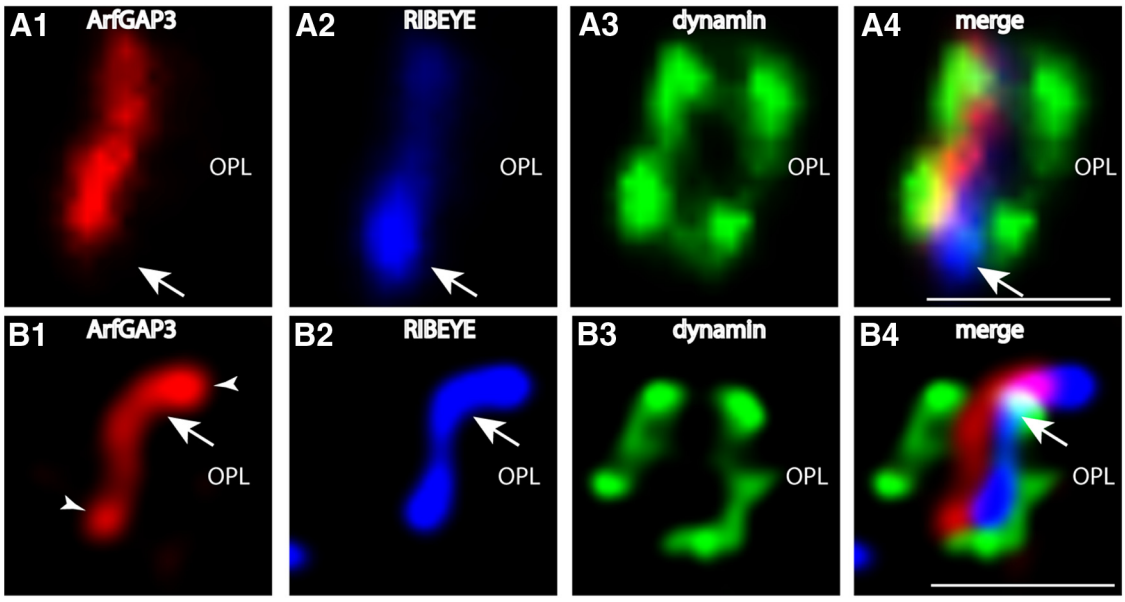

Figure 12. Localization of ArfGAP3 in the presynaptic photoreceptor terminal in relation to other presynaptic proteins. The 0.5-μm-thick retinal sections were triple immunolabeled with affinity-purified rabbit polyclonal antibodies against ArfGAP3 (Cterm3), mouse monoclonal antibodies against dynamin (hudy-1), and DyLight 650 directly labeled primary antibodies against RIBEYE(B)/CtBP2. ArfGAP3 and RIBEYE are located very close to each other (***A***, ***B***). The ArfGAP3 immunosignal is located within the ring-like dynamin immunosignal that demarcates the presynaptic plasma membrane of the periactive zone that surrounds the synaptic ribbon (Wahl et al., 2013). ***A*** was obtained by conventional imaging; ***B*** is a micrograph obtained by SR-SIM imaging. Arrows in ***A*** and ***B*** point to immunolabeled single synaptic ribbons. Arrowheads indicate ArfGAP3 immunoreactivity at the synaptic ribbon. OPL, Outer plexiform layer. Scale bars: ***A***, ***B***, 1 μm.

synaptic ribbon (Fig. 11*B*; see also discussion). Bassoon is localized to the arciform density and anchors the base of the synaptic ribbon (tom Dieck et al., 2005).

Previously, we have shown that dynamin is highly enriched at the presynaptic plasma membrane in close vicinity to the synaptic ribbon (Wahl et al., 2013). The dynamin immunosignal surrounds the synaptic ribbon in a ring-like manner in a very short distance (Wahl et al., 2013). Immunogold electron microscopy previously demonstrated that this ring of dynamin-1 immunoreactivity corresponded to the plasma membrane of the periactive zone (Wahl et al., 2013). We used dynamin as a landmark protein to further define the localization of ArfGAP3 at the synaptic ribbon complex using high-resolution fluorescence microscopy. We performed triple immunolabeling analyses with rabbit polyclonal antibodies against ArfGAP3, mouse monoclonal antibodies against dynamin (hudy-1), and Alexa 650 directly labeled primary mouse monoclonal antibodies against RIBEYE(B)-domain/CtBP2 (Fig. 12). In these triple immunolabeling analyses,

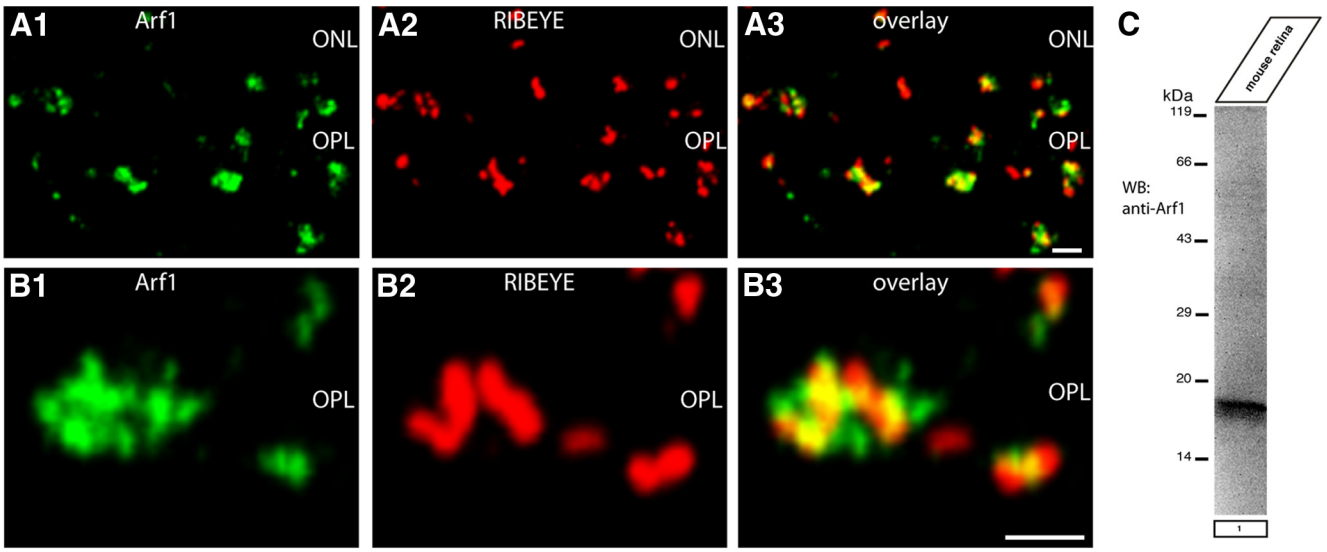

Figure 13. The ArfGAP3 effector Arf1 is enriched at the synaptic ribbon complex of photoreceptor synapses. ***A***, ***B***, Double immunolabeling experiments of 0.5-μm-thick retinal sections with mouse monoclonal antibodies against Arf1 and rabbit polyclonal antibodies against RIBEYE (U2656) demonstrated a close enrichment of Arf1 around the synaptic ribbon complex. ONL, Outer nuclear layer; OPL, outer plexiform layer. Scale bars: ***A***, ***B***, 1 μm. (***C***) Western blot analyses demonstrated that Arf1 is strongly expressed in the mouse retina.

the ArfGAP3 immunosignals were located very close to the RIBEYE-labeled synaptic ribbon and within the ring-like dynamin immunosignals that surrounded the synaptic ribbon (Fig. 12). Unfortunately, all the ArfGAP3 antibodies that we generated as well as various commercially available antibodies did not work at the ultrastructural level, so the ultrastructural localization remains to be elucidated by future examinations. ArfGAP3 is only weakly expressed in the inner plexiform layer (IPL) of the retina, which is probably due to the smaller size of the synaptic ribbons in bipolar cell terminals (data not shown).

RIBEYE(B) competes with Arf1 for binding to ArfGAP3

To get functional insights into the importance of the ArfGAP3/RIBEYE interaction we determined which Arf protein is interacting with ArfGAP3. In agreement with previous reports (Liu et al., 2001; Kartberg et al., 2010), we found that ArfGAP3 interacts with Arf1 (but not with Arf6; Fig. 2*E*, mating 1; data not shown). Western blot analyses demonstrated that Arf1 is strongly expressed in the retina and immunofluorescence microscopy documented enrichment of Arf1 in close vicinity to the synaptic ribbon complex (Fig. 13*A–C*).

Similar to RIBEYE(B), Arf1 also binds to the ArfGAP-domain of ArfGAP3 (data not shown). Therefore, we tested whether Arf1 and RIBEYE(B) can bind simultaneously to ArfGAP3 or whether they compete with each other in binding to ArfGAP3 (Fig. 14). To address this question, we used fusion protein pull-down experiments. We tested whether increasing concentrations of Arf1 (Fig. 14*A*) added to a fixed concentration of immobilized ArfGAP3 (0.15 μM) would inhibit binding of RIBEYE(B) to ArfGAP3. RIBEYE(B) was kept at a constant concentration in these experiments (0.15 μM). Similarly, we also tested whether increasing concentrations of RIBEYE(B) (Fig. 14*B*) added to a fixed concentration of immobilized ArfGAP3 (0.15 μM) would inhibit binding of Arf1 to ArfGAP3. Arf1 was kept at a constant concentration in these latter experiments (0.15 μM). In both sets of experiments, we observed a competitive behavior between Arf1 and RIBEYE(B) in binding to ArfGAP3: if Arf1 was increased, binding of RIBEYE(B) to ArfGAP3 was diminished and, vice versa, increasing concentrations of RIBEYE(B) inhibit binding of Arf1 to ArfGAP3. These data demonstrate that RIBEYE(B) competes with Arf1 for binding to a common binding site on ArfGAP3, indicating that binding of RIBEYE(B) and Arf1 to ArfGAP3 is mutually exclusive.

ArfGAP3 is involved in endocytic vesicle retrieval at the photoreceptor synapse

Next, we wanted to find out for which synaptic process ArfGAP3 is relevant at the synaptic ribbon. The synaptic ribbon is a site of intense membrane retrieval (Jackman et al., 2009; Snellman et al., 2011; Chen et al., 2013, Wahl et al., 2013). Therefore, we tested whether ArfGAP3 is involved in this process (Fig. 15). We added FM1–43 to the extracellular medium to compare endocytic uptake in photoreceptors that were either electroporated with ArfGAP3-mcherry or mcherry alone. In mcherry-electroporated photoreceptors, there was an intense uptake of FM1–43 (Fig. 15*A*,*B*). The uptake of FM1–43 in mcherry-transfected photoreceptors was similar to the FM1–43 uptake in nontransfected photoreceptors (data not shown). In contrast to mcherry-transfected photoreceptors, ArfGAP3-overexpressing transfected photoreceptors showed a very strong inhibition of FM1–43 uptake (Fig. 15*C*,*D*) indicating that ArfGAP3 is essentially involved in endocytosis at the photoreceptor synapse (see discussion).

Discussion

In the present study, we demonstrated that the Arf-GTPase-activating protein-3, ArfGAP3, is a novel component of the photoreceptor synaptic ribbon complex using various independent assays. Conventional immunofluorescence microscopy as well as SR-SIM on thin retinal resin sections demonstrated that ArfGAP3 is highly enriched at the photoreceptor synaptic ribbon complex *in situ*. ArfGAP3 is more weakly expressed in the IPL than in photoreceptor synapses of the OPL (data not shown). This is most likely because synaptic ribbons in the IPL are smaller than in photoreceptor synapses of the OPL and because the IPL is dominated by conventional, nonribbon-containing synapses.

ArfGAP3 has been previously characterized as a component of the Golgi apparatus (for review, see Spang et al., 2010). At the Golgi apparatus, ArfGAP3 regulates vesicle trafficking in an Arf1-

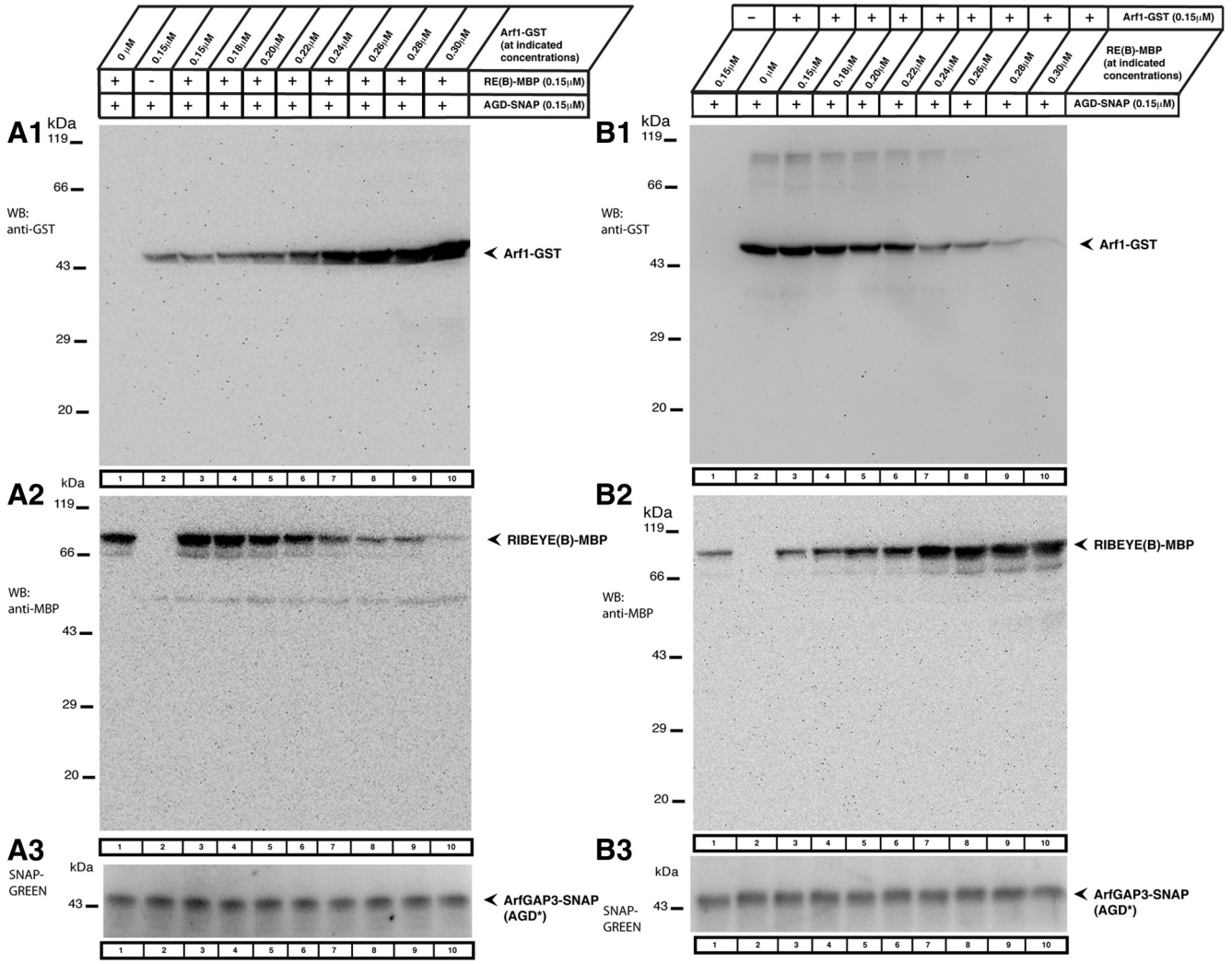

Figure 14. RIBEYE(B) and Arf1 compete with each other for binding to ArfGAP3. We tested in fusion protein pull-down experiments whether Arf1 and RIBEYE(B) can bind simultaneously to ArfGAP3 or whether they compete with each other for ArfGAP3-binding. ***A***, ***B***, Show representative Westerns blots incubated with the indicated antibodies to test for the binding of the respective fusion proteins. After detection of the GST-tagged protein (***A1***, ***B1***), blots were stripped and re-incubated with antibodies against MBP (***A2***, ***B2***). ***A3***, ***B3***, SNAP-tagged immobilized ArfGAP3 bait protein was visualized with SNAP-Vista Green (NEB). ***A***, We tested whether increasing concentrations of Arf1 added to a fixed concentration of immobilized ArfGAP3 would inhibit binding of RIBEYE(B) to ArfGAP3. RIBEYE(B) was kept at a constant concentration in these experiments. ***B***, We tested whether increasing concentrations of RIBEYE(B) added to a fixed concentration of immobilized ArfGAP3 would inhibit binding of Arf1 to ArfGAP3. Arf1 was kept at a constant concentration in these latter experiments. In both sets of experiments, we observed a competitive behavior between Arf1 and RIBEYE(B) in binding to ArfGAP3. These data demonstrate that RIBEYE(B) competes with Arf1 for binding to ArfGAP3. indicating that binding of RIBEYE(B) and Arf1 to ArfGAP3 is mutually exclusive. Abbreviations: AGD*, extended ArfGAP-domain of ArfGAP3.

dependent manner (Dogic et al., 1999; Eugster et al., 2000; Lewis et al., 2004; Watson et al., 2004; Frigerio et al., 2007; Saitoh et al., 2009; Kartberg et al., 2010; Spang et al., 2010; Yu et al., 2012). The localization of ArfGAP3 at the synaptic ribbon complex *in situ* was confirmed by two different antibodies directed against different regions of the ArfGAP3 C terminus. Both antibodies showed the same enrichment of ArfGAP3 at the photoreceptor synaptic ribbon complex. In agreement with these morphological data, ArfGAP3 and RIBEYE were coimmunoprecipitated from the bovine retina, further demonstrating enrichment of ArfGAP3 at the photoreceptor synaptic ribbon complex.

We propose that the interaction with RIBEYE recruits ArfGAP3 to the synaptic ribbons where ArfGAP3 subsequently exerts its activity. YTH data demonstrated that the catalytically active, highly conserved ArfGAP-domain of ArfGAP3 is responsible for the binding to RIBEYE. The recruitment of ArfGAP3 to RIBEYE(B) is unlikely to require a functional catalytic activity of the AGD-domain because the initial ArfGAP3 prey clone obtained from our YTH screen that strongly interacted with RIBEYE(B) displayed a deletion in the central Zn-finger motif of the AGD-domain (Goldberg, 1999; for review, see Gillingham and Munro, 2007; Kahn et al., 2008; Donaldson and Jackson, 2011). This finding does not exclude that ArfGAP3 exerts a catalytic activity at the synaptic ribbon. More likely, the ArfGAP3-RIBEYE complex is part of a larger catalytically active multiprotein complex that functions at the synaptic ribbon. In support of this proposal, the Arf GTP/GDP exchange factor IQ-ArfGEF BRAG1, which catalyzes exchange of GDP by GTP, has been shown to be associated with synaptic ribbons (Katsumata et al., 2009).

Interestingly, the interaction between RIBEYE(B) and ArfGAP3 is stimulated by NAD(H) in a redox-sensitive manner. NADH is more efficient than the oxidized NAD^+ in promoting RIBEYE(B)/ArfGAP3 interaction. Such a metabolism-dependent interaction is also known for the nuclear corepressor CtBP, which regulates transcription in a redox-sensitive manner (Zhang et al.,

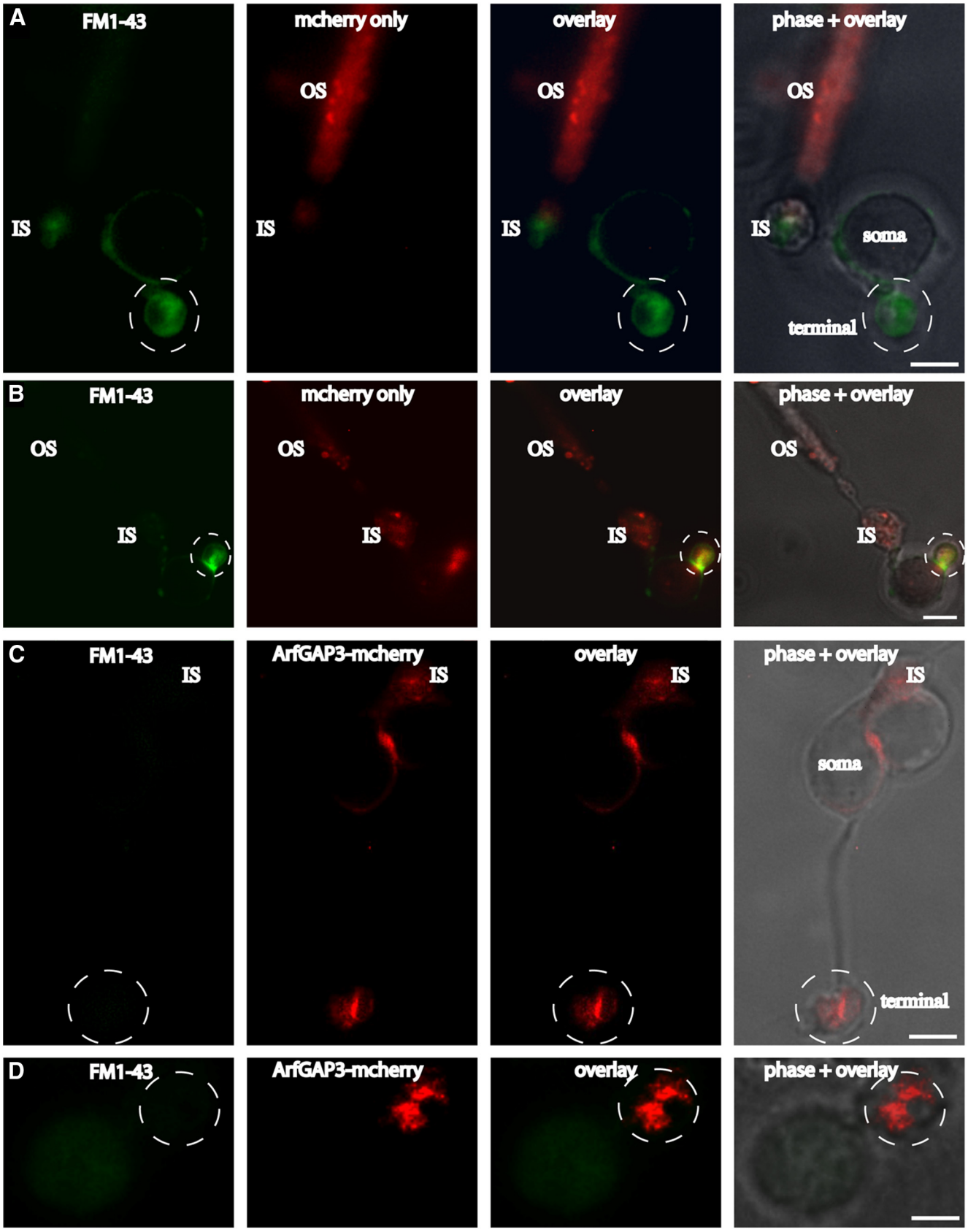

Figure 15. Overexpression of ArfGAP3 in mouse photoreceptors inhibits endocytic uptake of FM1–43. FM1–43 was used to compare endocytic uptake in photoreceptors that were either electroporated with mcherry alone (***A***, ***B***) or ArfGAP3-mcherry (***C***, ***D***). In mcherry-electroporated photoreceptors, there was an intense uptake of FM1–43 in the synaptic terminals (***A***, ***B***). The uptake of FM1–43 in mcherry-transfected photoreceptors was similar to the FM1–43 uptake in nontransfected photoreceptors (data not shown). In contrast to mcherry-transfected photoreceptors, ArfGAP3-mcherry-overexpressing photoreceptors showed a strong inhibition of FM1–43 uptake in the synaptic terminals (***C***, ***D***), indicating that ArfGAP3 is essential involved in endocytosis at the photoreceptor synapse. OS, Outer segment; IS, inner segment; Scale bars: ***A–C***, 1 μm; ***D***, 0.75 μm.

2002, 2006; Fjeld et al., 2003). A main function of this redox-sensitive interaction in ribbon synapses appears to be controlling Arf1 function. The small GTP-binding protein Arf1, an ArfGAP3 effector, is enriched at the synaptic ribbon. Arf1 is an important regulator of vesicle traffic at various intracellular compartments, including the Golgi apparatus and endosomal compartments (Gillingham and Munro, 2007; Kahn et al., 2008; Donaldson and Jackson, 2011) and might perform a similar role at the photoreceptor synaptic ribbon complex. We demonstrated that Arf1 and RIBEYE cannot bind at the same time. When RIBEYE is bound, e.g., at high levels of NADH, Arf1 can no longer bind to ArfGAP3. As a consequence, its GTPase activity will remain low and Arf1 will stay in its active, GTP-bound form.

Unfortunately, the antibodies against ArfGAP3 were not suitable for ultrastructural analyses. Super-resolution immunofluorescent microscopy indicated a particularly high enrichment of ArfGAP3 at the base of synaptic ribbon complex. Similarly, ArfGAP3 was also found close to bassoon, which is located at the base of the ribbon, and within the ring-like dynamin signal that surrounds the synaptic ribbon in the periactive zone. Dynamin was previously shown to be enriched at the presynaptic plasma membrane at the periactive zone (Wahl et al., 2013). Therefore, ArfGAP3 probably exerts its function at the base of the ribbon and in close proximity to the plasma membrane of the periactive zone. Clearly, future electron microscopic analyses need to demonstrate whether ArfGAP3 and Arf1 function directly at the presynaptic plasma membrane or on an endosomal compartment close to the plasma membrane.

Overexpression of ArfGAP3 in electroporated photoreceptors resulted in a strong inhibition of endocytic membrane retrieval as judged by an inhibition of uptake of FM1–43. Therefore, we propose that the RIBEYE/ArfGAP3 complex is involved in endocytic membrane retrieval at the synaptic ribbon. Recent studies demonstrated that the synaptic ribbon complex is important for endocytic membrane traffic in the tonically active ribbon synapse (Spassova et al., 2004; Griesinger et al., 2005; Khimich et al., 2005; Jackman et al., 2009; Babai et al., 2010; Frank et al., 2010; Schnee et al., 2011; Snellman et al., 2011; Tian et al., 2012; Chen et al., 2013; Wahl et al., 2013). Still, the molecular details and mechanisms used to accomplish this remain to be elucidated.

CtBP1/BARS, a close relative of RIBEYE(B)-domain/CtBP2 and component of the Golgi complex, is also localized to the synaptic ribbon complex (tom Dieck et al., 2005; for a review, see Corda et al., 2006). At the Golgi apparatus, CtBP1/BARS interacts with ArfGAP1 (Yang et al., 2005). This interaction has been proposed to be essential for vesicle formation and vesicle scission at the Golgi complex (Yang et al., 2002, 2005, 2006; Corda et al., 2006). The function of CtBP1/BARS at the synaptic ribbon is still unclear (Vaithianathan et al., 2013). There is a remarkable difference between the CtBP1/ArfGAP1 interaction compared with the RIBEYE/ArfGAP3 interaction. Interaction between CtBP1 and ArfGAP1 at the Golgi apparatus is mediated by the SBD of CtBP1, while the interaction between RIBEYE(B)domain and ArfGAP3 at the synaptic ribbons is mediated by the NBD of RIBEYE(B)-domain.

The recruitment of ArfGAP3 to the synaptic ribbon via an inducible, redox-dependent manner provides the synaptic ribbon with the possibility to regulate endocytic vesicle trafficking. The catalytically active ArfGAP-domain could control Arf1 activity in a redox-switchable manner by a competitive interaction with RIBEYE. The C terminus of ArfGAP3 could be involved in different tasks, e.g., the cargo sorting. The C terminus of ArfGAP3 has been shown to be involved in membrane-binding and cargo-binding/coat protein-binding at the Golgi apparatus (Rein et al., 2002; for review, see Nie and Randazzo, 2006; Schindler and Spang, 2007; Kliouchnikov et al., 2009; Schindler et al., 2009; Spang et al., 2010). A similar function might also apply in the ribbon synapse and would provide the RIBEYE-ArfGAP3 complex a central position in the vesicle recycling machinery.

References

Alpadi K, Magupalli VG, Käppel S, Köblitz L, Schwarz K, Seigel GM, Sung CH, Schmitz F (2008) RIBEYE recruits a mammalian ortholog of the C. elegans protein unc119 to synaptic ribbons of photoreceptor synapses. J Biol Chem 283:26461–26467. CrossRef Medline

Babai N, Bartoletti TM, Thoreson WB (2010) Calcium regulates vesicle replenishment at the cone ribbon synapse. J Neurosci 30:15866–15877. CrossRef Medline

Bigay J, Casella JF, Drin G, Mesmin B, Antonny B (2005) ArfGAP1 responds to membrane curvature through the folding of a lipid packing sensor motif. EMBO J 24:2244–2253. CrossRef Medline

Bradford MM (1976) A rapid and sensitive method for the quantitation of microgram quantities of protein utilizing the principle of protein-dye binding. Anal Biochem 72:248–254. CrossRef Medline

Briggman KL, Euler T (2011) Bulk electroporation and population calcium imaging in the adult mammalian retina. J Neurophysiol 105:2601–2609. CrossRef Medline

Chen M, Van Hook MJ, Zenisek D, Thoreson WB (2013) Properties of ribbon and non-ribbon release from rod photoreceptors revealed by visualizing individual synaptic vesicles. J Neurosci 33:2071–2086. CrossRef Medline

Corda D, Colanzi A, Luini A (2006) The multiple activities of CtBP/BARS proteins: the Golgi view. Trends Cell Biol 16:167–173. CrossRef Medline

Cukierman E, Huber I, Rotman M, Cassel D (1995) The Arf1 GTPase-activating protein: zinc finger motif and Golgi complex localization. Science 270:1999–2002. CrossRef Medline

Dogic D, de Chassey B, Pick E, Cassel D, Lefkir Y, Hennecke S, Cosson P, Letourneur F (1999) The ADP-ribosylation factor GTPase-activating protein glo3p is involved in ER retrieval. Eur J Cell Biol 78:305–310. CrossRef Medline

Donaldson JG, Jackson CL (2011) Arf family G proteins and their regulators: roles in membrane transport, development and disease. Nat Rev Mol Cell Biol 12:362–375. CrossRef Medline

Donovan SL, Dyer MA (2006) Preparation and square wave electroporation of retinal explant cultures. Nat Protoc 1:2710–2718. CrossRef Medline

Eugster A, Frigerio G, Dale M, Duden R (2000) COP I domains required for coatomer integrity and novel interactions with Arf and ArfGAP. EMBO J 19:3905–3917. CrossRef Medline

Fjeld CC, Birdsong WT, Goodman RH (2003) Differential binding of NAD+ and NADH allows the transcriptional corepressor C-terminal binding protein to serve as a metabolic sensor. Proc Natl Acad Sci U S A 100:9202–9207. CrossRef Medline

Frank T, Rutherford MA, Strenzke N, Neef A, Pangrsic T, Khimich D, Fejtova A, Gundelfinger ED, Liberman MC, Harke B, Bryan KE, Lee A, Egner A, Riedel D, Moser T (2010) Bassoon and the synaptic ribbon organize Ca^{2+}-channels and vesicles to add release sites and promote refilling. Neuron 68:724–738. CrossRef Medline

Frigerio G, Grimsey N, Dale M, Majoul I, Duden R (2007) Two human ArfGAPs associated with COP-I-coated vesicles. Traffic 8:1644–1655. CrossRef Medline

Gillingham AK, Munro S (2007) The small g proteins of the Arf family and their regulators. Annu Rev Cell Dev Biol 23:579–611. CrossRef Medline

Goldberg J (1999) Structural and functional analysis of the Arf1-Arfgap complex reveals a role for coatamer in GTP hydrolysis. Cell 96:893–902. CrossRef Medline

Griesinger CB, Richards CD, Ashmore JF (2005) Fast vesicle replenishment allows indefatigable signalling at the first auditory synapse. Nature 435:212–215. CrossRef Medline

Gustafsson MG, Shao L, Carlton PM, Wang CJ, Golubovskaya IN, Cande WZ, Agard DA, Sedat JW (2008) Three-dimensional resolution doubling in wide-field fluorescence microscopy by structured illumination. Biophys J 94:4957–4970. CrossRef Medline

Harper JW, Adami GR, Wei N, Keyomarsi K, Elledge SJ (1993) The p21 Cdk-interacting protein Cip1 is a potent inhibitor of G1 cyclin-dependent kinases. Cell 75:805–816. CrossRef Medline

Inoue H, Randazzo PA (2007) Arf GAPs and their interacting proteins. Traffic 8:1465–1475. CrossRef Medline

Jackman SL, Choi SY, Thoreson WB, Rabl K, Bartoletti TM, Kramer RH (2009) Role of the synaptic ribbon in transmitting the cone light response. Nat Neurosci 12:303–310. CrossRef Medline

Kahn RA, Bruford E, Inoue H, Logsdon JM Jr, Nie Z, Premont RT, Randazzo PA, Satake M, Theibert AB, Zapp ML, Cassel D (2008) Consensus nomenclature of the human ArfGAP domain-containing proteins. J Cell Biol 182:1039–1044. CrossRef Medline

Kartberg F, Asp L, Dejgaard SY, Smedh M, Fernandez-Rodriguez J, Nilsson T, Presley JF (2010) ArfGAP2 and ArfGAP3 are essential for COP I coat assembly on the Golgi membrane of living cells. J Biol Chem 285:36709–36720. CrossRef Medline

Katsumata O, Ohara N, Tamaki H, Niimura T, Naganuma H, Watanabe M, Sakagami H (2009) IQ-ArfGEF/BRAG1 is associated with synaptic ribbons in the mouse retina. Eur J Neurosci 30:1509–1516. CrossRef Medline

Khimich D, Nouvian R, Pujol R, Tom Dieck S, Egner A, Gundelfinger ED, Moser T (2005) Hair cell synaptic ribbons are essential for synchronous auditory signalling. Nature 434:889–894. CrossRef Medline

Kliouchnikov L, Bigay J, Mesmin B, Parnis A, Rawet M, Goldfeder N, Antonny B, Cassel D (2009) Discrete determinants in ArfGAP23/3 conferring Golgi localization and regulation by the COPI coat. Mol Biol Cell 20:859–869. CrossRef Medline

Kumar V, Carlson JE, Ohgi KA, Edwards TA, Rose DW, Escalante CR, Rosenfeld MG, Aggarwal AK (2002) Transcription corepressor CtBP is an NAD(+) regulated dehydrogenase. Mol Cell 10:857–869. CrossRef Medline

Lewis SM, Poon PP, Singer RA, Johnston GC, Spang A (2004) The ArfGAP Glo3 is required for the generation of COP I vesicles. Mol Biol Cell 15:4064–4072. CrossRef Medline

Liu X, Zhang C, Xing G, Chen Q, He F (2001) Functional characterization of novel human ArfGAP3. FEBS Lett 490:79–83. CrossRef Medline

Magupalli VG, Schwarz K, Alpadi K, Natarajan S, Seigel GM, Schmitz F (2008) Multiple RIBEYE-RIBEYE interactions create a dynamic scaffold for the formation of synaptic ribbons. J Neurosci 28:7954–7967. CrossRef Medline

Morgan JL, Soto F, Wong RO, Kerschensteiner D (2011) Development of cell type-specific connectivity patterns of converging excitatory axons in the retina. Neuron 71:1014–1021. CrossRef Medline

Nardini M, Spanò S, Cericola C, Pesce A, Massaro A, Millo E, Luini A, Corda D, Bolognesi M (2003) CtBP/BARS: a dual-function protein involved in transcriptional corepression and Golgi membrane fission. EMBO J 22:3122–3130. CrossRef Medline

Nie Z, Randazzo PA (2006) Arf GAPs and membrane traffic. J Cell Sci 119:1203–1211. CrossRef Medline

Olmsted JB (1981) Affinity purification of antibodies from diazotized paper blots of heterogeneous protein samples. J Biol Chem 256:11955–11957. Medline

Rea R, Li J, Dharia A, Levitan ES, Sterling P, Kramer RH (2004) Streamlined synaptic vesicle cycle in cone photoreceptor terminals. Neuron 41:755–766. CrossRef Medline

Rein U, Andag U, Duden R, Schmitt HD, Spang A (2002) ArfGAP-mediated interaction between ER-Golgi v-SNAREs and the COP I coat. J Cell Biol 157:395–404. CrossRef Medline

Saitoh A, Shin HW, Yamada A, Waguri S, Nakayama K (2009) Three homologous ArfGAPs participate in coat protein I-mediated transport. J Biol Chem 284:13948–13957. CrossRef Medline

Schermelleh L, Carlton PM, Haase S, Shao L, Winoto L, Kner P, Burke B, Cardoso MC, Agard DA, Gustafsson MG, Leonhardt H, Sedat JW (2008) Subdiffraction multicolor imaging of the nuclear periphery with 3D structured illumination microscopy. Science 320:1332–1336. CrossRef Medline

Schermelleh L, Heintzmann R, Leonhardt H (2010) A guide to superresolution fluorescence microscopy. J Cell Biol 190:165–175. CrossRef Medline

Schindler C, Spang A (2007) Interaction of SNAREs with ArfGAPs precedes recruitment of sec18p/NSF. Mol Biol Cell 18:2852–2863. CrossRef Medline

Schindler C, Rodriguez F, Poon PP, Singer RA, Johnston GC, Spang A (2009) The GAP domain and the SNARE, coatomer and cargo interaction region of the ArfGAP2/3 glo3 are sufficient for glo3 function. Traffic 10:1362–1375. CrossRef Medline

Schmitz F (2009) The making of synaptic ribbons: how they are built and what they do. Neuroscientist 15:611–624. CrossRef Medline

Schmitz F, Königstorfer A, Südhof TC (2000) RIBEYE, a component of ribbon synapses: a protein's journey through evolution provides insight into synaptic ribbon function. Neuron 28:857–872. CrossRef Medline

Schmitz F, Natarajan S, Venkatesan JK, Wahl S, Schwarz K, Grabner CP (2012) EF hand-mediated Ca and cGMP signaling in photoreceptor synaptic terminals. Front Mol Neurosci 5:26. CrossRef Medline

Schnee ME, Santos-Sacchi J, Castellano-Muñoz M, Kong JH, Ricci AJ (2011) Calcium-dependent synaptic vesicle trafficking underlies indefatigable release of the hair cell afferent fiber synapse. Neuron 70:326–338. CrossRef Medline

Schwarz K, Natarajan S, Kassas N, Vitale N, Schmitz F (2011) The synaptic ribbon is a site of phosphatidic acid generation in ribbon synapses. J Neurosci 31:15996–16011. CrossRef Medline

Snellman J, Mehta B, Babai N, Bartoletti TM, Akmentin W, Francis A, Matthews G, Thoreson W, Zenisek D (2011) Acute destruction of the synaptic ribbon reveals a role for the ribbon in vesicle priming. Nat Neurosci 14:1135–1141. CrossRef Medline

Spang A, Shiba Y, Randazzo PA (2010) ArfGAPs: gatekeepers of vesicle generation. FEBS Lett 584:2646–2651. CrossRef Medline

Spassova MA, Avissar M, Furman AC, Crumling MA, Saunders JC, Parsons TD (2004) Evidence that rapid replenishment of the synaptic ribbon mediates recovery from short-term adaptation at the hair cell afferent synapse. J Assoc Res Otolaryngol 5:376–390. CrossRef Medline

Tai AW, Chuang JZ, Bode C, Wolfrum U, Sung CH (1999) Rhodopsin's carboxyterminal cytoplasmic tail acts as a membrane receptor for cytoplasmic dynein by binding to the dynein light chain Ttctex-1. Cell 97:877–887. CrossRef Medline

Tian M, Xu CS, Montpetit R, Kramer RH (2012) Rab3a mediates vesicle delivery at photoreceptor ribbon synapses. J Neurosci 32:6931–6936. CrossRef Medline

tom Dieck S, Altrock WD, Kessels MM, Qualmann B, Regus H, Brauner D, Fejtová A, Bracko O, Gundelfinger ED, Brandstätter JH (2005) Molecular dissection of the photoreceptor ribbon synapse: physical interaction of Bassoon and RIBEYE is essential for the assembly of the ribbon complex. J Cell Biol 168:825–836. CrossRef Medline

Vaithianathan T, Akmentin W, Henry D, Matthews G (2013) The ribbon-associated protein C-terminal-binding protein 1 is not essential for the structure and function of retinal ribbon synapses. Mol Vis 19:917–926. Medline

Venkatesan JK, Natarajan S, Schwarz K, Mayer SI, Alpadi K, Magupalli VG, Sung CH, Schmitz F (2010) Nicotinamide adenine dinucleotide-dependent binding of the neuronal Ca^{2+}- sensor protein GCAP2 to photoreceptor synaptic ribbons. J Neurosci 30:6559–6576. CrossRef Medline

Vergara MN, Gutierrez C, O'Brien DR, Canto-Soler MV (2013) Ex vivo electroporation of retinal cells: a novel, high efficiency method for functional studies in primary retinal cultures. Exp Eye Res 109:40–50. CrossRef Medline

Wahl S, Katiyar R, Schmitz F (2013) A local, periactive zone endocytic machinery at photoreceptor synapses in close vicinity to photoreceptor synaptic ribbons. J Neurosci 33:10278–10300. CrossRef Medline

Watson PJ, Frigerio G, Collins BM, Duden R, Owen DJ (2004) gamma-COP appendage domain-structure and function. Traffic 5:79–88. CrossRef Medline

Williams PR, Morgan JL, Kerschensteiner D, Wong RO (2013) In vitro imaging of retinal whole mounts. Cold Spring Harb Protoc 2013. pii:pdb.prot072645. CrossRef Medline

Yang JS, Lee SY, Gao M, Bourgoin S, Randazzo PA, Premont RT, Hsu VW (2002) ArfGAP1 promotes the formation of COPI vesicles, suggesting function as a component of the coat. J Cell Biol 159:69–78. CrossRef Medline

Yang JS, Lee SY, Spanò S, Gad H, Zhang L, Nie Z, Bonazzi M, Corda D, Luini A, Hsu VW (2005) A role for BARS at the fission step of COP I vesicle formation from the Golgi membrane. EMBO J 24:4133–4143. CrossRef Medline

Yang JS, Zhang L, Lee SY, Gad H, Luini A, Hsu VW (2006) Key components of the fission machinery are interchangeable. Nat Cell Biol 8:1376–1382. CrossRef Medline

Yu X, Breitman M, Goldberg J (2012) A structure-based mechanism for Arf1-dependent recruitment of coatomer to membranes. Cell 148:530–542. CrossRef Medline

Zenisek D, Steyer JA, Almers W (2000) Transport, capture and exocytosis of single synaptic vesicles at active zones. Nature 406:849–854. CrossRef Medline

Zhang Q, Piston DW, Goodman RH (2002) Regulation of corepressor function by nuclear NADH. Science 295:1895–1897. Medline

Zhang Q, Wang SY, Nottke AC, Rocheleau JV, Piston DW, Goodman RH (2006) Redox sensor CtBP mediates hypoxia-induced tumor cell migration. Proc Natl Acad Sci U S A 103:9029–9033. CrossRef Medline